SAN DIEGO STATE UNIVERSITY AND UNIVERSITY OF CALIFORNIA
SANTA BARBARA

Salt Marsh Responses To Oil Contamination Following The Deepwater Horizon Oil Spill

A Dissertation submitted in partial satisfaction of the

requirements for the degree Doctor of Philosophy

in Geography

by
Michael Cooper Beland

Committee in charge:

Professor Trent Biggs, Chair

Professor Douglas Stow

Professor Dar Roberts

Professor Jennifer King

September 2018

The dissertation of Michael Cooper Beland is approved.

_____

Jennifer King

_____

Dar Roberts

_____

Douglas Stow

_____

Trent Biggs, Committee Chair

June 2018

Salt Marsh Responses to Oil Contamination following the *Deepwater Horizon* Oil Spill

by

Michael Cooper Beland

ABSTRACT OF THE DISSERTATION

Salt Marsh Responses To Oil Contamination Following The Deepwater Horizon Oil Spill

BY

MICHAEL BELAND

The *Deepwater Horizon* oil spill, which occurred from April to July of 2010, was the largest spill in U.S. history. Oil washed onto hundreds of kilometers of intertidal marsh shoreline resulting in widespread plant mortality and short-term reductions in ecosystem function. Past incidences of oiling have shown that marsh recovery trajectories can vary greatly over space and time. Accordingly, the long-term negative effects of an oil spill of this magnitude on marsh ecosystems remains largely unknown. This dissertation investigates the effects of oil contamination from the *Deepwater Horizon* oil spill on community dominant plant species distributions and land loss rates and, simultaneously, demonstrates the value of employing advanced remote sensing and GIS techniques to address landscape-scale ecological disturbances.

To examine the response of marsh plant communities to heavy oiling, dominant species in heavily oiled salt marshes, an image classification system was developed to map dominant species. This classification approach utilizes canonical discriminant analysis (CDA), along with a library of field-referenced image endmembers collected from a time series of Airborne Visible/Infrared Imaging Spectrometer (AVIRIS) images (2010-2012). Land loss rates were calculated using the normalized difference vegetation index (NDVI)

applied to a time series (2006-2016) of high resolution (0.30-0.64 m) orthorectified image datasets. Finally, a simple, fetch-limited wind-wave model was integrated into the analysis of shoreline oiling and land loss to examine the interacting effects of wave characteristics and oiling on bay-wide land loss rates.

This dissertation's findings suggest that the most important impact of oiling along marsh boundaries is the acceleration of shoreline retreat and land loss. Further, the results imply that marsh responses to oil contamination are highly variable, and wave action is a significant factor in determining marsh recovery trajectories. Without high wave energy, marsh plant communities show signs of recovery within 3 years of oil contamination. Conversely, oiled shorelines that are exposed to high wave energy can accelerate land loss exponentially. Finally, the results demonstrate the value of advanced remote sensing techniques in examining landscape-scale ecosystem changes that are impractical to assess using traditional, field-based quantitative methods.

ABBREVIATED VITA MICHAEL COOPER BELAND

August 2018

EDUCATION

Doctor of Philosophy in Geography, University of California, Santa Barbara & San Diego State University, September 2018 (expected)
Master of Arts in Geography, California State University, Northridge, CA, Spring 2008
Bachelor of Science in Geography, East Carolina University, Fall 1999

PROFESSIONAL EXPERIENCE

2017- *present*: Adjunct Professor, California State University, Los Angeles, CA
2013-2015: Research Fellow, NASA Earth and Space Science Fellowship
2011-2013: Research Assistant, Visualization & Image Processing for Environmental Research Lab, UCSB
2008-2012: Teaching and Research Assistant, Department of Geography San Diego State University, San Diego, CA
2007-2008: Teaching and Research Assistant, Department of Geography, Department of Geography & Center for Geographic Studies
2000-2006: Geographic Analyst, NAVTEQ Corp. Los Angeles, CA, Austin, TX, Charlotte, NC

PUBLICATIONS

Beland, M., Biggs, T.W., Roberts, D. A., Peterson S.H., Kokaly, R.F. (*in preparation*). Interactive Contributions of Oiling and Wave Energy on Land Loss along Salt Marsh Boundaries. Intended for *Journal of Coastal Research.*

Beland, M., Biggs, T.W., Roberts, D. A., Peterson S.H., Kokaly, R.F., Piazza, S. (2017). Oiling accelerates loss of salt marshes, southeastern Louisiana. *PloS one, 12*(8).

Beland, M., Roberts, D. A., Peterson S.H., Biggs, T.W., Kokaly, R.F., Piazza, S., Roth, K.L., Khanna, S., Ustin, S.L. (2016). Mapping changing distributions of dominant species in oil-contaminated salt marshes of Louisiana using imaging spectroscopy. *Remote Sensing of Environment*, *182*, 192-207.

Roth, K. L., Roberts, D. A., Dennison, P. E., Alonzo, M., Peterson, S. H., & **Beland, M.** (2015). Differentiating plant species within and across diverse ecosystems with imaging spectroscopy. *Remote Sensing of Environment*, *167*, 135-151.

Peterson, S. H., Roberts, D. A., **Beland, M.**, Kokaly, R. F., & Ustin, S. L. (2015). Oil detection in the coastal marshes of Louisiana using MESMA applied to band subsets of AVIRIS data. *Remote Sensing of Environment*, *159*, 222-231.

Stein, E., Dark, S., Longcore, T., Grossinger, R., Hall, N. & **Beland, M.** (2010) Historical Ecology as a Tool for Assessing Landscape Change and Informing Wetland Restoration Priorities. *Wetlands* 30(3): 589-601.

Biggs T.W., **Beland M.** 2009. Hydrologic Functions and the Effects of Climate Change on Himalayan Wetlands. Unpublished manuscript for Regional Program on Himalayan Glaciers, Rivers and High-altitude Wetlands, WWF – India.

Stein, E.D., S. Dark, T. Longcore, N. Hall, **M. Beland**, R. Grossinger, J. Casanova & M. Sutula (2007). *Historical ecology and landscape change of the San Gabriel River and floodplain*. Southern California Coastal Water Research Project. Costa Mesa, CA.

TABLE OF CONTENTS

LIST OF FIGURES

LIST OF TABLES

ACKNOWLEDGEMENTS

To Sarah, my wife, thank you for your love, support and the countless sacrifices you have made throughout this journey. I thank my daughter Leni for the therapeutic distraction she has provided and our dog Tuna for the many contemplative walks that sometimes led to new ideas. I also owe much gratitude to my parents, Becky and Marvin, my brother, Jeff, and in-laws, Margie and Harlan, for their continued support throughout my academic career.

This dissertation has evolved considerably over the years, and critical to the success of its evolution has been the expertise and input of my outstanding committee; Trent Biggs, Dar Roberts, Doug Stow and Jennifer King. I owe a special thanks to Trent Biggs for his support and direction, and perhaps more importantly, for sticking with me during the ups-and-downs. I also owe a great deal of gratitude to Dar Roberts and Seth Peterson for their invaluable input in the early stages of this project, without which this dissertation would have never progressed.

I've had the privilege to collaborate with many talented people of the years. In particular, I want to thank Ray Kokaly, Sarai Piazza, Brett Patton and the USGS team for their contributions to the dissertation, and specifically, for making the field research campaigns possible. Finally, I want to thank the brilliant Viper Lab'ers: Keely Roth, Susan Meerdink, Andrew Thorpe, Mike Alonzo and others; who have made this process an enjoyable learning experience.

Chapter 1: Introduction

Salt marshes are highly productive, resilient ecosystems that provide a myriad of important ecological services and possess unique physiological traits for coping with stressful environmental conditions (Turner, 1976; Niering et al., 1977; Pennings and Bertness, 2001; Gedan et al., 2009). For nearly two centuries, human activities in the northern Gulf of Mexico have altered natural hydrologic regimes and changed the magnitude of system perturbations beyond salt marsh resilience thresholds (Deegan et al., 1984; van de Koppel et al., 2005), resulting in accelerated rates of wetland loss (> 250 $km^2\ yr^{-1}$: Stedman and Dahl, 2008). Since the 1970s, land loss has been a major topic of concern in the region, particularly for coastal Louisiana (Barrett, 1970; Gagliano et al., 1970; Chabreck, 1972; Craig et al., 1979), which lost an estimated 4833 km^2 of intertidal wetland area from 1932-2016 ($\backsim$58 $km^2 yr^{-1}$: Couvillion et al., 2017).

The largest oil spill in U.S. history occurred in the Gulf of Mexico on April 20, 2010, when an explosion at the BP/Deepwater Horizon (DWH) Macondo wellhead released 780,000 m^3 of crude oil into the Gulf before being capped on July 15 (Lehr et al., 2010). Oil washed onto approximately 796 km of shoreline comprised of intertidal marshes, disproportionally impacting salt marshes of Louisiana (Michel et al., 2013). Oiling was concentrated along the marsh shoreline edge (Silliman et al., 2012; Kokaly et al., 2013; Peterson et al., 2015), causing plant stress, mortality, and reductions in above- and belowground biomass (Silliman et al., 2012; Lin and Mendelssohn, 2012; McClenachan et al., 2013). The long-term effects of an oil spill of this magnitude remain difficult to predict,

due to the variability in oiling characteristics, plant responses and landscape position (Pezeshki et al., 2000; Lin and Mendelssohn, 2012; McClenachan et al., 2013).

Varying oiling characteristics, such as oil-type, timing of exposure, concentration, thickness, degree of weathering and emulsification, and surface distribution, have been shown to elicit highly variable plant community and ecosystem responses (Pezeshki et al., 2000; DeLaune et al., 2003). For example, leaf tissue that is exposed directly to oil exhibits immediate, yet, short-term effects, while oil contamination of marsh sediment may cause longer-term effects on ecosystem processes, like gas exchange capacity (DeLaune et al., 2003). The timing of an oil spill may determine the degree of plant mortality, as plants respond more adversely to oiling during the growing season than during pre-dormancy and dormancy periods (Webb, 1994; Lin, 1996). Furthermore, oil spills that occur during an active storm year may cause more extensive marsh injury and mortality, due to higher storm tides' capacity for transporting oil into previously unaffected areas (Pezeshki et al., 2000).

Dominant plant species shape community structure and are a useful indicator of ecosystem health following disturbances (Frieswyk et al., 2007). Most petroleum crude oils (e.g. south Louisiana crude) are nonionic, and therefore, associate more readily with organic particles (Pezeshki et al. 2000). The level of soil organic matter (SOM) in a marsh substrate impacts oil concentrations, and SOM content varies depending on plant species composition (Lin and Mendelssohn, 1996). For example, Lin and Mendelssohn (1996) reported, in a comparative greenhouse study, both higher SOM content and higher oil residual concentrations in plots dominated by *Spartina patens* than those dominated by *Spartina alterniflora*. Additionally, the distribution of commonly occurring species is a valuable indicator of ecosystem response, due to the variable growth responses of species to oil

contaminated soils. For instance, *Spartina alterniflora* has exhibited a greater recovery rate than other common dominant marsh species in field experiments, indicating a higher tolerance limit for oil contamination (Lin and Mendelssohn, 2012). Therefore, identifying the distribution of marsh species and documenting vegetation changes in relation to oiling characteristics are critical steps in assessing the landscape-scale ecological impacts of oil contamination.

Exposure of marsh plants to oil can lead to plant mortality and reduced biomass production, resulting in destabilization of the root-soil matrix (Lin and Mendelssohn, 1996; Silliman et al., 2012; Hester et al., 2016). Soil strength and sediment accretion are directly related to belowground biomass as roots and rhyzomes create a binding matrix for sediment accumulation (Gabet, 1998; Michel and Kirchner, 2002). Reductions in belowground biomass caused by oiling and subsequent remediation efforts increased the vulnerability of shorelines to both episodic (i.e. storm surge) and chronic (i.e. subsidence, sea-level rise) erosional forces (Hershner and Lake, 1980; Silliman et al., 2012; McClenachan et al., 2013; Zengel et al., 2015).

Limited resources and the inaccessibility of many areas have made ecological assessments using traditional field-based methods infeasible. In light of these limitations, remote sensing products have become attractive tools for "scaling up" *in situ* observations to a landscape scale, evaluating post-disturbance responses, and monitoring ecosystem changes. Time series, or multitemporal, image processing models have become important tools for ecosystem ecologists and conservation biologists, as these techniques provide accurate and reliable measurements of vegetation cover and biophysical parameters (i.e. aboveground green biomass, leaf area index and vegetation stress) that are used to support estimates of

primary productivity for terrestrial ecosystems (Asner, 1998; Ustin and Gamon, 2010). More recently, narrow-band, hyperspectral sensors, like the Airborne Visible / Infrared Imaging Spectrometer (AVIRIS), have produced images with fine enough spectral resolution (10 nm) to discriminate ground constituents that were previously indistinguishable with broadband sensors. Consequently, advanced techniques, like increasingly sophisticated feature extraction and spectral unmixing algorithms, have been developed to attain more detailed information from spectroscopic data (Gamon et al., 1997; Asner, 1998; Roberts et al., 1998; Ceccato et al., 2001; Serrano et al., 2002; Asner et al., 2003; Nagler et al., 2003; Feret et al., 2008; Kokaly et al., 2009; Ustin et al., 2009).

The objective of this dissertation is to investigate the impact of oil contamination on dominant plant species distributions (2010-2012) and marsh boundary land loss (2010-2013 and 2013-2016) in Barataria Bay, Louisiana following the DWH oil spill and, simultaneously, to demonstrate the value of employing advanced remote sensing and GIS techniques to address landscape-scale ecological disturbances. The dissertation is divided into three main chapters that each address different questions related to this objective. Chapter 2, titled "Mapping changing distributions of dominant species in oil-contaminated salt marshes of Louisiana using imaging spectroscopy" and published in *Remote Sensing of Environment*, analyzes the post-oiled, changing spatial distribution of dominant salt marsh communities using a time series of airborne imaging spectroscopic data (AVIRIS; Beland et al., 2016). An image classification system was employed for mapping dominant marsh species, and novel imaging spectroscopy techniques were developed to distinguish spectrally similar plant species. The goal was to develop and implement an image classification strategy that would obtain satisfactory and consistent classification results.

Chapter 3, titled "Oiling accelerates loss of salt marshes, southeastern Louisiana" and published in *PLoS ONE*, analyzes landscape and reach-scale land loss trajectories in oil impacted salt marshes (Beland et al., 2017). Normalized Difference Vegetation Index (NDVI) was applied to a time series (2006-2016) of high resolution satellite and airborne color-infrared images to map changes in marsh land cover and open water before and after oiling. Marsh boundaries were segmented into non-oiled and oiled reaches, and land-loss rates were calculated to determine if losses were significantly different than background rates. Further, standardized land-loss rates per unit shoreline were calculated to provide results that can be easily compared with future assessments of marsh shoreline change in the Louisiana Coastal Zone.

Chapter 4, titled "Interactive Contributions of Oiling and Wave Energy on Land Loss along Salt Marsh Boundaries", integrates a simple, fetch-limited wave climate model with shoreline oiling and land loss observations to better explain the variability in land losses after oiling by generating a spatially-explicit model of background rates of erosion before and after oil contamination. This chapter examines the relationship between marsh boundary oiling and exposure to wave energy and calculates land loss rates along heavily-oiled and non-oiled marsh boundaries across a range of wave energy exposures.

The last chapter, Chapter 5, summarizes the overall findings of the dissertation work and concludes with an examination of future research questions.

1.1. References

Asner, G. P. (1998). Biophysical and biochemical sources of variability in canopy reflectance. *Remote Sensing of Environment*, 64(3), 234-253.

Asner, G. P., Borghi, C. E., & Ojeda, R. A. (2003). Desertification in Central Argentina: Changes in ecosystem carbon and nitrogen from imaging spectroscopy. *Ecological Applications*, 13, 629−648.

Barrett, B. (1970). Water measurements of coastal Louisiana: Louisiana Wildlife and Fisheries Commission, Division of Oysters, Water Bottoms and Seafood, p. 196.

Beland, M., Biggs, T. W., Roberts, D. A., Peterson, S. H., Kokaly, R. F., & Piazza, S. (2017). Oiling accelerates loss of salt marshes, southeastern Louisiana. *PloS one*, 12(8), e0181197.

Beland, M., Roberts, D. A., Peterson, S. H., Biggs, T. W., Kokaly, R. F., Piazza, S., ... & Ustin, S. L. (2016). Mapping changing distributions of dominant species in oil-contaminated salt marshes of Louisiana using imaging spectroscopy. *Remote Sensing of Environment*, 182, 192-207.

Ceccato, P., Flasse, S., Tarantola, S., Jacquemoud, S., & Gregoire, J. -M. (2001). Detecting vegetation leaf water content using reflectance in the optical domain. *Remote Sensing of Environment*, 77, 22−33.

Chabreck, R. H. (1972). Vegetation, water and soil characteristics of the Louisiana coastal region. *Louisiana State University Agricultural Experiment Station Bulletin No. 664.* Louisiana State University, Baton Rouge, Louisiana.

Couvillion, B.R., Beck, Holly, Schoolmaster, Donald, and Fischer, Michelle (2017) Land area change in coastal Louisiana 1932 to 2016: U.S. Geological Survey Scientific Investigations Map 3381, 16 p. pamphlet.

Craig, N. J., Turner, R. E., & Day Jr, J. W. (1979). Land loss in coastal Louisiana (USA). *Environmental Management*, 3(2), 133-144.

Deegan L., Kennedy H., and Neill C. (1984). Natural factors and human modifications contributing to marsh loss in Louisiana's Mississippi River deltaic plain. *Environmental Management*, 8 519–27.

DeLaune, R. D., Pezeshki, S. R., Jugsujinda, A., & Lindau, C. W. (2003). Sensitivity of US Gulf of Mexico coastal marsh vegetation to crude oil: Comparison of greenhouse and field responses. *Aquatic Ecology*, 37(4), 351-360.

Feret, J. B., François, C., Asner, G. P., Gitelson, A. A., Martin, R. E., Bidel, L. P., ... & Jacquemoud, S. (2008). PROSPECT-4 and 5: Advances in the leaf optical properties model separating photosynthetic pigments. *Remote Sensing of Environment*, 112(6), 3030-3043.

Frieswyk, C. B., Johnston, C. A., & Zedler, J. B. (2007). Identifying and characterizing dominant plants as an indicator of community condition. *Journal of Great Lakes Research*, 33(sp3), 125-135.

Gabet, E. J. (1998). Lateral migration and bank erosion in a saltmarsh tidal channel in San Francisco Bay, California. *Estuaries*, 21(4), 745-753.

Gagliano, S. M., Kwon, H. J., & Van Beek, J. L. (1970). Deterioration and restoration of coastal wetlands. *Coastal Engineering Proceedings*, 1(12).

Gamon, J .A., Serrano, L., & Surfus, J. S. (1997). The photochemical reflectance index: an optical indicator of photosynthetic radiation-use efficiency across species, functional types, and nutrient levels. *Oecologia*, 112, 492-501.

Gedan, K. B., Silliman, B. R., and Bertness, M. D. (2009). Centuries of human-driven change in salt marsh ecosystems. *Annual Review of Marine Science*, 1, 117–141.

Hershner, C., & Lake, J. (1980). Effects of chronic oil pollution on a salt-marsh grass community. *Marine Biology*, 56(2), 163-173.

Hester, M. W., Willis, J. M., Rouhani, S., Steinhoff, M. A., & Baker, M. C. (2016). Impacts of the Deepwater Horizon oil spill on the salt marsh vegetation of Louisiana. *Environmental Pollution*, 216, 361-370.

Kokaly, R. F., Asner, G. P., Ollinger, S. V., Martin, M. E., & Wessman, C. A. (2009). Characterizing canopy biochemistry from imaging spectroscopy and its application to ecosystem studies. *Remote Sensing of Environment*, 113, S78–S91.

Kokaly, R. F., Couvillion, B. R., Holloway, J. M., Roberts, D. A., Ustin, S. L., Peterson, S. H., et al. (2013). Spectroscopic remote sensing of the distribution and persistence of oil from the Deepwater Horizon spill in Barataria Bay marshes. *Remote Sensing of Environment*, 129, 210-230.

Lehr, B., Nristol, S., & Possolo, A. (2010). Oil Budget Calculator—Deepwater Horizon, technical documentation: a report to the National Incident Command. Coastal Response Research Center.

Lin, Q., 1996. Factors Controlling the Impact of South Louisiana Crude Oil on Vegetation and Revegetation of Coastal Wetlands. PhD thesis, Louisiana State University, Baton Rouge, LA.

Lin, Q., & Mendelssohn, I. A. (1996). A comparative investigation of the effects of south Louisiana crude oil on the vegetation of fresh, brackish and salt marshes. *Marine Pollution Bulletin*, 32(2), 202-209.

Lin, Q., & Mendelssohn, I. A. (2012). Impacts and recovery of the Deepwater Horizon oil spill on vegetation structure and function of coastal salt marshes in the northern Gulf of Mexico. *Environmental science & technology*, 46(7), 3737-3743.

McClenachan, G., Eugene Turner, R., & Tweel, A. W. (2013). Effects of oil on the rate and trajectory of Louisiana marsh shoreline erosion. *Environmental Research Letters*, 8(4), 044030.

Michel, E. R., & Kirchner, J. W. (2002). Effects of wet meadow riparian vegetation on streambank erosion. 2. Measurements of vegetated bank strength and consequences for failure mechanics. *Earth Surface Processes and Landforms*, 27(7), 687-697.

Michel, J., Owens, E. H., Zengel, S., Graham, A., Nixon, Z., Allard, T., et al. (2013). Extent and degree of shoreline oiling: Deepwater Horizon oil spill, Gulf of Mexico, USA. *PloS one*, *8*(6), e65087.

Nagler, P. L., Inoue, Y., Glenn, E. P., Russ, A. L., & Daughtry, C. S. T. (2003). Cellulose absorption index (CAI) to quantify mixed soil–plant litter scenes. *Remote Sensing of Environment*, 87, 310−325.

Niering W.A., Warren R.S., Weymouth C.G. (1977). Our dynamic tidal marshes: vegetation changes as revealed by peat analysis. *Connecticut Arboretum Bulletin*, 22:2–12.

Pennings S.C., Bertness M.D. (2001). Salt marsh communities. In: M.D. Bertness SDG, Hay ME, editors. Marine Community Ecology: Sinauer Associates.

Peterson, S. H., Roberts, D. A., Beland, M., Kokaly, R. F., & Ustin, S. L. (2015). Oil detection in the coastal marshes of Louisiana using MESMA applied to band subsets of AVIRIS data. *Remote Sensing of Environment*, 159, 222-231.

Pezeshki, S. R., Hester, M. W., Lin, Q., & Nyman, J. A. (2000). The effects of oil spill and clean-up on dominant US Gulf coast marsh macrophytes: a review. *Environmental pollution*, 108(2), 129-139.

Roberts, D. A., Gardner, M., Church, R., Ustin, S., Scheer, G., & Green, R. O. (1998). Mapping chaparral in the Santa Monica Mountains using multiple endmember spectral mixture models. *Remote Sensing of Environment*, 65(3), 267-279.

Serrano, L., Penuelas, J., & Ustin, S. L. (2002). Remote sensing of nitrogen and lignin in Mediterranean vegetation from AVIRIS data: Decomposing biochemical from structural signals. Remote Sensing of Environment, 81, 355−364.

Silliman, B. R., van de Koppel, J., McCoy, M. W., Diller, J., Kasozi, G. N., Earl, K., et al. (2012). Degradation and resilience in Louisiana salt marshes after the BP–Deepwater Horizon oil spill. *Proceedings of the National Academy of Sciences* , 109(28), 11234–11239.

Stedman, S. M., & Dahl, T. E. (2008). Status and trends of wetlands in the coastal watersheds of the eastern United States, 1998 to 2004. National Oceanic and Atmospheric Administration, National Marine Fisheries Service.

Turner R.E. (1976). Geographic variations in salt marsh macrophyte production: a review. *Contributions in Marine Science*, 20:47–68.

Ustin, S. L., & Gamon, J. A. (2010). Remote sensing of plant functional types. *New Phytologist*, 186(4), 795-816.

Ustin, S. L., Gitelson, A. A., Jacquemoud, S., Schaepman, M., Asner, G. P, Gamon, J. A., & Zarco-Tejada, P. J. (2009). Retrieval of foliar information about plant pigment systems from high resolution spectroscopy. *Remote Sensing of Environment*, 113, 67−77.

van de Koppel, J., van der Wal, D., Bakker, J. P., & Herman, P. M. (2005). Self-organization and vegetation collapse in salt marsh ecosystems. *The American Naturalist*, 165(1), E1-E12.

Webb, J.W. (1994) Effects of Oil on Saltmarshes. Symp. Proc. Gulf of Mexico and Caribbean Oil Spill in Coastal Ecosystems: Assessing Effects, Natural Recovery, and Progress in Remediation Research. US Department of the Interior, Minerals Management Service, OCS Study/MMS 95-0063, New Orleans, LA, pp. 55-61.

Zengel, S., Bernik, B. M., Rutherford, N., Nixon, Z., & Michel, J. (2015). Heavily oiled salt marsh following the Deepwater Horizon oil spill, ecological comparisons of shoreline cleanup treatments and recovery. *PloS one*, 10(7), e0132324.

Chapter 2: Mapping changing distributions of dominant species in oil-contaminated salt marshes of Louisiana using imaging spectroscopy

Abstract

The April 2010 Deepwater Horizon (DWH) oil spill was the largest coastal spill in U.S. history. Monitoring subsequent change in marsh plant community distributions is critical to assess ecosystem impacts and to establish future coastal management priorities. Strategically deployed airborne imaging spectrometers, like the Airborne Visible/Infrared Imaging Spectrometer (AVIRIS), offer the spectral and spatial resolution needed to differentiate plant species. However, obtaining satisfactory and consistent classification accuracies over time is a major challenge, particularly in dynamic intertidal landscapes.

Here, we develop and evaluate an image classification system for a time series of AVIRIS data for mapping dominant species in a heavily oiled salt marsh ecosystem. Using field-referenced image endmembers and canonical discriminant analysis (CDA), we classified 21 AVIRIS images acquired during the fall of 2010, 2011 and 2012. Classification results were evaluated using ground surveys that were conducted contemporaneously to AVIRIS collection dates. We analyzed changes in dominant species cover from 2010-2012 for oiled and non-oiled shorelines.

CDA discriminated dominant species with a high level of accuracy (overall accuracy = 82%, kappa = 0.78) and consistency over three imaging dates ($overall_{2010}$ = 82%, $overall_{2011}$ = 82%, $overall_{2012}$ = 88%). Marshes dominated by *Spartina alterniflora* were the most spatially abundant in shoreline zones (≤ 28m from shore) for all three dates (2010

=79%, 2011 = 61%, 2012 = 63%), followed by *Juncus roemerianus* (2010 = 11%, 2011 = 19%, 2012 = 17%) and *Distichlis spicata* (2010 = 4%, 2011 = 10%, 2012 = 7%).

Marshes that were heavily contaminated with oil exhibited variable responses from 2010-2012. Marsh vegetation classes converted to a subtidal, open water class along oiled and non-oiled shorelines that were similarly situated in the landscape. However, marsh loss along oil-contaminated shorelines doubled that of non-oiled shorelines. Only S*partina alterniflora* dominated marshes were extensively degraded, losing 15% (354,604 m^2) cover in oiled shoreline zones, suggesting that *Spartina alterniflora* marshes may be more vulnerable to shoreline erosion following hydrocarbon stress, due to their landscape position.

2.1. Introduction

Coastal wetlands of the Gulf of Mexico provide a wide range of vital ecosystem services, including storm surge protection, water quality enhancements, carbon sequestration, wildlife habitat, fisheries and recreational opportunities (Mitsch and Gosselink, 2000; Reddy and DeLaune, 2008). However, for nearly two centuries, the states around the northern Gulf of Mexico have experienced elevated rates of intertidal wetland loss (> 250 km^2yr^{-1}: Stedman and Dahl, 2008), due to a combination of natural disturbances (e.g. hurricanes, tropical storms), and anthropogenic activities (e.g. wetland drainage, canal dredging, river channelization and reduced sediment loads from the Mississippi River). Louisiana alone lost an estimated 4800 km^2 of intertidal wetland area from 1932-2010 ($\backsim$62 km^2yr^{-1}: Couvillion et al., 2011).

On April 20, 2010, an explosion occurred on the Deepwater Horizon (DWH) offshore drilling unit at the Macondo well about 64 km off the coast of Louisiana. An estimated

780,000 m^3 of crude oil was released into the Gulf before the well was successfully capped on July 15, 2010 (Lehr et al., 2010). Oil washed onto shorelines of several Gulf States, including approximately 796 km of Louisiana shoreline composed of intertidal marshes (Michel et al., 2013). Past incidences of oiling have shown that marsh recovery trajectories can vary greatly, from temporary reductions in stomatal conductance and photosynthetic rates (Pezeshki et al., 1993) to plant mortality, substrate destabilization and marsh shoreline erosion (Lin and Mendelssohn, 1996; Lin and Mendelssohn, 2012). The long-term effects of an oil spill of this magnitude on marsh ecosystems remain unknown due to variations in exposure properties (Alexander and Webb, 1985; Pezeshki et al., 2000), landscape characteristics, such as marsh surface elevation (Hester and Mendelssohn, 2000), distance to shoreline (Khanna et al. 2013) or exposure to wave action (Silliman et al., 2012) and plant community composition (Pezeshki and Delaune, 1993; Lin and Mendelssohn, 1996; Lin and Mendelssohn, 2012).

Studies conducted after the DWH spill suggest that oil coverage extended less than 15 m inland from the seaward edge of marshes (Silliman et al., 2012), reaching a maximum of 21 m (Kokaly et al., 2013), and vegetation stress was largely restricted to the zone extending 14 m from the shoreline (Khanna et al., 2013). Lin and Mendelssohn's (2012) findings indicate that impacts to salt marsh plant communities were variable depending upon oiling intensity, and suggested that the locations most impacted by oiling were dominated by *Spartina alterniflora* and *Juncus roemerianus.* However, the distribution of plant communities that were impacted, and the degree of community change have not been quantitatively determined.

Dominant species shape community structure and are a useful indicator of plant community condition (Frieswyk et al., 2007). More specifically, identifying dominant species and changes in spatial distribution can help explain long-term marsh ecosystem responses to oil (Lin and Mendelssohn, 1996; DeLaune et al., 2003). Most crude oils are nonionic, and associate more readily with organic particles (Pezeshki et al., 2000). Consequently, soil organic matter (SOM) in a marsh substrate impacts the persistence of oil residues, and SOM content in turn varies with plant species composition (Lin and Mendelssohn, 1996). In a comparative greenhouse study, Lin and Mendelssohn (1996) reported both higher SOM content and higher oil residual concentrations in plots dominated by *Spartina patens* than in plots dominated by *S. alterniflora*. Additionally, *S. alterniflora* has exhibited a greater recovery rate than other common dominant marsh species (e.g. *Distichlis spicata*, *S. patens* and *J. roemerianus*) in field experiments, indicating a higher tolerance threshold for oil contamination (Mendelssohn et al., 1990; Lin and Mendelssohn, 2012).

Accordingly, mapping community dominants and changes in distribution are valuable components of ecosystem assessments. Yet, quantitative assessments of plant community impacts are infeasible using field-based methods, due to the large size of the DWH oil-affected area. Remote sensing has become an attractive tool for evaluating responses of vegetation to disturbance and for "scaling up" *in situ* observations to landscape scales, due to the relatively high cost and time requirements of traditional field assessments and the inaccessibility of many areas. More recently, narrow-band, hyperspectral sensors, like the Airborne Visible / InfraredImaging Spectrometer (AVIRIS), have produced images with fine enough spectral resolution ($\backsim$10 nm) to discriminate ground constituents that were previously

indistinguishable with broadband sensors. As a result, increasingly sophisticated image classifiers, feature extraction and spectral unmixing algorithms have been developed to derive more detailed information from spectroscopic data, including pigment (Demmig-Adams and Adams, 1996; Gamon et al., 1997; Feret et al., 2008; Ustin et al., 2009), non-pigment (Ceccato et al., 2001; Asner et al., 2003; Serrano et al., 2002; Nagler et al., 2003; Kokaly et al., 2009) and biochemical constituents of vegetation (Asner, 1998).

Species-level classification, however, remains a substantial challenge due to the spectral similarity of many species, particularly those within the same functional type (Ustin and Gamon, 2010; Roth et al., 2015), and spatial, temporal and spectral variability of a single species (Somers et al., 2009; *see* Somers, et al., 2011, *for review of endmember variability*). Mapping coastal vegetation is further complicated by sharp environmental gradients, such as salinity and anaerobic stress, phenology, and the tidal regime, all of which enhance spectral variability over space and time (Schmidt and Skidmore, 2003; Adam et al., 2010).

Developing techniques that optimize the use of training data to minimize spectral variability within classes and reduce data dimensionality are active areas of remote sensing research as they may improve classification accuracies both spatially (Roth et al., 2015) and temporally (Peterson et al., 2015). A broad range of endmember optimization (Somers et al., 2011), dimension reduction (Dópido et al., 2012) and classification techniques (Lu and Weng, 2007) have been applied to hyperspectral images for vegetation mapping (Xie et al., 2008 *for review of vegetation mapping*), all of which have advantages and limitations that should be considered in relation to the analysis objectives, spatial and temporal factors, and landscape complexity (Lu and Weng, 2007). With high dimensional data, like AVIRIS, reducing the number of spectral bands used for classification is often necessary to retrieve

satisfactory results, due to the redundancy and collinearity of some bands (Hughes, 1968), particularly those close in spectral distance. Canonical discriminant analysis (CDA) with a linear discriminant allocation rule has performed well in addressing class discrimination problems (Palacios-Orueta, 1996; Guang and McLean, 2000; Pu and Liu, 2011; Alonzo et al., 2013; Roth et al., 2015). CDA is a combined dimension reduction and classification method that transforms high-dimensional datasets into discriminant functions that maximize the difference ratios between class means and standard deviations. Subsequently, CDA selects variables with significant discriminating power, discarding unexplained noise and redundancy (Fisher, 1936; Guang and McLean, 2000; Roth et al., 2015). As a result, CDA is well suited for distinguishing spectrally similar image constituents, such as perennial marsh grasses, because it removes spectral bands that are collinear (Plaza et al., 2009).

Field surveys have reported that Barataria Bay was among the most heavily impacted areas by oil following the DWH spill (Michel et al., 2013). Three recent studies have detected oil and mapped the extent of oil and persistence in Barataria Bay with greater detail using imaging spectroscopy (Khanna et al., 2013; Kokaly et al., 2013; Peterson et al., 2015). Kokaly et al. (2013) compared AVIRIS data with field-collected spectra of oiled marsh, focusing on the spectral absorption features related to the hydrocarbon (C-H) bond, to delineate the distribution of oiled marshes. Khanna et al. (2013) used a continuum removal technique centered on two oil absorption features to detect oil contamination on AVIRIS images. Peterson et al. (2015) used stable zone unmixing (SZU: Somers et al., 2010) and synthetic mixture analysis to determine which bands had discriminating power for oiled and non-oiled marshes. Nine bands (1-visible (685 nm), 4-short-wave infrared 1 (SWIR1, 1263, 1622, 1732, 1772 nm), and 4 SWIR2 (2038, 2208, 2238, 2277 nm)) effectively discriminated

oiled marsh from live and dead vegetation (Peterson et al., 2015). Here, we used the approach from Peterson et al. (2015) to identify oiled zones, and applied CDA to all bands to map dominant species. We evaluated the suitability of time series imaging spectroscopy for mapping dominant species and for assessments of plant community distribution change after the spill. The following questions provide a framework for examining the suitability of the approach:

1. How well can spectrally similar salt marsh species be discriminated using airborne imaging spectroscopy? Do the maps of dominant species correspond to expectations based on expert knowledge of regional species distributions?

2. Which plant communities, defined by dominant species, were most affected by oiling, and how did the spatial distribution of those communities change?

3. How did marsh area conversion to open water compare between oiled and non-oiled shoreline reaches and for different dominant species?

S. alterniflora and *J. roemerianus* were the primary dominants inhabiting oil-contaminated marshes of Barataria Bay (Lin and Mendelssohn, 2012; Kokaly et al., 2013). No study has quantitatively or spatially documented the cover of these species or of other less common salt marsh dominants (e.g. *Phragmites australis, D. spicata*, and *S. patens*) in the impacted area. Further, no studies have documented changes in the distribution of those dominants following the incident. Here, we devise an image classification scheme and examine the spatial distribution of salt marsh dominants on a landscape-scale, including *S. alterniflora, J. roemerianus, P. australis*, *D. spicata* and *S. patens* (Figure 2.1). Finally, we evaluate the dominant species cover change in oiled and in adjacent, non-oiled zones for potential oil-related impacts to marsh community distributions, including conversion of

marsh to open water.

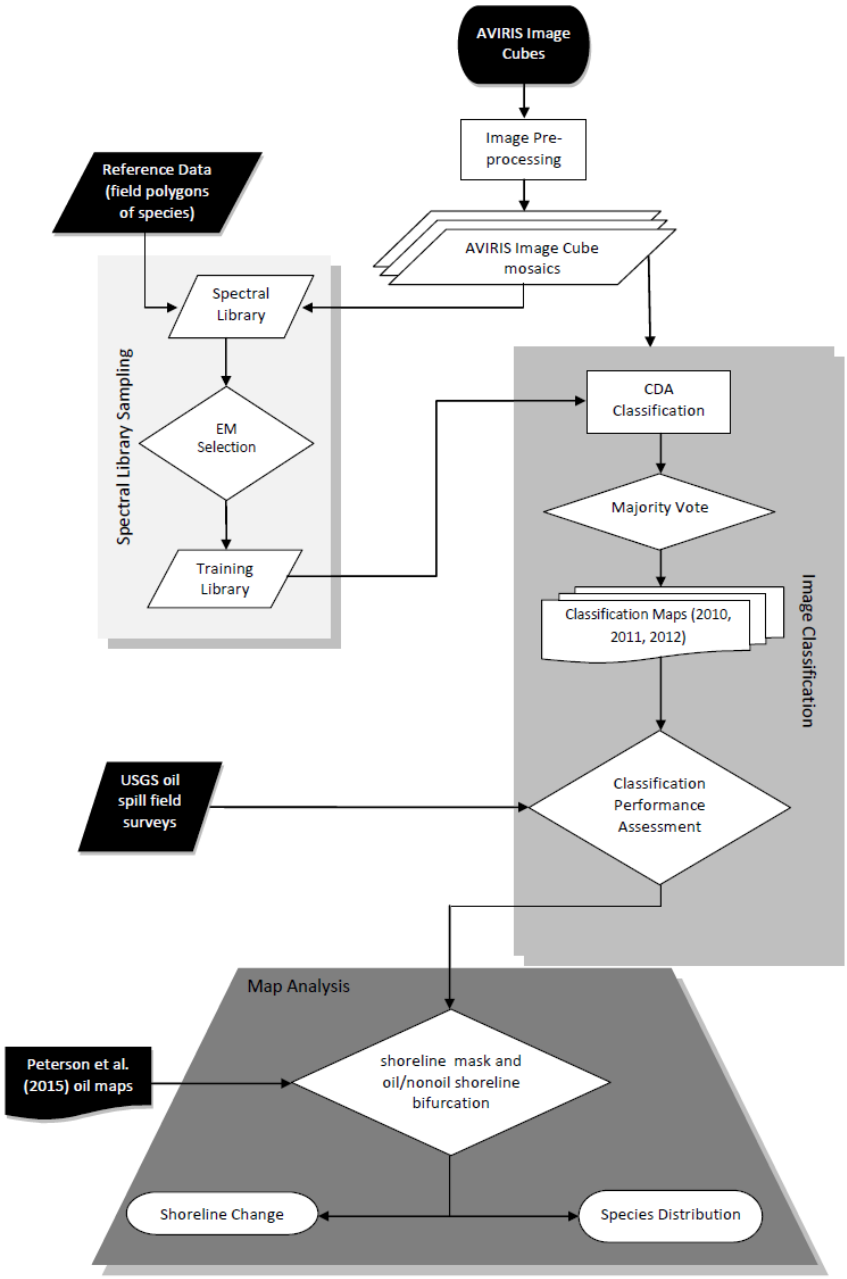

Figure 2.1: Work flow schematic illustrating the AVIRIS and reference datasets (black boxes) image processing, spectral sampling, classification and map analysis methodology.

2.2. Material and Methods

2.2.1 Study Area

Following the 2010 DWH spill, the most heavily oiled marsh shorelines were located in northern Barataria Bay, Louisiana (29.43°N, 89.88°W, approximately 60 km south of New Orleans) (Figure 2.2B). The marsh ecosystems of this study area, which cover approximately 197 km^2, are typical of coastal wetlands throughout the Mississippi Delta region and are strongly influenced by the subtropical climate as well as by oceanic and fluvial processes. Salt marshes of Barataria Bay are fractions of a meter from sea level and are being impacted greatly by sea level rise (Penland and Ramsey, 1990). The vegetation types commonly found in the northern portion of Barataria Bay are characterized by low species richness (Visser et al., 1998). The common dominant species were identified using the 2007 Louisiana coastwide vegetation survey (Visser et al., 1998; Sasser et al., 2008). A dataset of more than 8,000 records was queried to determine which dominant species were commonly observed at Braun-Blanquet cover-abundance category 6 levels (>75%: *see* Moore and Chapman, 1986 *for cover-scale*). Five species met the criteria of dominant species in Barataria Bay, including *D. spicata, J. roemerianus, P. australis, S. alterniflora* and *S. patens*, of which four are grasses (*D. spicata*, *S. alterniflora*, *P. australis* and *S. patens*), and one is a grass-like rush (*J. roemerianus*).

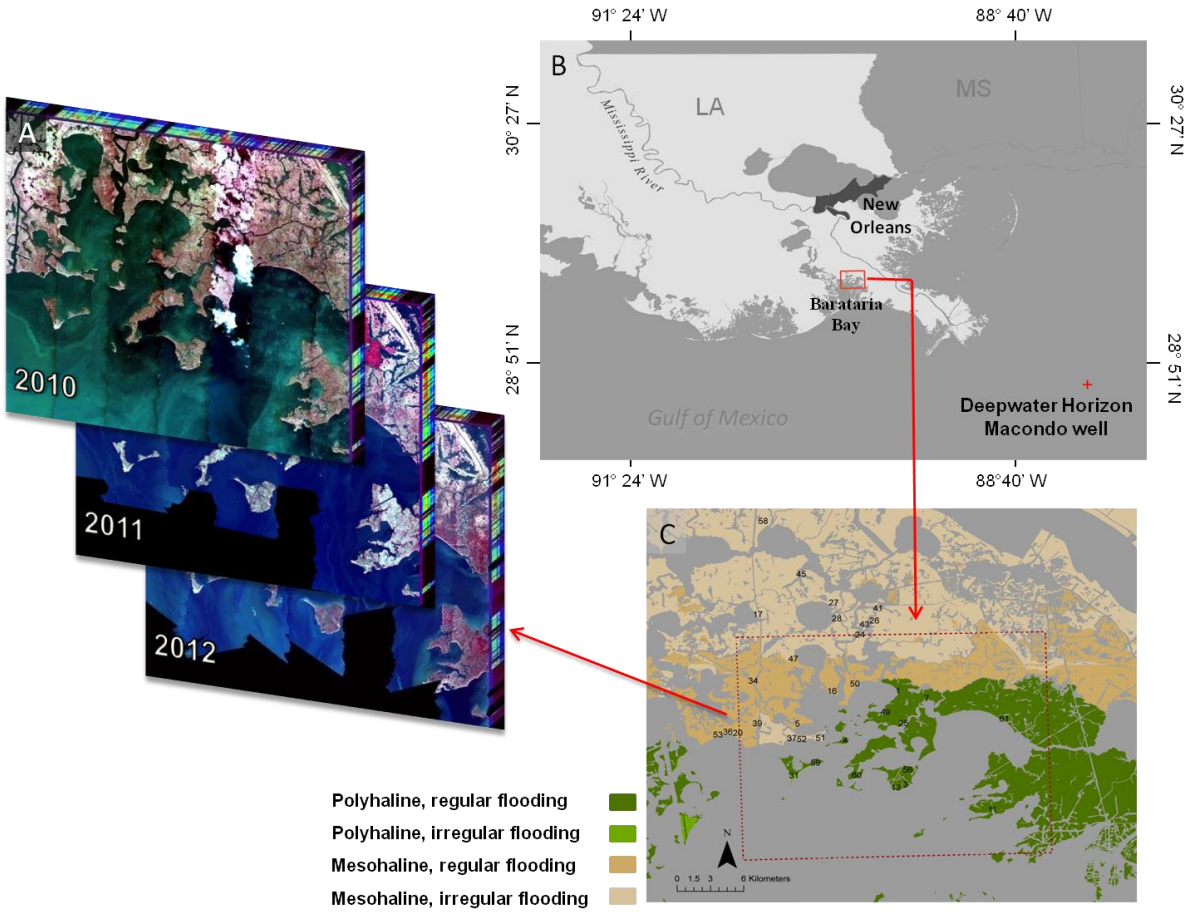

Figure 2.2: Maps show the A) three AVIRIS image mosaicks used for classification, B) location of study area (red box) and Deepwater Horizon well (red cross) in Louisiana, and C) field collection sites (n = 59) for reference polygons in Barataria Bay. The spatial distribution of salinity and flooding conditions is based on U.S. Fish and Wildlife Service's National Wetlands Inventory maps.

Polyhaline marsh zones (salinity 8-29 ppt) of Barataria Bay are dominated by *S. alterniflora* and *J. roemerianus* with *J. roemerianus* more frequently dominant in the mesohaline zones (salinity 4-18 ppt: Chabreck, 1972; Visser et al., 1998). Additionally, *P. australis* is commonly present in patches as a dominant in mesohaline zones. Commonly intermixed with these dominants are the subdominants, *D. spicata*, *S. patens*, *Schoenoplectus americanus* and *Schoenoplectus robustus*. *D. spicata* and *S. patens* are found as dominants in mesohaline zones, and *D. spicata* is commonly present in polyhaline, irregularly flooded

zones as a dominant, and particularly in locations where a disturbance has recently occurred (Chabreck, 1972; Visser et al., 1998).

All five species differ in the timing of peak productivity and in the volume of dead biomass buildup, which impacts their spectral profile, or reflectance. The two extreme species, in terms of fluctuations in biomass and seasonality, are *S. alterniflora* and *S. patens*. *S. alterniflora* has the most seasonal fluctuations of biomass, and consistently exhibits peak biomass in September, while *S. patens* grows throughout the year and the biomass shows little, if any, seasonal pattern (Kirby and Gosselink, 1976; Morris and Haskin, 1990; Pezeshki and DeLaune, 1991).

2.2.2 Image Acquisition and Preprocessing

In an effort to investigate the large-scale impacts and monitor the long-term recovery of coastal ecosystems following the DWH oil spill, the National Aeronautics and Space Administration (NASA) deployed the ER-2 and Twin Otter International aircrafts equipped with AVIRIS to collect spectrometer data of the post-spill environment. AVIRIS is a whiskbroom scanner that measures upwelling radiance between 365 and 2495 nm at 10 nm intervals (total of 224 bands) (Green et al., 1998), and produces 700 - 800 ortho-corrected pixels for 224 detectors on each scan. Here, the AVIRIS data used for analysis and mapping were collected for ecosystem impact assessments while deployed on the Twin Otter in October, 2010, 2011 and 2012 and had a native resolution of 3.3-3.5m (http://aviris.jpl.nasa.gov/) (Figure 2.2A). The images were acquired with full navigation and georectification information.

The AVIRIS radiometric calibration took place at the Jet Propulsion Laboratory (JPL). Following image acquisition, atmospheric calibration and reflectance retrieval was

performed in two steps using ACORN 6 (ImSpec LLC, Seattle). ACORN 6 performs forward inversion that fits modeled radiance against measured radiance to retrieve surface reflectance based on geographic, temporal and atmospheric parameters. In this study, water vapor was fit using the 940 nm water vapor band. After initial reflectance retrieval, a ground target was used to remove high-frequency noise in retrieved reflectance (Clark et al., 2002).

Georectification was completed in two steps, starting with a geocorrection procedure using JPL's georeferencing information derived from inertial navigation data and GPS in a geographic lookup table (Boardman, 1999). Further georeferencing was done using Aerometric Inc. (http://gis.aerometric.net/dirlists.htm) aerial photos ($0.30m^2$) as base maps that were resampled by pixel aggregation to 3.5 m to more closely match the resolution of the first AVIRIS datasets. Registration error of less than one pixel (RMSE < 1.0) was achieved for all images.

Environmental conditions are confounding factors in multitemporal analysis of vegetation cover, and therefore, studies commonly seek to acquire data under similar illumination, hydrologic and phenological conditions (Rogan et al., 2002). AVIRIS collection is generally restricted to within two hours of solar noon, due to the increased atmospheric scattering (atmospheric noise) that occurs early and later in the daytime hours. Atmospheric conditions were favorable (i.e. low humidity and cloud-free) on all three dates. A gap in coverage exists for the October 4, 2010 data. We attempted to fill this gap with a dataset from an earlier date (September 24, 2010), but poor atmospheric conditions made calibration unsatisfactory. Therefore, we excluded this area from the analysis for all three dates.

The AVIRIS collection dates had a maximum separation of 16 days on the Julian calendar (Julian dates 277, 288, 293). However, the precipitation patterns preceding the October collection dates varied appreciably from year-to-year, likely causing variable phenological conditions (Figure 2.3C). As a result, spectral signatures also varied for some species (Figure 2.3A & B). The 2010 water year (October 2009-September 2010) was the wettest and vegetation was generally greener on 2010 imagery. Precipitation in both 2011 and 2012 was below average in relation to the 44-year climate record (Galliano, LA), which may have contributed to the differences in spectra (Figure 2.3B & C). For instance, all species but *J. roemerianus* showed increased reflectance in the red region and red-edge shifts in the later October dates, which implies a shift from green to yellow and brown vegetation caused by the onset of natural senescence (Figure 2.3B).

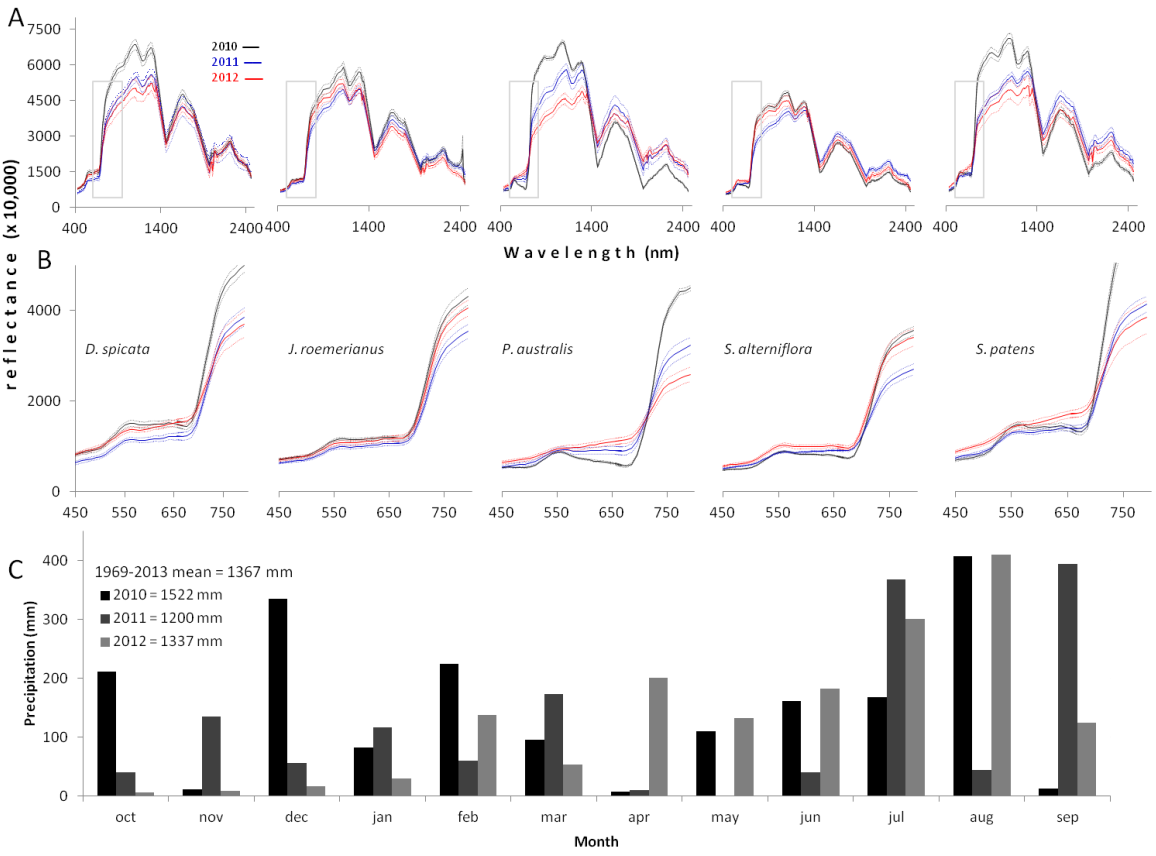

Figure 2.3: Shows the full spectrum (A) and subset (B) mean reflectance curves (solid line) with 95% confidence intervals (dashed lines) of dominant species training data and monthly precipitation (C) for each water year leading up to the AVIRIS collection dates.

Tidal conditions at the time of AVIRIS data acquisition are important because varying water levels can affect image registration (i.e. shorelines differ on multitemporal datasets) and classification results (Jensen et al., 1993, Allen et al., 2012). AVIRIS data capture in northern Barataria Bay occurred between 16:39 and 19:27 UTC on October 4, 2010. Tide levels over that timeframe ranged from 0.246 to 0.138 m above mean lower low water height (MLLW: NOAA Station ID 8761724, Grand Isle, LA). On October 15, 2011, data capture occurred from 16:22 to 18:04 PM UTC with tides ranging from 0.026 to 0.036 m above MLLW. On October 19, 2012, data capture occurred from 15:48 to 17:11 PM UTC

with tides ranging from 0.097 to 0.034 m above MLLW. The AVIRIS collection time on the two later acquisition dates (October 15, 2011 and October 19, 2012) were during lower tides, and therefore any decreases in land cover on those dates would not be due to higher water levels. Water levels were highest on the first image date, so the use of that image as the base layer for identification of increased open water would result in conservative estimates of the area experiencing conversion to open water.

2.2.3 Data Collection, Spectral Library Development & Endmember Selection

Classification accuracies are highly dependent upon: a) how representative the collected reference spectra are of the classes of interest (Foody et al., 1995; Chen and Stow, 2002), and b) whether the spectral separability among classes is greater than the variability within a class (Somers et al., 2011). Spectra used for classification can be collected from measurements of reflectance taken from the field, lab or imagery. Here, we used image-derived spectra because image pixels can more effectively capture the broad range in live (green) and senesced vegetation composition as well as the background components (i.e. water or soil) found in scenes (Figure 2.4). Selecting pixels that cover a single class is difficult, due to the composite nature of surface materials, resulting in problems with class separability (Somers et al., 2009). We used field-referenced polygons of relatively pure stands to minimize class intermixing that may result in classification error.

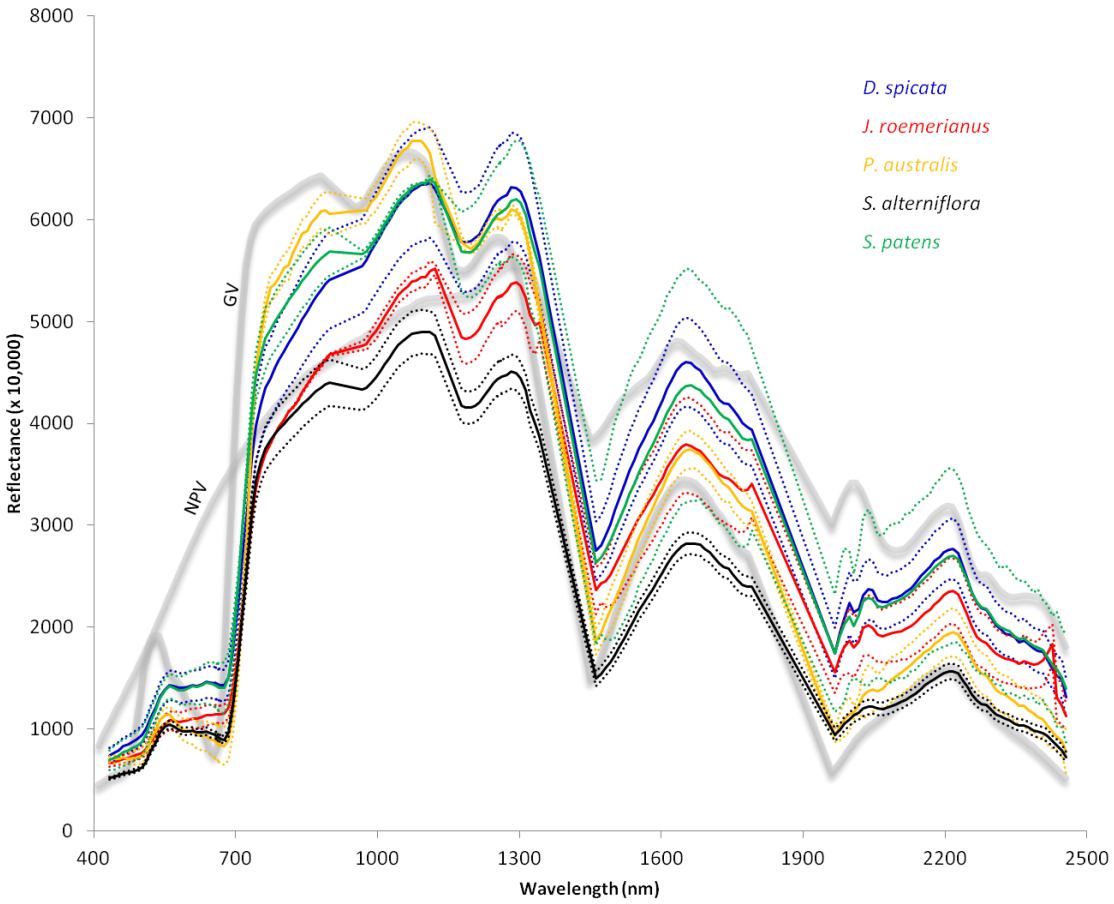

Figure 2.4: Mean spectral reflectance profiles and 95% confidence intervals for the five dominant species (*Distichlis spicata*, *Juncus roemerianus*, *Phragmites australis*, *Spartina alterniflora*, *Spartina patens*), and examples of "pure" green vegetation (GV: *S. alterniflora*) and non-photosynthetic vegetation (NPV: *S. alterniflora*). Training data (image spectra) of dominant species are composites of mostly live vegetation, but also include dead vegetation, water and soil. Image spectra of dominants differ from "pure" GV and NPV endmembers (gray), and illustrates where spectral confusion among species classes is likely occur.

Class training spectra (herein referred to as endmembers) were collected from spatially referenced dominant species polygons overlaid onto AVIRIS image mosaics for each date. To minimize spectral mixing of dominants and subdominants or understory species, selected training data were limited to dense monotypic stands by using only the Braun-Blanquet cover-abundance category 6 range (75-100% cover). Image-derived

endmembers were collected from reference polygons of dominant species stands delineated during field visits in October 2012 and May and October of 2013. Field polygons (n = 95) of variable size were delineated using a global positioning system (GPS) and species percent cover estimates were recorded (Figure 2.2C). Due to a lack of large stands observed during field visits, supplemental polygons were established for *P. australis* using the 2007 CRMS coast-wide vegetation survey (Sasser et al., 2008; *see* Visser et al., 1998 *for details in regards to Louisiana coast-wide vegetation survey methods*). Endmembers for water and soil classes were collected using visual spectra interpretation, and oil endmembers were selected using a hydrocarbon absorption index to detect oil on marsh surfaces (Kühn et al. 2004). In total, 9639 image spectra from 281 field-delineated polygons were used for training and validation of dominant species and non-vegetated surfaces, including wet and dry soil, water/glint and oiled-marsh.

The full spectral library of classes was separated into training and validation datasets. Polygons from each image date, comprising at least two-thirds of the spectra for a given class, were reserved for validation of classification results. Next, image spectra were selected from training and validation polygons, until one of two predefined thresholds was met to ensure that both small and large polygons were well-represented in the training and classification testing process, either an absolute sampling limit of 50% of the spectra from a polygon, or a limit of 10 spectra (Roth et al., 2012). The percentages of image spectra used in classification training for all classes ranged 4-15%, and for validation ranged 15-27%. The percentages were determined by the number of polygons, number of image spectra per polygon and the aforementioned thresholds for partitioning. A total of 547 image endmembers were used for classification training. A summary of the reference polygons,

total image spectra and endmembers (i.e. training pixels) for each class is shown in Table 2.1. Twenty random training and validation libraries were generated and tested for CDA classification. Generating the relatively large number of paired training and validation libraries was considered an important step, due to the potential intrinsic variability of the image spectra.

Table 2.1: Summary table of Dominant Species dataset, including reference polygons, total reference spectra (pixels), training and test samples.

Class Name	polygons	total pixels	training	validation
Distichlis spicata	19	597	41	87
Juncus roemerianus	29	742	41	144
Phragmites australis	51	1898	91	228
Spartina alterniflora	78	3127	135	346
Spartina patens	21	570	38	97
soil	3	100	15	24
water	72	2362	185	290
oiled marsh	2	7	1	2

2.2.4 CDA classification

CDA was applied to the training data to maximize the between-class variance by selecting bands with significant discriminating power, and discarding unexplained noise and redundancy (Pu and Gong, 2011; Alonzo et al., 2013). A set of standardized coefficients were multiplied through the original spectra in MATLAB (The Mathworks, Inc., 2012) to derive canonical weighted functions (one per band), and determine the bands which are significant contributors to class discrimination (Roth et al., 2015). Following CDA dimension reduction, a linear discriminant classifier was used in ENVI/IDL (www.exelisvis.com)to assign image spectra to the class that produces the highest discriminant function score. AVIRIS image mosaics were classified (October 2010, 2011 & 2012), and a post-classification majority vote of the 20 different maps generated by the random training pulls was used to eliminate noise in areas of higher classification inconsistency, and improve overall map outputs.

2.2.5 Map Validation

Two data sets were used to validate the dominant species classification maps. The first assessment was done using spectra in the validation dataset that were excluded from the random sampling process. A total of 7043 pixels were used as validation spectra for each of the 20 random pairs of training and validation libraries, and confusion matrices were assessed for errors of omission (producer error) and commission (user error) among classes (species).

A classification performance assessment was conducted using USGS post-oil spill vegetation surveys (USGS unpublished data). Researchers from the USGS revisited six sites (three oiled and three non-oiled) contemporaneously with AVIRIS collection in October, 2010, 2011 and 2012 (Figure 2.5A & B). The surveys consisted of four 4 m^2 plots along 50 m transects that were spaced 30 m apart for a total of 72 plots. The 12 plots from site 5 were

excluded from the classification assessment because it was located in the data gap in the October, 2010 image. Transects A, B and C were positioned from west to east at each site, and plots were randomly spaced along each 50 m transect with plot 1 being the closest and plot 4 being the farthest from the shoreline. This dataset provided field observations of species composition that corresponded with AVIRIS collection dates. Observations included species identification and richness, cover fractions and abundance estimates of live, green (GV) and senesced, non-photosynthetic (NPV) vegetation. Using this dataset for classification validation introduces several challenges and limitations. For instance, the reliability of classification evaluation is potentially diminished, due to georectification error of up to one pixel (12.25 m^2) and the uncertainty of the GPS accuracy for the plot locations ($\backsim$ 5m). Because of differences in plot and pixel size, and positional uncertainty, we created 2 m buffers around the USGS plots. We evaluated the classification performance based on one or more pixels within the 4 m^2 buffer area being classified as the targeted species.

Some of the dominant species are not represented well by the reference dataset, as 95% of the observations were either *S. alterniflora* or *J. roemerianus*. Therefore, the validation library (first approach) is the more comprehensive method, but the USGS plots provide an assessment of each individual map in the time series, and validation by shoreline zone. We defined the dominant species as the one with the highest cover fraction per plot, because some plots lacked a dominant with GV cover >50%.

2.2.6 Oiled and non-oiled shoreline identification

Marsh oiling was concentrated in the first 15 m of the shoreline with a maximum distance of 21 m (Silliman et al., 2012; Khanna et al., 2013; Kokaly et al., 2013; Peterson et al., 2015). Therefore, the focus of our analysis of dominant species distributions was on the shoreline zones. To establish a shoreline vector, we masked all pixels that were modeled as GV, NPV, oiled vegetation or soil that summed to ≥5%. We used 5% to match minimum fraction criteria used in model selection by Multiple Endmember Spectral Mixture Analysis (MESMA: Roberts et al., 1998; Halligan, 2002; Dennison and Roberts, 2003). Next, we removed mudflats and lakes located within the marsh interior that had no connectivity with large channels and bays by converting the raster of water pixels into a polygon. We separated the multi-part polygons into individual features, and deleted the features that were disconnected from the Barataria Bay polygon. This procedure removed shorelines that we assumed would not have been exposed to oil following the DWH spill (Khanna et al., 2013). An 8 pixel (28 m) buffer from the edge pixels was used to create shoreline zones.

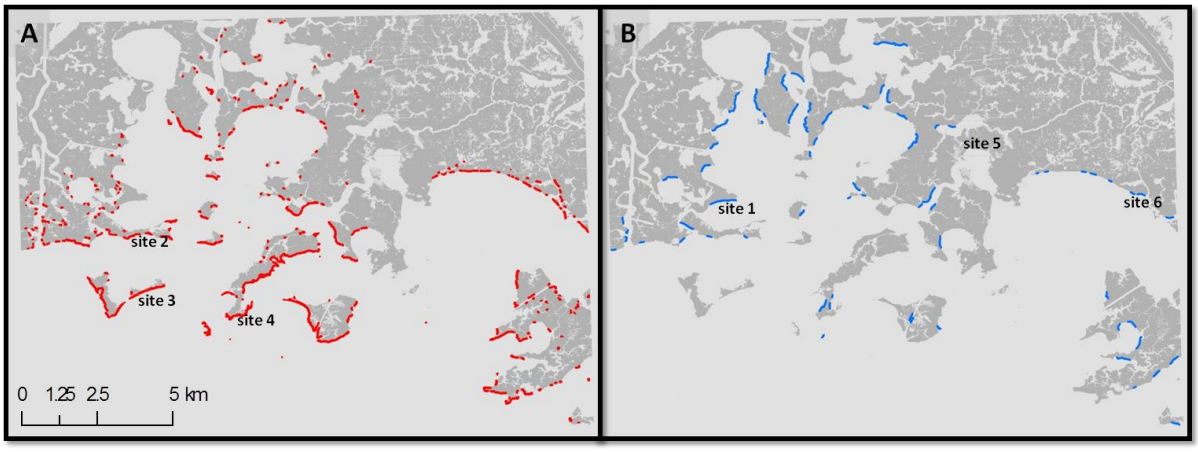

Figure 2.5: USGS site locations are shown on study area maps of A) oiled (red), B) and non-oiled shoreline zones (blue) in similar landscape positions.

Oiled marsh cover was determined using MESMA (Roberts et al., 1998; Peterson et al., 2015), because oil fractions (per pixel) generated with MESMA provide a more comprehensive spatial coverage of oil than produced by discrete CDA classification. For a detailed description of the method used to generate oil fractional cover, refer to Peterson et al. (2015). In summary, iterative endmember selection (IES: Roth et al., 2012) was used to produce a spectral library of GV, NPV, soil and oiled marsh endmembers. Stable Zone Unmixing (SZU: Somers et al., 2010), InStability Index (ISI: Somers et al., 2009) and synthetic mixture modeling were used to identify an optimal subset of bands for discriminating endmembers. Finally, two, three and four endmember models were run on each image, followed by an automated extraction process in which endmember combinations with the lowest RMSE and least complexity (fewest endmembers) were selected for each pixel and merged into a multiple endmember fractional cover dataset.

We created a mask of pixels that were oiled (≥5% oil fraction) using AVIRIS images (same spatial resolution) from September 14, October 4, 2010 and May 4, 2011 to capture maximum oil coverage, and applied it to the mask of the shoreline zone maps (Figure 2.5A). The mask was used to examine the changes in marsh vegetation cover at oiled locations and to compare change in oiled marshes to changes in marshes that were not affected directly by oil, but were in a similar landscape position (elevation and distance from shoreline). Furthermore, we refined the non-oiled zone filter to only include shorelines that were oriented towards the south (90° to 270°) as these were the locations most heavily contaminated by oil (Khanna et al., 2013; Kokaly et al., 2013; Peterson et al., 2015) (Figure 2.5B).

2.3. Results

2.3.1 Spectral Library (Endmember) and Classification Validation

Twenty randomly sampled (paired) training and validation libraries were spectrally transformed into CDA functions and assessed for classification performance using a linear classifier in MATLAB 7.9. Twenty paired libraries had an average overall accuracy of 82% and kappa of 0.78 (Table 2.2). Little variability was found among classification accuracies for all training libraries, so we opted to use all libraries for CDA classification and a majority rule classifier to aggregate the final results. Average producer's and user accuracies for the species classes was 72% (Table 2.2). The highest accuracies (producer) were for *S. alterniflora* and *J. roemerianus*, and *P. australis* and *S. alterniflora* reported the highest classification reliability (user) (Table 2.2). As expected, accuracies were higher for non-vegetated classes with the exception of oiled marsh, which had a small sample size (Table 2.2). We anticipated *D. spicata* and *S. patens* would be difficult to distinguish, due to their similar morphology and spatial association. *S. patens* reported the lowest combined accuracy and reliability, while *D. spicata* reported the lowest reliability overall. Yet, *D. spicata* endmembers were more likely to be confused with *J. roemerianus* and *S. alterniflora* (Table 2.2). Confusion occurred among the *Spartina* species (*S. patens* misclassified 30% of training samples as *S. alterniflora*). However, as expected, *S. patens* is more dominant in the northern portion of the study area where the marshes transition from polyhaline (indicator species *S. alterniflora*) to mesohaline (indicator species *S. patens*) (Figure 2.6: Visser et al., 1998).

Table 2.2: Matrix of training endmember allocations, producer and user accuracies and averaged kappa and overall accuracies for the 20 sample libraries.

	D. spicata	J. roemerianus	P. australis	S. alterniflora	S. patens	soil	oiled marsh	water	unclassified
D. spicata	**61**	17	14	14	6	0	0	0	0
J. roemerianus	17	**108**	7	22	4	0	0	0	0
P. australis	2	0	**157**	6	0	0	0	0	0
S. alterniflora	5	16	23	**300**	29	0	0	0	0
S. patens	1	3	27	3	**58**	0	0	0	0
soil	0	0	0	0	0	**24**	0	0	0
oiled marsh	1	0	0	0	0	0	**2**	0	0
water	0	0	0	1	0	0	0	**290**	0
unclassified	0	0	0	0	0	0	0	0	0
producer (%)	70	75	69	87	60	100	100	100	
user (%)	54	68	95	80	63	100	67	100	
overall accuracy (%)	**82.10**								
kappa	**0.78**								

Figure 2.6: Highlighted marsh dominants (red) for 2010 (top), 2011 (middle) & 2012 (bottom). *Spartina alterniflora* covered 70% of the marsh area, followed by *Juncus roemerianus* with 14% and *Spartina patens* with 10%.

2.3.2 Dominant Species Distribution

A total of 41,248,359 m^2 were classified as one of the five dominant species, soil, water (shallow water, deep water and glint), or oiled marsh (Figure 2.6; Table 2.3A). *S. alterniflora* was the most widespread over all three years, averaging 76% cover, followed by *J. roemerianus* (9%), *S. patens* (9%), *D. spicata* (3%) and *P. australis* (1%) (Figures 2.6; Table 2.3A). The percent cover was relatively stable between years for the less common dominants, however, *S. alterniflora* and *J. roemerianus* exhibited considerable change (Table

2.3A). There was an overall loss of 7% (2,909,585m^2) of the marsh area to open water from 2010-2012, with a greater loss occurring from 2011-2012 (1,807,285m^2) (Table 2.3A).

Table 2.3: Coverage area and percent cover per dominant species and non-vegetation classes for 2010, 2011 & 2012 in full study area (A), oiled shoreline zones (B) and non-oiled (C) shoreline zones. DISP = *Distichlis spicata*; JURO = *Juncus roemerianus*; PHAU = *Phragmites australis*; SPAL = *Spartina alterniflora*; and SPPA = *Spartina patens*

A

Species	2010 (m^2)	% Cover	2011 (m^2)	% Cover	2012 (m^2)	% Cover
DISP:	554,082	1	2,126,780	5	957,628	2
JURO:	1,496,604	4	5,530,035	14	3,861,497	9
PHAU:	95,093	0	53,863	0	766,352	2
SPAL:	35,514,804	87	27,721,139	68	29,491,320	72
SPPA:	3,236,254	8	4,421,259	11	2,966,840	7
drysoil:	1,934	0	539	0	2,338	0
oiled:	59,470	0	2,326	0	2,681	0
water:	0	0	1,102,300	3	2,909,585	7
total:	40,958,241		40,958,241		40,958,241	

B

Species	2010 (m^2)	% Cover	2011 (m^2)	% Cover	2012 (m^2)	% Cover
DISP:	76,498	3	216,922	10	146,031	7
JURO:	228,944	10	333,316	15	261,066	12
PHAU:	25,242	1	7,798	0	63,314	3
SPAL:	1,801,580	80	1,444,124	64	1,446,976	65
SPPA:	51,562	2	130,900	6	47,779	2
drysoil:	575	0	135	0	539	0
oiled:	57,058	3	220	0	453	0
water:	0	0	108,045	5	275,303	12
total:	2,241,460		2,241,460		2,241,460	

Table 2.3 continued

C

Species	2010 (m^2)	% Cover	2011 (m^2)	% Cover	2012 (m^2)	% Cover
DISP:	27,336	4	64,746	10	42,417	6
JURO:	83,953	12	157,709	23	143,827	21
PHAU:	6,757	1	1,126	0	25,426	4
SPAL:	521,788	77	392,541	58	403,118	60
SPPA:	33,505	5	27,213	4	15,461	2
drysoil:	0	0	0	0	0	0
oiled:	49	0	0	0	12	0
water:	0	0	30,053	4	43,127	6
total:	673,389		673,389		673,389	

S. alterniflora and *J. roemerianus* covered greater than 80% of the marsh area in the oiled and non-oiled shoreline zones (Figure 2.5; Table 2.3B & C). Distributions of species in oiled and non-oiled shoreline zones changed substantially during the two periods, however, the distribution patterns were similar for both zones. *S. alterniflora* decreased markedly from 2010-2011 and remained relatively stable from 2011-2012 in both oiled and non-oiled shoreline zones (Table 2.3B & C). *J. roemerianus* increased substantially from 2010-2011 and decreased slightly from 2011-2012 in both oiled and non-oiled shoreline zones (3B & C). *D. spicata* exhibited similar increases from 2010-2011 and decreases in 2011-2012 in oiled and non-oiled shoreline zones (Table 2.3B & C). *S. patens* increased in oil zones and decreased in non-oiled shoreline zones from 2010-2011, and decreased in both oiled and non-oiled zones from 2011-2012. *P. australis* cover was negligible in 2010 and 2011, but increased considerably from 2011-2012 in both oiled and non-oiled shoreline zones (Table 2.3B &C).

Cover change detection from 2010-2012, in areas initially dominated by *S. alterniflora* and *J. roemerianus*, indicate that marsh area loss was proportionately similar for both species in oiled shoreline zones. Marsh loss to open water for both species was higher along oiled shorelines (12% and 10%, respectively) than non-oiled shorelines (7% and 4%, respectively). *S. alterniflora* retained a comparable proportion of its initial cover distribution in oiled (72%) and non-oiled (69%) shoreline zones, however, *J. roemerianus* retained 20% less of its initial cover distribution along oiled shorelines (37% and 57%, respectively). *J. roemerianus* was largely converted to *S. alterniflora* (34%) along oiled shorelines, while only 8% of *S. alterniflora* converted to *J. roemerianus*. A relatively small percentage changed to any of the three other classified dominants (<5% for *D. spicata*, *P. australis*, *S. patens*) in oiled and non-oiled zones.

The overall loss of vegetated marsh in the oiled zone was 12% compared to 6% in the non-oiled zone, as indicated by the increases in water classes found in oiled (0% to 5% to 12%) and non-oiled (0% to 4% to 6%) zones (Table 2.3B & C). The loss of *S. alterniflora* from 2011-2012 is not replaced by the other marsh dominants. Rather, it largely transitions to the water class indicating a net loss of marsh area.

2.3.3 Site-Specific Assessments of Dominant Species Maps

The data used for map validation (USGS) were not collected for the purposes of assessing discrete classification performance. Rather, the surveys were conducted to evaluate plot-scale changes in community composition, and to measure belowground and aboveground biomass. Consequently, the quantity (i.e. 60 plots) and spatial distribution of sites is limited, in part due to the time-consuming nature of the data being collected. The USGS sites were the only data available that could be used to evaluate multitemporal

classification performance, and to document the change in cover at both oiled and non-oiled shoreline locations. USGS data were used to examine species composition and plot-specific cover attributes in comparison with classification maps to assess the performance of the classifier on a per-pixel basis.

Overall, CDA classifications were consistent with field observations across sites with 84% agreement between USGS plots and CDA classified maps, and the lowest accuracy reported for site 1 (75%) and the highest accuracy for sites 2 & 3 (94%). The dominant species were mapped accurately for 82% of the USGS plots in 2010, 82% in 2011 and 88% in 2012. The overall accuracy based on the USGS field observations (84%) was comparable to the spectral library validation accuracy (82%). When the USGS observations were separated into Braun-Blanquet cover-abundance category 6 (>75%) levels and below, the classifier was 88% accurate for ≥75% single dominant cover and 82% accurate for <75% cover of a single dominant, indicating spectral mixing of dominants is accountable for some class confusion. In general, CDA-classifications were more accurate for plots greater than 25 m from both oiled and non-oiled shorelines. For plots farther than 25 m from the shoreline, the classified maps were in 89% agreement with field observations, while plots within 25 m of the shoreline were 80% accurate.

From 2010 to 2012, all plots at non-oiled sites (sites 1 & 6) had greater than 80% vegetation cover and an overall decrease in cover of 4% and 7% (Figure 2.7). Of the plots closest to the shoreline, only C1 exhibited a decrease in vegetation cover of greater than 10% (95% to 80%), suggesting that shoreline erosion did not occur or was minimal at these non-oiled sites (Figure 2.7; Table 2.4).

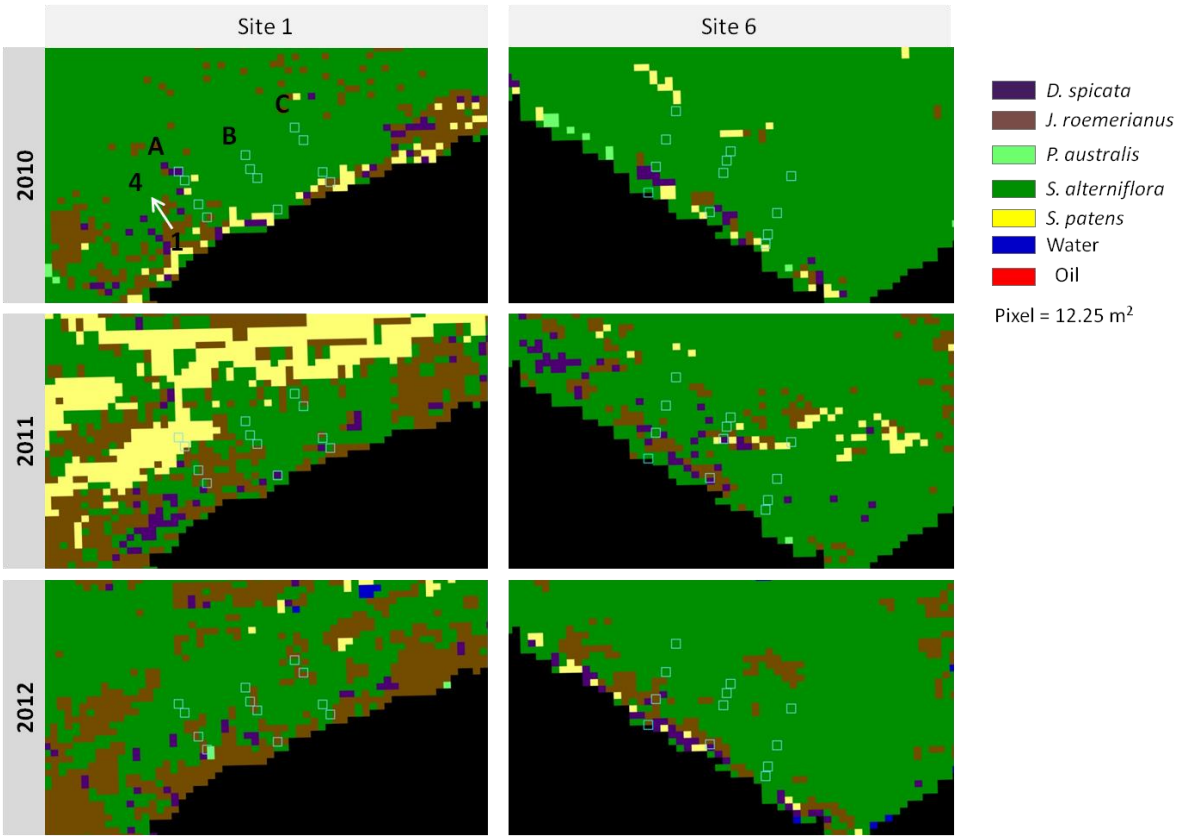

Figure 2.7: Location of plots (light blue square, N = 24) used for 2010, 2011 & 2012 classification and survey comparisons of USGS *non-oiled sites* 1 & 6. Four randomly positioned plots (1 closest and 4 farthest from shoreline) were located along transects A(west), B(middle) and C(east). Black pixels represent initial (2010) open water.

Table 2.4: Prevalent species and cover-abundance (%) at non-oiled site 1 (left) and site 6 (right) in 2010, 2011 and 2012 from USGS plots (1-4).

Site 1

2010

Plot	transect A	transect B	transect C
1			JURO(40)
	JURO(98)	JURO(69)	SPAL(45)
2		SPAL(15)	
	JURO(95)	JURO(45)	SPAL(80)
3	SPAL(10)	SPAL(30)	SPAL(40)
	JURO(85)	JURO(60)	JURO(50)
4	SPAL(10)	JURO(30)	SPAL(25)
	JURO(88)	SPAL(50)	JURO(70)

2011

1	JURO(45)	JURO(20)	JURO(40)
	SPAL(54)	SPAL(80)	SPAL(60)
2	JURO(45)	SPAL(15)	
	SPAL(54)	JURO(80)	SPAL(95)
3	SPAL(49)	SPAL(35)	
	JURO(60)	JURO(45)	JURO(80)
4	JURO(6)	JURO(15)	JURO(<5)
	SPAL(<5)	SPAL(80)	SPAL(<5)

2012

1	SPAL(40)	JURO(10)	JURO(15)
	JURO(45)	SPAL(85)	SPAL(75)
2	JURO(40)	SPAL(10)	JURO(10)
	SPAL(50)	JURO(75)	SPAL(80)
3		SPAL(10)	SPAL(15)
	SPAL(50)	JURO(35)	JURO(55)
4		SPAL(25)	JURO(20)
	SPAL(70)	JURO(50)	SPAL(35)

Site 6

2010

Plot	transect A	transect B	transect C
1	SPAL(10)	DISP(10)	SPPA(15)
	DISP(30)	SPAL(30)	DISP(40)
	SPPA(45)	JURO(75)	SPAL(85)
2	SPAL(10)	SPAL(30)	
	JURO(60)	JURO(65)	SPAL(98)
3	SPAL(85)	SPAL(85)	SPAL(98)
4	SPAL(75)	SPAL(90)	SPAL(90)

2011

1	DISP(13)	JURO(15)	SPPA(20)
	SPPA(80)	SPAL(15)	SPAL(70)
		SPPA(40)	
2	SPAL(10)		
	JURO(85)	JURO(15)	SPAL(90)
3	SPAL(70)	SPAL(40)	SPAL(70)
4	SPAL(50)	SPAL(60)	SPAL(30)

2012

1	DISP(10)	SPPA(10)	SPPA(10)
	SPAL(10)	SPAL(15)	SPAL(50)
	SPPA(40)	JURO(65)	
2	JURO(50)	SPAL(30)	
	SPAL(<5)	JURO(45)	SPAL(93)
3		SPAL(75)	SPAL(95)
	SPAL(77)	JURO(<5)	JURO(<5)
4		SPAL(80)	
	SPAL(70)	JURO(<5)	SPAL(70)

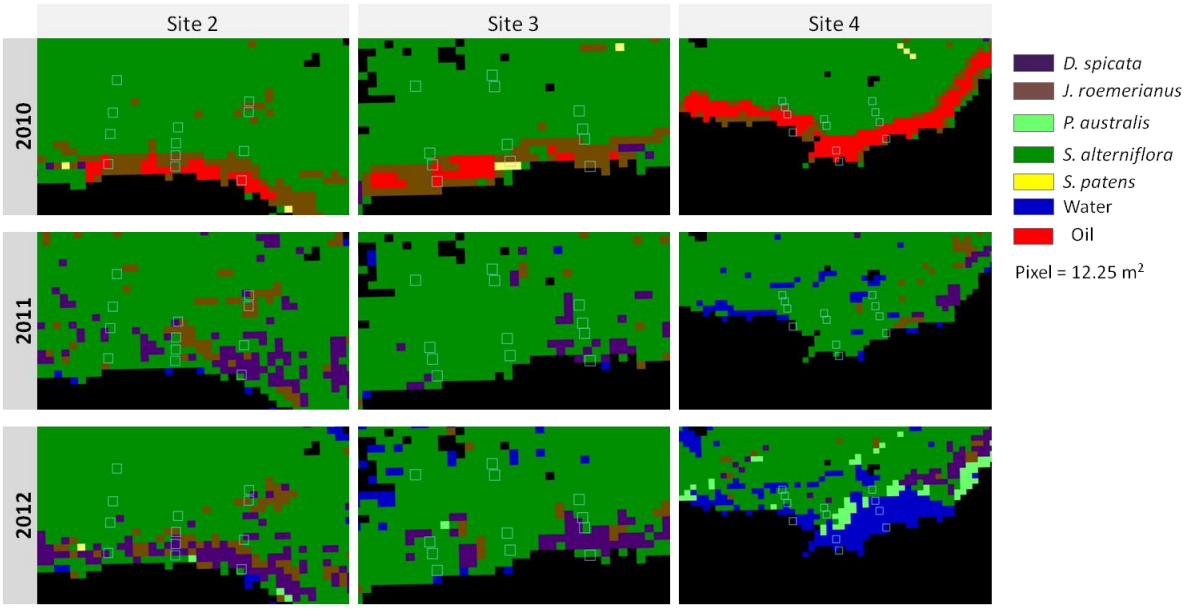

Figure 2.8: Location of plots (light blue square, N = 36) used for 2010, 2011 & 2012 classification and survey comparisons with USGS *oiled sites* 2, 3 & 4. Four randomly positioned plots (1 closest and 4 farthest from shoreline) were located along transects A(west), B(middle) and C(east). Black pixels represent initial (2010) open water.

Table 2.5: Prevalent species and cover-abundance (%) at oiled sites in 2010, 2011 and 2012 from USGS plots with percent cover in parentheses (1-4).

Site 2

2010

Plot	transect A	transect B	transect C
1	DISP(8) SPAL(<5)	JURO(90)	no vegetation
2	JURO(85)	JURO(99)	JURO(45) SPAL(50)
3	SPAL(85)	SPAL(30) JURO(68)	SPAL(15) JURO(90)
4	JURO(45) SPAL(80)	SPAL(25) JURO(65)	SPAL(20) JURO(60)

2011

1	no vegetation	SPAL(15) DISP(25) JURO(35)	DISP(50)
2	JURO(35) SPAL(45)	DISP(20) JURO(20) SPAL(50)	JURO(15) SPAL(70)
3	SPAL(90)	JURO(40) SPAL(45)	JURO(50)
4	SPAL(20) JURO(30)	JURO(10) SPAL(80)	JURO(10) SPAL(35)

2012

1	SPAL(70)	SPAL(20) JURO(30)	DISP(40)
2	JURO(20) SPAL(60)	DISP(10) SPAL(15) JURO(35)	JURO(25) SPAL(40)
3	SPAL(80)	SPAL(35) JURO(45)	JURO(60)
4	JURO(35) SPAL(50)	JURO(20) SPAL(50)	JURO(10) SPAL(35)

Site 3

2010

Plot	transect A	transect B	transect C
1	DISP(20) SPAL(40)	SPAL(30) JURO(40)	DISP(10) SPAL(20)
2	JURO(25) SPAL(60)	SPPA(20) SPAL(82)	JURO(10) SPAL(80)
3	JURO(15) SPAL(75)	JURO(25) SPAL(75)	SPAL(90)
4	SPAL(93)	JURO(15) SPAL(75)	SPAL(95)

2011

1	SPPA(15) SPAL(25) DISP(50)	SPPA(15) SPAL(30) JURO(55)	SPAL(20) DISP(60)
2	JURO(15) SPAL(45)	SPPA(10) SPAL(45)	SPAL(80)
3	JURO(25) SPAL(40)	JURO(18) SPAL(20)	SPAL(90)
4	JURO(10) SPPA(10) SPAL(30)	JURO(10) SPAL(50)	JURO(25) SPAL(30)

2012

1	SPPA(10) SPAL(85)	JURO(15) SPAL(60)	SPAL(70)
2	JURO(20) SPAL(60)	SPAL(45)	SPAL(20)
3	SPAL(40)	JURO(25) SPAL(40)	SPAL(65)
4	JURO(15) SPAL(70)	JURO(20) SPAL(55)	SPAL(90)

Site 4

2010

Plot	transect A	transect B	transect C
1	SPAL(8)	SPAL(<5)	no vegetation
2	SPAL(90)	JURO(50)	SPAL(95)
3	SPAL(25) JURO(60)	SPAL(85)	SPAL(90)
4	SPAL(10) JURO(85)	JURO(10) SPAL(70)	SPAL(34) JURO(36)

2011

1	SPAL(15)	SPAL(70)	no vegetation
2	SPAL(10)	SPAL(98)	SPAL(80)
3	SPAL (<5)	DISP(10) SPAL(55)	SPAL(45)
4	JURO(15) SPAL(55)	JURO(15) SPAL(45)	SPAL(15) JURO(25)

2012

1	no vegetation	no vegetation	SPAL(<5)
2	JURO(5) SPAL(5)	no vegetation	no vegetation
3	SPAL(60)	no vegetation	no vegetation
4	JURO(6)	SPAL(20)	no vegetation

USGS field sites 2, 3, & 4 were impacted by heavy oiling in 2010 and exhibited signs of oil-induced vegetation stress, including widespread chlorosis and plant mortality, particularly in the plots that were closest to the shoreline. Field observations indicated site 4 was the most heavily oiled site with oil covering both the vegetation stems and/or soil substrate. Oil was present on plant stems and soil substrate in five of the six plots that were closest to the shoreline at site 4, and vegetation in these plots exhibited near-complete mortality (>90%: Table 2.5). Plot C2 was the only plot within 15 m of the shoreline to show signs of live vegetation cover (98% live) with only light oil impact to vegetation stems (Table 2.5). The CDA map successfully classified oil in the five plot locations with oil cover, and correctly classified plot C2 as *S. alterniflora*. Site 3 was also extensively oiled with plots

A1, B1 and C1 showing heavy impacts, including 70% (C1) and 40% (A1 & B1) plant mortality (Table 2.5). CDA successfully classified A1 as oiled marsh (Figure 2.8; Table 2.5). Plot B1 was inhabited by *J. roemerianus* (40%) and *S. alterniflora* (30%), and CDA classified the two pixels encompassed by the plot as *J. roemerianus* and *S. patens* (Figure 2.8; Table 2.5). Plot C1 was inhabited by *S. alterniflora* (20%) and *D. spicata* (10%), and this location was misclassified as *J. roemerianus* (Figure 2.8; Table 2.5). At plots A1 and C1 of site 2 near-complete mortality (>90%) was also observed, and the CDA map successfully identified the oiled-vegetation in these plot locations (Figure 2.8; Table 2.5).

All plots that showed heavy oiling exhibited plant stress (>50% chlorosis) in 2010, however, mortality was not observed at all plots. For example, heavy oiling and greater than 50% chlorosis was observed at plots B1 and B2 of site 2, but plant mortality was less than 10%, and CDA successfully classified these plots as *J. roemerianus* (Figure 2.8; Table 2.5). Plots A3, B3 and C3 of site 4 showed only light oiling and live vegetation cover between 85-90%, and these plots were classified accurately as *J. roemerianus* (A3) and *S. alterniflora* (Figure 2.8B3 & C3; Table 2.5). Plots A4, B4 and C4 all had live vegetation cover greater than 70%, and exhibited only trace oil impacts (i.e. speckled chlorosis on stems) with no visible oil present on stems or substrate. CDA misclassified one of these plots as *S. alterniflora* (A4), and classified accurately plots B4 and C4 as *S. alterniflora*. *S. alterniflora* dominated cover with only trace oil impacts were observed at the nine plots greater than 5 m from the shoreline at site 3, and the 2010 CDA map was correctly classified as *S. alterniflora* for all these plot locations (Figure 2.8; Table 2.5). Additionally, *D. spicata* was classified in pixels adjacent to the plots and observed as a subdominant in plots in 2011 and 2012 (Figure 2.8; Table 2.5).

Heavy oiling of stems and soil substrate was only seen at site 4 in 2011. Heavy oiling and dead stems were observed at A1 & C1 of site 4. These plots were characterized by low to no live aboveground biomass (<15%), while B1 showed heavy oiling, but *S. alterniflora* live biomass of 75% (Figure 2.8). The 2011 CDA map did not classify plots A1 & C1 as oiled, but captured the *S. alterniflora* in plot B1. All other plots of site 4 were classified accurately as *S. alterniflora* with the exception of C4, which was reportedly a mixed plot of *J. roemerianus* and *S. alterniflora*, but with low live vegetation cover (40%) (Figure 2.8).

The CDA classifier performed poorly at sites 2 and 3 in 2011 where vegetation had begun to recover, due to the lack of a single, clear dominant in the plots and an apparent increase in species richness (Table 2.5). For instance, no oil was observed on stems or substrate within plots A1, B1 or C1 of site 3, and only trace impacts were observed to stems (speckled chlorosis). Vegetation had largely recovered and was characterized by mixtures of *S. alterniflora, D. spicata, J. roemerianus* and *S. patens* with live vegetation composing at least 80% of the plots (Table 2.5). *S. alterniflora* was observed in the field and classified for all three plots. However, *D. spicata* cover (50-60%) was dominant in plots A1 and C1, and therefore the classification of *S. alterniflora* was viewed as an error (Figure 2.8; Table 2.5). The green vegetation on most plots were *S. alterniflora*-dominated for site's 2 and 3 with the exceptions of B3 and C4 of site 2, which were inhabited by *S. alterniflora* and *J. roemerianus* in comparable cover-abundance. The classification products were accurate for all plots 2 through 4, except for B4 which was classified as *D. spicata* and *J. roemerianus* rather than *S. alterniflora* as observed in the field (Figure 2.8; Table 2.5).

In 2012, no oil was observed at sites 2, 3 or 4. At site 4, only four plots exhibited any vegetation cover (A2 =15%, A3 = 95%, A4 = 15%, B4 = 30%) and only one plot had live

vegetation cover of >20%. The CDA maps are in general agreement with most of the survey observations (Figure 2.8; Table 2.5). At sites 2 & 3, *S. alterniflora* was the most abundant dominant along all transects, however, the cover was below 50% for several plots in 2012. Likewise, the classification results in those plot locations reflect *S. alterniflora* dominance. Several plots that were misclassified (e.g. A3 and C2 of site 3) had low live vegetation cover, low average stem heights (52-73 cm) and the presence of wrack (Figure 2.8; Table 2.5).

2.4. Discussion

2.4.1 Accuracy Assessment

Oiling factors, such as oil-type, timing of exposure, concentration, thickness, degree of weathering and emulsification, and surface distribution, have been shown to elicit highly variable vegetation and ecosystem responses (Pezeshki et al., 2000). Subsequent to the DWH spill, ground-based and remotely sensed surveys of oil contamination in marshes have been conducted to measure these oiling factors (Kokaly et al., 2013; Michel et al., 2013; Peterson et al., 2015). The distribution of dominant species in oil-contaminated marshes is an important factor in explaining ecosystem response. We set out to generate a time series of classified maps that consistently meet or exceed previous efforts to map salt marsh dominant species. An overall accuracy 82% (kappa = 0.78) was obtained when comparing training and validation spectra (Table 2.2), indicating CDA performed well in discriminating classes despite the spectral similarity of the dominant species. The CDA classifier performed well in locations with little spectral mixing among dominant species classes. For instance, the classified pixels in Figure 2.9A & D are in agreement with the observations from validation polygons, despite presence of subdominant species (Figure 2.9A). In contrast, the classifier

performed poorly in areas characterized by wrack zones in 2011 and low vegetation cover (Figure 2.9B) or intermixed dominant species in 2012 (Figure 2.9C).

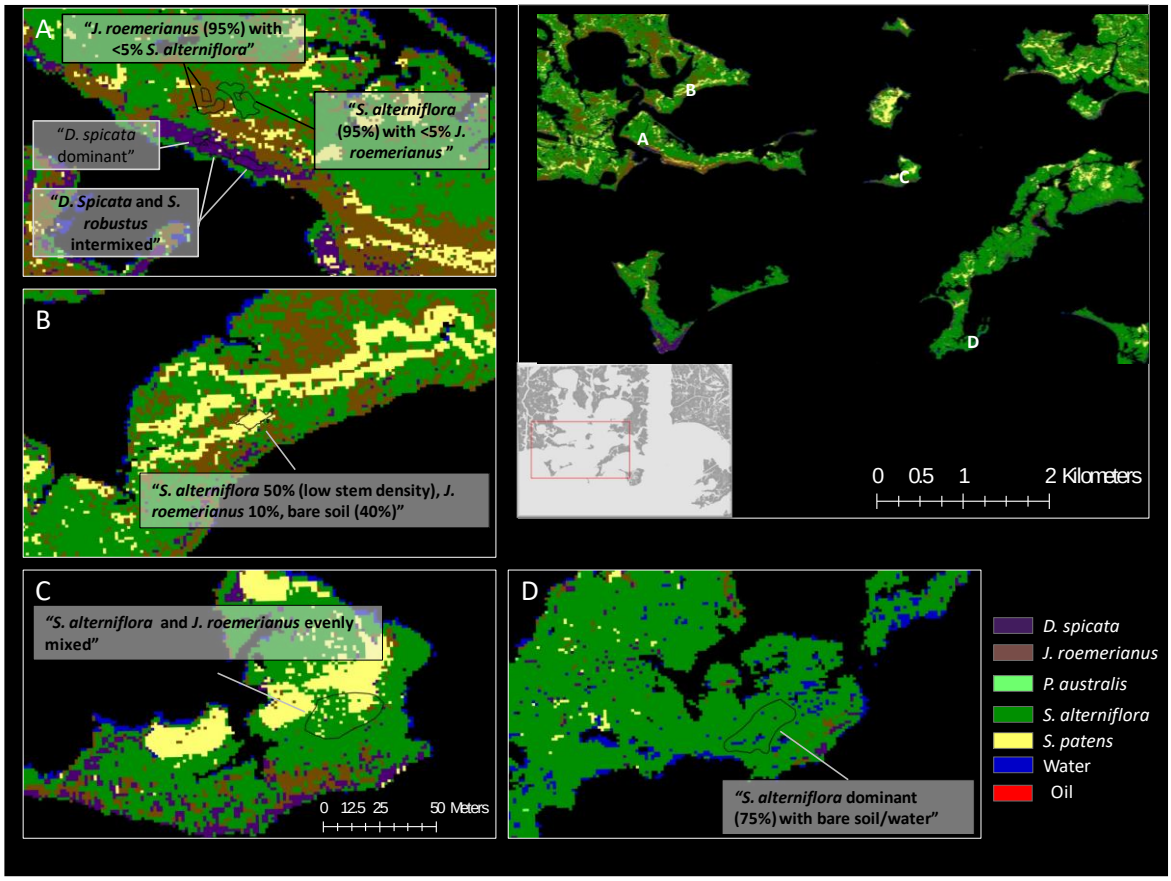

Figure 2.9: Classification map of dominant species in October 2011. Expanded view boxes A and D show areas with validation polygons where the CDA classifier performed well, and expanded view boxes B and C show areas of poor classification results.

In comparison with a time series of field (USGS) surveys along oiled and non-oiled shorelines, CDA classifications were in agreement with 84% of the plot observations (n = 180), and in 88% agreement if plots with mixed dominants (<75%) are removed. *S. alterniflora* is clearly the most commonly occurring dominant in the polyhaline marshes of Barataria Bay, but appears to be overly classified in shoreline zones in place of *J. roemerianus* on the 2010 classified map (Figure 2.6). Dense mixtures of *J. roemerianus* and

S. alterniflora are commonly observed within ~30m of shoreline, and due to the influence of distinctive phenological properties on spectral features, the species that is classified as dominant in a given location (i.e. pixel) may change depending on the timing of the AVIRIS data collection. *J. roemerianus*, for instance, has continuous aboveground biomass production throughout the year and lacks a clear "greening up" pattern (Hopkinson et al., 1978). Conversely, *S. alterniflora* has clear seasonal trends in aboveground green biomass with increasing live leaf production through the spring and summer (Hopkinson et al., 1978; Gosselink, 1984). *S. alterniflora* canopies were potentially greener in 2010, due to the greater annual rainfall leading up to the collection date (Figure 2.3C). This would potentially explain some of the decrease in *S. alterniflora* and increase in *J. roemerianus* from 2010 to 2011. The seasonality of *S. alterniflora* also may be responsible for the *S. alterniflora* to *S. patens* conversion from 2010 to 2011 seen in Figures 2.6 and 2.7. This conversion to *S. patens* is likely an artifact in the classification occurring in locations where mats of dead grass (wrack) have suppressed new vegetation growth. The large wrack zones were only observed in the 2011 data, and the inclusion of a senesced grass class could have addressed this classification problem. However, we determined a non-specific plant class, like senesced grass, would aggregate pixels from all species classes where heavily mixtures of live and senesced grass occurred. This was considered a departure from the focus of the paper, and was excluded from the classification scheme. The accuracy of the CDA-classified maps are acceptable in comparison to previous efforts to map species in intertidal environments using imaging spectroscopy. Sadro et al. (2007) used spectral angle mapper (SAM) and a mixture-tuned matched filter to classify salt marsh vegetation species on AVIRIS images and generated overall accuracy of 59% (kappa = 0.40). Similarly, Schmidt et al. (2004) produced wetland

species maps with an overall classification accuracy of 66% (kappa = 0.64) using an expert system and HyMap imagery (Integrated Spectronics Pty Ltd). Judd et al. (2007) achieved higher classification accuracies (overall accuracy 85%, kappa= 0.76) using Navy Research Laboratory Portable Hyperspectral Imager for Low Light Spectroscopy II (PHILLS II) sensor and a linear unmixing algorithm.

2.4.2 Assessment of Vegetation Cover Change

The loss in overall vegetation cover (and increase in bare soil) suggests post-spill productivity was reduced, but the conversion from dead to live vegetation also suggests there were signs of recovery. For example, green vegetation increased to 45% cover or more in the oil-impacted plots of sites 2 and 3 in 2012. *D. spicata* (40%) was dominant and the classification map was in agreement with the field observations (Figure 2.8; Table 2.5). Additionally, the colonization by *D. spicata* following disturbance makes ecological sense as it has been described as an opportunistic species (Shumway, 1995). Previous research has suggested that *D. spicata* can more effectively compete for resources under nutrient-limited conditions than other salt marsh dominants (Levine et al., 1998). Further, in Gulf Coast marshes, it has been shown to occur as a colonizing species following disturbances, such as storm surges (Clewell et al., 1999).

In contrast to stability at some sites (2 and 3), site 4 exhibited heavy vegetation damage and shoreline erosion following the oiling and additional disturbance caused by Hurricane Isaac in August 2012 (Figures 2.8 & 2.9B). A comparison of the reported observations and our classified maps indicate we successfully captured the land-cover change documented in this marsh location. The marsh shoreline retreated 27 to 31 m along these transects, and our classifications reflect this shoreline loss (Figure 2.8). The most remarkable

changes at site 4 (and along other shorelines) occurred between 2011-2012, as the open water intruded from the shoreline into the interior marshes by more than 30 m in some locations (Figure 2.8). The shoreline change is more complicated than shoreline retreat. The shoreline change appears to be a function of retreat plus the formation of new tidal channels and mudflats in the near-shore marsh interior, perhaps developed following the storm surge from Hurricane Isaac (Figures 2.8 & 2.9B).

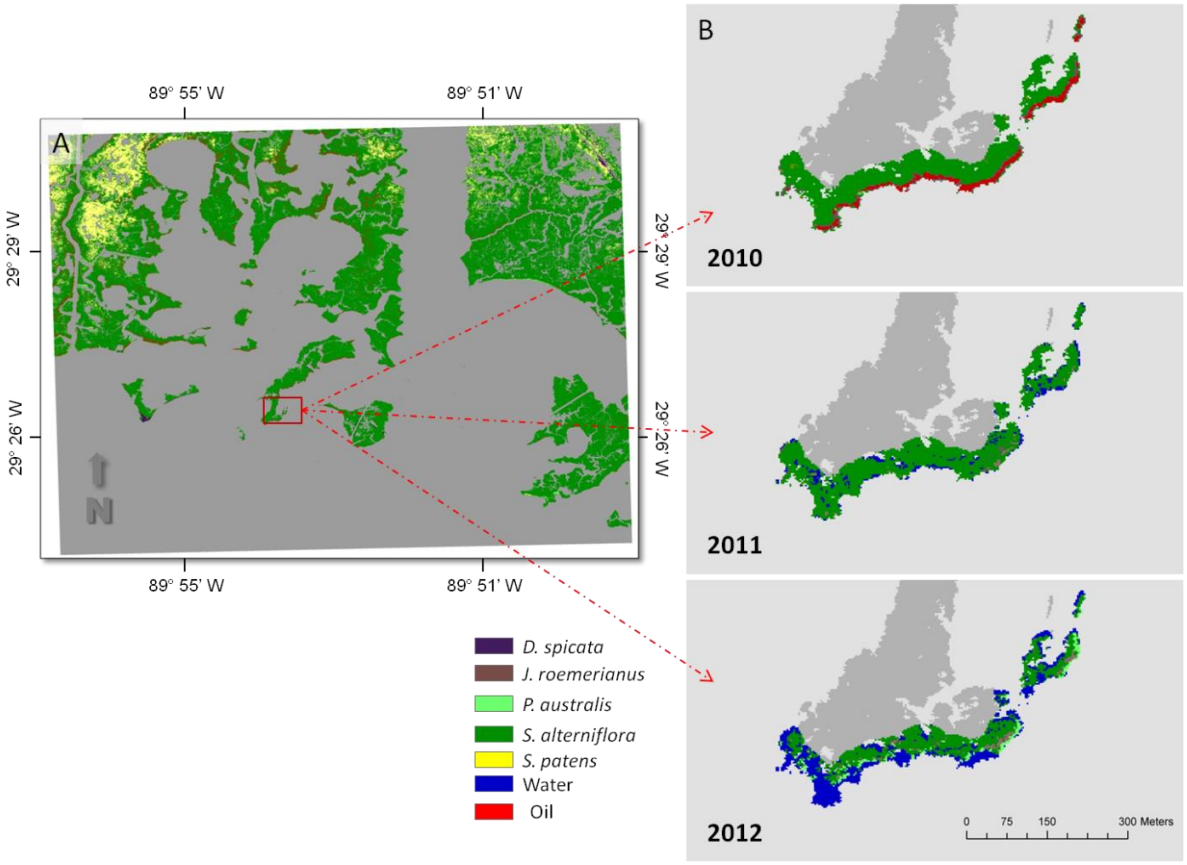

Figure 2.10: A) Map of dominant species in 2010. The shorelines in the north were among the most heavily oiled marshes following the DWH spill. B) Progression of marsh loss from 2010-2012 on a heavily oiled shoreline.

The most striking result from the times series analysis is the decrease in overall marsh area in the oiled shoreline zones. Figure 2.10B illustrates the transition from oiled marsh to subtidal, open water over the period of the study. Our examination of a subset of generally

south-facing (i.e. 70° to 270°) shorelines that are bifurcated into oiled and non-oiled locations indicate that both shoreline zones exhibited retreat, however, oiled marshes loss appreciably more area (Table 2.3B & C). We found an 8% (15,351 m^2) greater decrease in total marsh area for oiled shoreline zones (-12%) than for non-oiled shoreline zones (-6%) from 2010-2012 suggesting that, in comparison to similarly situated marsh shorelines, oil contamination exacerbated marsh area loss. Furthermore, the results point to the potential vulnerability of shorelines lacking vegetated soil stability to storms that are common in the region.

Tidal stage is widely known to influence vegetation reflectance characteristics and estimates of wetland area, resulting in classification and change detection assessment uncertainty (Jensen et al., 1993; Dobson et al., 1995; Kearney et al., 2009). We anticipated *S. alterniflora* and *P. australis* to have the near-infrared reflectance similar to that of the "pure" GV spectra shown in Figure 2.4, due to the leaf structure (i.e. high leaf area) of these species, and *P. australis* exhibits comparable reflectance in this region. Yet, *S. alterniflora* reflectance is much lower than expected, which could be attributable to the influence of background water, resulting from a relatively high tidal stage during the AVIRIS collection period in 2010 (0.246 - 0.138 m above MLLW).

The percent loss of wetlands in oiled zones (12%, 173,799 m^2) is likely an underestimate of the actual loss, due to the offset caused by lower water levels in 2011 and 2012 compared with the base image (2010). The maximum tidal difference between data capture periods (2010 and 2011) is 22 cm, and a minimum difference of 4 cm from low tide in 2010 to high tide in 2012. In determining the effect of tidal stage on remotely sensed classification/ change detection products in *S. alterniflora* dominated marshes of South Carolina, Jensen et al. (1993) found that for every 10 cm of water level change wetland area

changed by 1-2%. Using this metric, a 22 cm decrease in water level (maximum difference during data capture periods) could increase wetland loss in oiled zones as much as 4% (43,955 m^2). However, a great deal of uncertainty lies in predicting the impacts of water level on wetland area change estimates.

The salt marshes where the heaviest oiling occurred were dominated by *S. alterniflora* and *J. roemerianus*, but only *S. alterniflora* were extensively degraded or lost in the oiled zones (Table 2.3B). The relative even distribution of *J. roemerianus* from 2010-2012 (10-12%) suggest that *J. roemerianus* was less sensitive to oiling than *S. alterniflora*. This assertion contradicts field and greenhouse mesocosm experiments which have shown *S. alterniflora* to have a higher tolerance threshold for oil contamination (Lin et al., 2002, Lin and Mendelssohn, 2012). An alternative explanation is that the disproportional negative response of *S. alterniflora* is due to its spatial distribution and landscape position. For example, *J. roemerianus* commonly dominates intermediate marsh zones and is not as widely spread on the shoreline edge, or on the southern, bayside islands that are closest to the Gulf of Mexico (Figure 2.6). Conversely, *S. alterniflora* is widespread on the marsh shoreline edges of these islands, which suggests that *S. alterniflora* marshes may be more vulnerable to wave action and storm surge erosion following oiling, due to their landscape position (Figure 2.6).

Our results showing variable marsh responses to heavy oiling are supported by previous field observations (Lin and Mendelssohn, 2012; Silliman et al., 2012). Silliman et al. (2012) highlighted the importance of landscape position and biogeomorphological feedbacks in the variable responses of marsh ecosystems to disturbance, and that heavily oiled shorelines amplified erosion in areas already experiencing elevated rates of retreat, due

to multiple human stressors. Erosion rates along heavily oiled shorelines of already receding platforms were more than twice that of reference sites one-and-a-half years after the spill began. Conversely, shoreline erosion was suppressed at heavily oiled sites with different geomorphic and/or vegetation properties as these sites showed evidence of recovery with plant cover meeting or exceeding that of reference sites through lateral (clonal) regrowth originating from the marsh interior (Silliman et al., 2012). More recently, Zengel et al. (2015) has indicated that manual oil treatments (i.e. oil and oiled debris removal) conducted by small crews improved habitat conditions by exposing residual oiling to natural degradation processes and minimizing additional detrimental effects (Zengel et al., 2015). Furthermore, *S. alterniflora* planting, following treatment, increased vegetation recovery and reduced shoreline erosion (Zengel et al., 2015). Going forward, marsh shoreline change should be further examined, with consideration of different treatment and re-vegetation methods, using imaging spectroscopy.

2.5. Conclusion

We demonstrated the capacity of a time series of airborne imaging spectroscopic data (AVIRIS) to distinguish spectrally similar plant species in a salt marsh ecosystem heavily impacted by oil. We used canonical discriminant analysis (CDA) to classify dominant species, and verified distributions with temporally corresponding field data. Finally, we compared changes in dominant species percent cover during three years (October 2010, 2011 and 2012) along oiled and non-oiled shorelines with comparable locations, inshore distance and orientation.

S. alterniflora was by far the most widespread dominant in oiled zones. *J. roemerianus* and *S. patens* were common dominants, but were not frequently dominant in the southern portion of the study area that was most impacted by oil. *D. spicata* was a pioneer species following oiling disturbance. Both oiled and non-oiled shorelines showed signs of shoreline erosion, but oiled shorelines exhibited more than twice as much loss 2.5 years after initial oiling. Damage to vegetation from oil may have increased the vulnerability of the shoreline to erosion during subsequent extreme events. Marshes that were heavily oiled exhibited variable degrees of loss and recovery, suggesting other factors may have contributed to the marsh responses.

Future research will build upon the findings here by analyzing marsh transitions following oiling using sub-pixel mixture modeling techniques, and determine whether observed marsh responses (i.e. recovery, type-conversion, degradation, or loss) are functions of oil distribution (oil EM fractions, oil penetration and persistence) and/or tidal and wave height properties. The goal is to improve predictions of marsh ecosystem responses (i.e. degradation and resiliency), and in doing so, advance mitigation and management efforts.

2.6. References

Adam, E., Mutanga, O., & Rugege, D. (2010). Multispectral and hyperspectral remote sensing for identification and mapping of wetland vegetation: a review. *Wetlands Ecology and Management*, *18*(3), 281-296.

Alexander, S. K., & Webb Jr, J. W. (1985). Oil in the salt marsh: what have we learned. In *Proceedings, Fourth Coastal Marsh and Estuary Management Symposium. Louisiana State University Printing Office, Baton Rouge, LA* (pp. 49-62).

Allen, Y. C., Couvillion, B. R., & Barras, J. A. (2012). Using multitemporal remote sensing imagery and inundation measures to improve land change estimates in coastal wetlands. *Estuaries and Coasts*, *35*(1), 190-200.

Alonzo, M., Roth, K., & Roberts, D. (2013). Identifying Santa Barbara's urban tree species from AVIRIS imagery using canonical discriminant analysis. *Remote Sensing Letters*, *4*(5), 513-521.

Asner, G. P. (1998). Biophysical and biochemical sources of variability in canopy reflectance. *Remote sensing of Environment*, *64*(3), 234-253.

Asner, G. P., Borghi, C. E., & Ojeda, R. A. (2003). Desertification in Central Argentina: Changes in ecosystem carbon and nitrogen from imaging spectroscopy. *Ecological Applications*, 13, 629−648.

Boardman, J. W. (1999, February). Precision geocoding of low altitude AVIRIS data: lessons learned in 1998. In *AVIRIS 1999 Proceedings*.

Ceccato, P., Flasse, S., Tarantola, S., Jacquemoud, S., & Gregoire, J. -M. (2001). Detecting vegetation leaf water content using reflectance in the optical domain. Remote Sensing of Environment, 77, 22−33.

Chabreck, R. H. (1972). Vegetation, water and soil characteristics of the Louisiana coastal region.*Louisiana State UniversityAgricultural Experiment Station Bulletin No. 664.* Louisiana State University, Baton Rouge, Louisiana.

Chen, D., & Stow, D. (2002). The effect of training strategies on supervised classification at different spatial resolutions. *Photogrammetric Engineering and Remote Sensing*, *68*(11), 1155-1162.

Clark, R.N., Swayze, G.A., Livo, K.E., Kokaly, R.F., King, T.V.V., Dalton, J.B., Vance, S., Rockwell, B.W., Hoefen, T., and McDougal R.R., (2002). Surface reflectance calibration of terrestrial imaging spectroscopy data, in Proceedings of the Eleventh JPL Airborne Earth Science Workshop , (ed.) Green R.O., *JPL Publication 03-04*. 43-64.

Clewell, A. F., R. S. Beaman, C. L. Coultas, and M. E. Lasley. 1999. Suwannee River Tidal Marsh Vegetation and its Response to External Variables and Endogenous Community Processes. Final Report. Report prepared for the Suwannee River Water Management District, Live Oak, FL. 119 pp.

Couvillion, B.R., Barras, J.A., Steyer, G.D., Sleavin, W., Fischer, M., Beck, H., Trahan, N., Griffin, B., Heckman, D. (2011). Land area change in coastal Louisiana from 1932 to 2010: U.S. Geological Survey Scientific Investigations Map 3164, scale 1:265,000, 12 p. pamphlet.

DeLaune, R. D., Pezeshki, S. R., Jugsujinda, A., & Lindau, C. W. (2003). Sensitivity of US Gulf of Mexico coastal marsh vegetation to crude oil: Comparison of greenhouse and field responses. *Aquatic Ecology*, *37*(4), 351-360.

Demmig-Adams B, A. & Adams, W. W.III (1996).The role of xanthophyll cycle carotenoids in the protection of photosynthesis.*Trends Plant Science*, *1*(1), 21–26.

Dennison, Philip E, Roberts, D.A. (2003). Endmember Selection for Multiple Endmember Spectral Mixture Analysis using Endmember Average RSME. *Remote Sensing of Environment*, *87*(2-3), 123-135.

Dobson, J.E., E.A. Bright, R.L. Ferguson, D.W. Field, L.L. Wood, K.D. Haddad, H. Iredale, J.R. Jensen, V.V. Klemas, R.J. Orth, J.P. Thomas (1995) NOAA Coastal Change Analysis Program (C-CAP): Guidance for Regional Implementation. NOAA Technical Report NMFS 123, NOAA NMFS, Seattle, Washington, 92 p.

Dópido,I. Villa, A. Plaza, A. and P. Gamba,(2012) A quantitative and comparative assessment of unmixing-based feature extraction techniques for hyperspectral image classification. IEEE J. Sel. Topics Applied Earth Observations and Remote Sens., vol. 5, no. 2, pp. 421–435.

Feret, J. -B., Francois, C., Asner, G. P., Gitelson, A. A., Martin, R. E., Bidel, L. P. R., Ustin, S. L., le Maire, G., & Jacquemoud, S. (2008). PROSPECT-4 and 5: Advances in the leaf optical properties model separating photosynthetic pigments. Remote Sensing of Environment.

Fisher, R. A. (1936). The use of multiple measurements in taxonomic problems. *Annals of eugenics*, *7*(2), 179-188.

Foody, G. M., McCulloch, M. B., & Yates, W. B. (1995). Classification of remotely sensed data by an artificial neural network: issues related to training data characteristics. *Photogrammetric Engineering and Remote Sensing*, *61*(4), 391-401.

Frieswyk, C. B., Johnston, C. A., & Zedler, J. B. (2007). Identifying and characterizing dominant plants as an indicator of community condition. *Journal of Great Lakes Research*, *33*(sp3), 125-135.

Gamon, J.A., Serrano, L., & Surfus, J. S. (1997). The photochemical reflectance index: an optical indicator of photosynthetic radiation-use efficiency across species, functional types, and nutrient levels. *Oecologia*, *112*, 492-501.

Gosselink, J., & Pendleton, E. C. (1984). *The ecology of delta marshes of coastal Louisiana: a community profile*. Center for Wetland Resources, Louisiana State University, Baton Rouge.

Green, R. O., Eastwood, M. L., Sarture, C. M., Chrien, T. G., Aronsson, M., Chippendale, B. J., ... & Williams, O. (1998). Imaging spectroscopy and the airborne visible/infrared imaging spectrometer (AVIRIS). *Remote Sensing of Environment*, *65*(3), 227-248.

Guang, Z., & Maclean, A. L. (2000). A comparison of canonical discriminant analysis and principal component analysis for spectral transformation. *PE&RS, Photogrammetric Engineering & Remote Sensing*, *66*(7), 841-847.

Halligan, K. Q. (2002). *Multiple endmember spectral mixture analysis of vegetation in the northeast corner of Yellowstone national park*. Master's Thesis, University of California Santa Barbara.

Hester, M. W., & Mendelssohn, I. A. (2000). Long-term recovery of a Louisiana brackish marsh plant community from oil-spill impact: vegetation response and mitigating effects of marsh surface elevation. *Marine Environmental Research*, *49*(3), 233-254.

Hopkinson, C. S., Gosselink, J. G., & Parrando, R. T. (1978). Aboveground production of seven marsh plant species in coastal Louisiana. *Ecology*, 760-769.

Hughes, G. (1968). On the mean accuracy of statistical pattern recognizers. *Information Theory, IEEE Transactions on*, *14*(1), 55-63.

Jensen, J. R., Cowen, D. J., Althausen, J. D., Narumalani, S., & Weatherbee, O. (1993). The detection and prediction of sea level changes on coastal wetlands using satellite imagery and a geographic information system. *Geocarto International*, *8*(4), 87-98.

Judd, C., Steinberg, S., Shaughnessy, F., & Crawford, G. (2007). Mapping salt marsh vegetation using aerial hyperspectral imagery and linear unmixing in Humboldt Bay, California. *Wetlands*, *27*(4), 1144-1152.

Kearney, M. S., Stutzer, D., Turpie, K., & Stevenson, J. C. (2009). The effects of tidal inundation on the reflectance characteristics of coastal marsh vegetation. *Journal of Coastal Research*, 1177-1186.

Khanna, S., Santos, M. J., Ustin, S. L., Koltunov, A., Kokaly, R. F., & Roberts, D. A. (2013). Detection of salt marsh vegetation stress and recovery after the deepwater horizon oil spill in barataria bay, Gulf of Mexico using AVIRIS data. *PloS one*, *8*(11), e78989.

Kirby, C. J., & Gosselink, J. G. (1976). Primary production in a Louisiana Gulf Coast *S. alterniflora* marsh. *Ecology*, 1052-1059.

Kokaly, R. F., Asner, G. P., Ollinger, S. V., Martin, M. E., & Wessman, C. A. (2009). Characterizing canopy biochemistry from imaging spectroscopy and its application to ecosystem studies. *Remote Sensing of Environment*, 113, S78–S91.

Kokaly, R. F., Couvillion, B. R., Holloway, J. M., Roberts, D. A., Ustin, S. L., Peterson, S. H., ... & Piazza, S. C. (2013). Spectroscopic remote sensing of the distribution and

persistence of oil from the Deepwater Horizon spill in Barataria Bay marshes. *Remote Sensing of Environment*, *129*, 210-230.

Kühn, F., Oppermann, K., & Hörig, B. (2004). Hydrocarbon Index–an algorithm for hyperspectral detection of hydrocarbons. *International Journal of Remote Sensing*, *25*(12), 2467-2473.

Lehr, B., Nristol, S., & Possolo, A. (2010). Oil Budget Calculator—Deepwater Horizon, technical documentation: a report to the National Incident Command. *Coastal Response Res. Cent*.

Levine, J. M., Brewer, J. S., & Bertness, M. D. (1998). Nutrients, competition and plant zonation in a New England salt marsh. *Journal of Ecology*, *86*(2), 285-292.

Lin, Q., & Mendelssohn, I. A. (1996). A comparative investigation of the effects of south Louisiana crude oil on the vegetation of fresh, brackish and salt marshes. *Marine Pollution Bulletin*, *32*(2), 202-209.

Lin, Q., & Mendelssohn, I. A. (2012). Impacts and recovery of the Deepwater Horizon oil spill on vegetation structure and function of coastal salt marshes in the northern Gulf of Mexico. *Environmental science & technology*, *46*(7), 3737-3743.

Lu, D. and Weng, Q. (2007) A Survey of Image Classification Methods and Techniques for Improving Classification Performance. *Int. J. Remote Sens.* 28(5)823-870.

Mendelssohn, I. A., Hester, M. W., Sasser, C., & Fischel, M. (1990). The effect of a Louisiana crude oil discharge from a pipeline break on the vegetation of a southeast Louisiana brackish marsh. *Oil and chemical pollution*, *7*(1), 1-15.

Michel, J., Owens, E. H., Zengel, S., Graham, A., Nixon, Z., Allard, T., ... & Taylor, E. (2013). Extent and degree of shoreline oiling: Deepwater Horizon oil spill, Gulf of Mexico, USA. *PloS one*, *8*(6), e65087.

Mitsch, W.J., Gosselink, J.G., 2000. Wetlands, 3rd ed. John Wiley, New York.

Moore, P.D. & Chapman, S.B. 1986. Methods in plant ecology. Blackwell Scientific Publications, Oxford.

Morris, J. T., & Haskin, B. (1990). A 5-yr record of aerial primary production and stand characteristics of *S. alterniflora*. *Ecology*, 2209-2217.

Nagler, P. L., Inoue, Y., Glenn, E. P., Russ, A. L., & Daughtry, C. S. T. (2003). Cellulose absorption index (CAI) to quantify mixed soil–plant litter scenes. *Remote Sensing of Environment*, 87, 310−325.

Palacios-Orueta, A., & Ustin, S. L. (1996). Multivariate statistical classification of soil spectra. *Remote sensing of environment*, *57*(2), 108-118.

Penland, S., & Ramsey, K. E. (1990). Relative sea-level rise in Louisiana and the Gulf of Mexico: 1908-1988. *Journal of Coastal Research*, 323-342.

Peterson, S.H., Roberts, D.A., Beland M., Kokaly, R.F., Ustin, S.L. (2015). Oil detection in the coastal marshes of Louisiana using MESMA applied to band subsets of AVIRIS data, *Remote Sensing of Environment*.

Pezeshki, S. R., & DeLaune, R. D. (1991). A comparative study of above-ground productivity of dominant US Gulf Coast marsh species. *Journal of Vegetation Science*, *2*(3), 331-338.

Pezeshki, S. R., & De Laune, R. D. (1993). Effect of crude oil on gas exchange functions of *J. roemerianus* and *S. alterniflora*. *Water, Air, and Soil Pollution*, *68*(3-4), 461-468.

Pezeshki, S. R., Hester, M. W., Lin, Q., & Nyman, J. A. (2000). The effects of oil spill and clean-up on dominant US Gulf coast marsh macrophytes: a review. *Environmental Pollution*, *108*(2), 129-139.

Plaza, A., Benediktsson, J. A., Boardman, J. W., Brazile, J., Bruzzone, L., Camps-Valls, G., ... & Trianni, G. (2009). Recent advances in techniques for hyperspectral image processing. *Remote sensing of environment*, *113*, S110-S122.

Pu, R., & Liu, D. (2011). Segmented canonical discriminant analysis of in situ hyperspectral data for identifying 13 urban tree species. *International Journal of Remote Sensing*, *32*(8), 2207-2226.

Ranwell, D. S. (1964). *Oil pollution in Poole Harbour and its effect on birds*.

Reddy, K. Ramesh, Delaune, Ronald, D. (2008). *Biogeochemistry of Wetlands: Science and Applications*. Boca Raton, FL: CRC Press, Taylor and Francis Group (757 pp).

Roberts, D. A., Gardner, M., Church, R., Ustin, S., Scheer, G., & Roberts Gardner, M., Church, R., Ustin, S., Scheer, G. & Green, R. O., D. A. (1998). Mapping Chaparral in the Santa Monica Mountains Using Multiple Endmember Spectral Mixture Models. *Remote Sensing of Environment*, *65*(3), 267–279.

Rogan, J., Franklin, J., & Roberts, D. A. (2002). A comparison of methods for monitoring multitemporal vegetation change using Thematic Mapper imagery. *Remote Sensing of Environment*, *80*(1), 143-156.

Roth, K. L., Dennison, P. E., & Roberts, D. A. (2012). Comparing endmember selection techniques for accurate mapping of plant species and land cover using imaging spectrometer data. *Remote Sensing of Environment*, *127*(null), 139–152.

Roth, K. L., Roberts, D. A., Dennison, P. E., Alonzo, M., Peterson, S. H., & Beland, M. (2015). Differentiating plant species within and across diverse ecosystems with imaging spectroscopy. *Remote Sensing of Environment*.

Sasser, C.E., Visser, J.M., Mouton, Edmond, Linscombe, Jeb, and Hartley, S.B., 2008, Vegetation types in coastal Louisiana in 2007: U.S. Geological Survey Open-File Report 2008–1224, 1 sheet, scale 1:550,000.

Schmidt, K. S., & Skidmore, A. K. (2003). Spectral discrimination of vegetation types in a coastal wetland. *Remote sensing of Environment*, *85*(1), 92-108.

Serrano, L., Penuelas, J., & Ustin, S. L. (2002). Remote sensing of nitrogen and lignin in Mediterranean vegetation from AVIRIS data: Decomposing biochemical from structural signals. Remote Sensing of Environment, 81, 355−364.

Silliman, B. R., Van de Koppel, J., McCoy, M. W., Diller, J., Kasozi, G. N., Earl, K., Adams, P. N., et al. (2012). Degradation and resilience in Louisiana salt marshes after the BP–Deepwater Horizon oil spill. *Proceedings of the National Academy of Sciences ,109* (28), 11234–11239.

Somers, B., Asner, G. P., Tits, L., & Coppin, P. (2011). Endmember variability in spectral mixture analysis: A review. *Remote Sensing of Environment*, *115*(7), 1603-1616.

Somers, B., Delalieux, S., Stuckens, J., Verstraeten, W. W., & Coppin, P. (2009). A weighted Linear Spectral Mixture Analysis approach to address endmember variability in agricultural production systems. *International Journal of Remote Sensing*, 30, 139−147.

Somers, B., Delalieux, S., Verstraeten, W. W., Van Aardt, J. A. N., Albrigo, G. L., & Coppin, P. (2010). An automated waveband selection technique for optimized hyperspectral mixture analysis. *International Journal of Remote Sensing*, *31*(20), 5549-5568.

Stedman, S. & Dahl, T.E. (2008). Status and trends of wetlands in the coastal watersheds of the Eastern United States 1998 to 2004. National Oceanic and Atmospheric Administration, National Marine Fisheries Service and U.S. Department of the Interior, Fish and Wildlife Service.

Steyer, G. D., Sasser, C. E., Visser, J. M., Swenson, E. M., Nyman, J. A., & Raynie, R. C. (2003). A proposed coast-wide reference monitoring system for evaluating wetland restoration trajectories in Louisiana. In *Coastal Monitoring through Partnerships* (pp. 107-117). Springer Netherlands.

Shumway, S. W. (1995). Physiological integration among clonal ramets during invasion of disturbance patches in a New England salt marsh. *Annals of Botany*, *76*(3), 225-233.

The Mathworks Inc. (2012). MATLAB and Statistics Toolbox. (Natick, MA).

Ustin, S. L., & Gamon, J. A. (2010). Remote sensing of plant functional types. *New Phytologist*, *186*(4), 795-816.

Ustin, S. L., Gitelson, A. A., Jacquemoud, S., Schaepman, M., Asner, G. P, Gamon, J. A., & Zarco-Tejada, P. J. (2009). Retrieval of foliar information about plant pigment systems from high resolution spectroscopy. Remote Sensing of Environment, 113, 67−77.

Visser, J. M., Sasser, C. E., Chabreck, R. H., & Linscombe, R. G. (1998). Marsh vegetation types of the Mississippi River deltaic plain. *Estuaries*, *21*(4), 818-828.

Xie, Yichun , Zongyao Sha and Mei Yu (2008) Remote sensing imagery in vegetation mapping: a review Journal of Plant Ecology (2008) 1 (1): 9-23.

Zengel, S., Bernik, B. M., Rutherford, N., Nixon, Z., & Michel, J. (2015). Heavily Oiled Salt Marsh following the Deepwater Horizon Oil Spill, Ecological Comparisons of Shoreline Cleanup Treatments and Recovery. *PloS one*, *10*(7), e0132324.

Chapter 3: Oiling accelerates loss of salt marshes, southeastern Louisiana

Abstract

The 2010 BP Deepwater Horizon (DWH) oil spill damaged thousands of km^2 of intertidal marsh along shorelines that had been experiencing elevated rates of erosion for decades. Yet, the contribution of marsh oiling to landscape-scale degradation and subsequent land loss has been difficult to quantify. Here, we applied advanced remote sensing techniques to map changes in marsh land cover and open water before and after oiling. We segmented the marsh shorelines into non-oiled and oiled reaches and calculated the land loss rates for each 10% increase in oil cover (e.g. 0% to >70%), to determine if land loss rates for each reach oiling category was significantly different before and after oiling. Finally, we calculated background land-loss rates to separate natural and oil-related erosion and land loss. Oiling caused significant increases in land losses, particularly along reaches of heavy oiling (>20% oil cover). For reaches with ≥20% oiling, land loss rates increased abruptly during the 2010-2013 period, and the loss rates during this period are significantly different from both the pre-oiling ($p < 0.0001$) and 2013-2016 post-oiling periods ($p < 0.0001$). The pre-oiling and 2013-2016 post-oiling periods exhibit no significant differences in land loss rates across oiled and non-oiled reaches ($p = 0.557$). We conclude that oiling increased land loss by more than 50%, but that land loss rates returned to background levels within 3-6 years after oiling, suggesting that oiling results in a large but temporary increase in land loss rates along the shoreline.

3.1. Introduction

Coastal wetlands provide a myriad of important ecosystem services, including flood mitigation, pollution removal, carbon sequestration, wildlife habitat and recreational opportunities, but they are threatened by an array of human activities, both directly by dredging, channelization and construction, and indirectly by sea level rise and reduced sediment input. Intertidal ecosystems, particularly salt marshes, are resilient to physical disturbances, which has been attributed to their high productivity (Turner, 1976; Pennings and Bertness, 2001; Gedan et al., 2009) and their physiological traits for coping with stressful environmental conditions (Niering et al., 1977; Smart and Barko, 1978; Pezeshki and DeLaune, 1993; Lin and Mendelssohn, 1996; Weis and Weis, 2004).

For nearly two centuries, human activities in the northern Gulf of Mexico have altered natural hydrologic regimes and changed the magnitude of system perturbations beyond salt marsh resilience thresholds (Deegan et al., 1984; van de Koppel et al., 2005), resulting in accelerated rates of wetland loss (> 250 $km^2\ yr^{-1}$: Stedman and Dahl, 2008). Since the 1970's, land loss has been a major topic of concern with broad management implications for the region, particularly for coastal Louisiana (Barrett 1970; Gagliano and van Beek, 1970; Chabreck 1972; Adams et al., 1976; Craig et al., 1979). Louisiana alone lost an estimated 4800 km^2 of intertidal wetland area from 1932-2010 ($\backsim$62 $km^2\ yr^{-1}$: Couvillion et al., 2011). A combination of natural (e.g. subsidence, sea-level-rise, abandoned river delta decay, wave energy and storm events) and anthropogenic (e.g. levees, impoundments, canal dredging and subsequent channel erosion) forces have contributed to the alarming rates of wetland loss, which has been popularly expressed in media outlets as "a football field per hour" (Couvillion et al., 2011).

Barataria Bay, a rapidly eroding abandoned delta where aggradation is no longer keeping pace with the effects of eustasy and subsidence (Evers et al., 1992), perhaps best illustrates the challenge of managing land loss (Craig et al., 1979; FitzGerald et al., 2007), as it has been losing 15.1 km^2 of wetland area per year since 1932 (Britsch and Dunbar 1993; Couvillion et al., 2011). Yet, these land losses in the Barataria Basin have not increased monotonically over the past century (Couvillion et al., 2011; Turner 2011). Episodic disturbances, like oil spills and hurricanes, can accelerate land loss, particularly along marsh edges, in areas already experiencing marsh degradation or loss (Hester and Mendelssohn, 2000; Ko and Day, 2004; Culbertson et al., 2008; Silliman et al., 2012; McClenachan et al., 2013).

The largest oil spill in U.S. history occurred in the Gulf of Mexico on April 20, 2010, when an explosion on the Deepwater Horizon (DWH) offshore drilling unit released 780,000 m^3 of crude oil into the Gulf before being capped on July 15 (Lehr et al., 2010). Oil washed onto approximately 796 km of shoreline comprised of intertidal marshes, disproportionally impacting salt marshes of Louisiana (Michel et al., 2013). Oiling was concentrated along the marsh shoreline edge (Silliman et al., 2012; Kokaly et al., 2013; Khanna et al., 2013), causing plant stress, mortality, and reductions in above- and belowground biomass (Lin and Mendelssohn, 2012; McClenachan et al., 2013). Exposure of marsh macrophytes to oil can lead to reduced function (i.e. transpiration and photosynthesis) followed by recovery through new shoot regeneration (Pezeshki and Delaune 1993; DeLaune et al. 2003), or plant mortality and reduced biomass production, resulting in destabilization of the root-soil matrix (Lin and Mendelssohn 1996; Silliman et al., 2012; Hester et al., 2016). Soil strength and sediment accretion are directly related to belowground biomass as roots and rhizomes create a binding

matrix for sediment accumulation (Gabet,1998; Michel and Kirchner, 2002; Turner, 2011). Reductions in belowground biomass caused by oiling and subsequent remediation efforts increases the vulnerability of shorelines to both episodic (i.e. storm surge) and chronic (i.e. subsidence, sea-level rise) erosional forces forces (Hershner and Lake, 1980; Silliman et al., 2012; McClenachan et al., 2013; Zengel et al., 2015).

Barataria Bay was among the areas most heavily impacted by oil following the DWH spill (Michel et al., 2013). The threat of accelerated erosion is of particular concern for the rapidly deteriorating marsh platforms of the lower Barataria Basin (Lin and Mendelssohn, 2012; Silliman et al., 2012; McClenachan et al., 2013; Zengel et al., 2015). Land loss in the lower basin over the last century has been caused by a combination of natural and anthropogenic erosional forces, including reduced sediment deposition from the Mississippi River, compaction and subsidence of underlying deltaic deposits, flood control practices and canal dredging (Craig et al., 1979; Ko and Day, 2004; Wilson and Allison 2008). Oiling from the DWH spill in Barataria Bay was concentrated within the first 15 m from the marsh edge (maximum of 19m; Kokaly et al., 2013, Khanna et al., 2015), with only 1% reaching beyond 15m (Peterson et al., 2015). Oiling accelerated shoreline erosion, contributing to erosion rates at oiled sites that were more than double that of reference (non-oiled) sites a year after exposure (Silliman et al., 2012; Zengel et al., 2015). However, existing studies were conducted over relative small areas (60 m of shoreline in Silliman et al, 2012; 300 m of shoreline in McClenachan et al., 2013; ∽630 m of shoreline in Zengel et al, 2015). Extrapolating results from these small study areas to regional scales can be problematic, due to the variability in shoreline orientation and exposure to wave action, degree of oiling, and variable responses of aboveground and belowground biomass to oiling (Pezeshki et al., 2000;

Lin and Mendelssohn, 2012; McClenachan et al., 2013). Consequently, the magnitude of marsh shoreline retreat and land loss attributed to oiling is difficult to quantify over regional scales by extrapolating from specific study reaches.

Three recent studies used remote sensing techniques to examine the impacts of oiling on salt marshes of Barataria Bay on a landscape-scale (Beland et al., 2016; Rangoonwala et al., 2016; Turner et al., 2016). Beland et al. (2016) found that only *Spartina alterniflora* dominated marshes were extensively degraded and that vegetation classes converted to an open water class along oiled shorelines at more than double the rate of non-oiled shorelines from 2010-2012. In comparing pre-oiling (2009-2010) shoreline recession rates, Rangoonwala et al. (2016) documented a fourfold and threefold increase in shorelines experiencing >4 m recession for the first and second years after oiling. Turner et al. (2016) assessed shoreline loss by measuring the change in width (east-west) and length (north-south) of 46 marsh islands in Barataria Bay, and reported erosion rates of oiled islands were 3 times that of non-oiled islands for the first 2.5 years after oiling. To date, however, a bay-wide and reach-scale assessment of wetland loss attributable to oiling has yet to be conducted. Further, previous studies have not accounted for variability in background erosion rates for oiled shorelines, or determined if land loss rates remained above pre-oiling rates or returned to background levels beyond the first 2.5 years.

In this chapter, our objectives were to: a) map changes in land loss along the shoreline in a bay affected by the DWH oil spill for three time periods: before, 3 years after, and 6 years after the spill, b) determine if rates of land loss were significantly different before and 3 and 6 years after the spill, and c) quantify the impact of oiling on reach-scale and bay-wide loss rates, controlling for temporal variability in natural background erosion rates. Land loss

rates per unit shoreline ($m^2\ m^{-1}\ yr^{-1}$) were calculated to standardize the loss rates for varying shoreline lengths, and to provide results that can be easily compared with future assessments of marsh loss along the shoreline in the Louisiana Coastal Zone. The rationale for examining the land loss rates at three-year time intervals derived from the temporal response patterns documented in prior research (Hester et al., 2016; Rangoonwala et al., 2016; Turner et al., 2016). Additionally, the time intervals (i.e. length of time between image acquisition dates) were constrained by the availability of high resolution satellite and airborne datasets capturing Barataria Bay.

3.2. Materials and Methods

We used a combination of remote sensing and GIS techniques and simple statistical algorithms to map shoreline change. Marsh shorelines were segmented into non-oiled (i.e. reference) and oiled reaches, and land loss rates were calculated to determine if loss rates were significantly different for oiled and non-oiled reaches, and for pre- (3 years before oiling) and post-oiling (0-3 years, 3-6 years) time periods. Last, we calculated background land loss rates for oiled reaches, using a combination of oiled (pre-spill) and non-oiled (pre- and post-spill) shoreline loss rates, to estimate the magnitude of oil-related land losses that are not attributable to temporal variability in background loss rates.

3.2.1 Study area description

The study area covers approximately 197 km^2 in northern Barataria Bay, Louisiana (29.43°N, 89.88°W), and consists of 41 km^2 of marsh area and 133 km of marsh shoreline (excluding interior channel and canal banks) (Figure 3.1). Barataria Bay is an

interdistributary bay, formed between the active Plaquemines delta lobe and Lafourche headland, which is experiencing some of the highest relative sea level rise rates in the continental United States (0.94 cm/yr from 1947-2006; FitzGerald et al., 2007). Salt marshes of Barataria Bay are fractions of a meter from sea level and are being impacted by sea level rise (Penland and Ramsey, 1990), and are highly vulnerable to natural and anthropogenic disturbances (Craig et al., 1979; Day et al., 2000; Ko and Day, 2004).

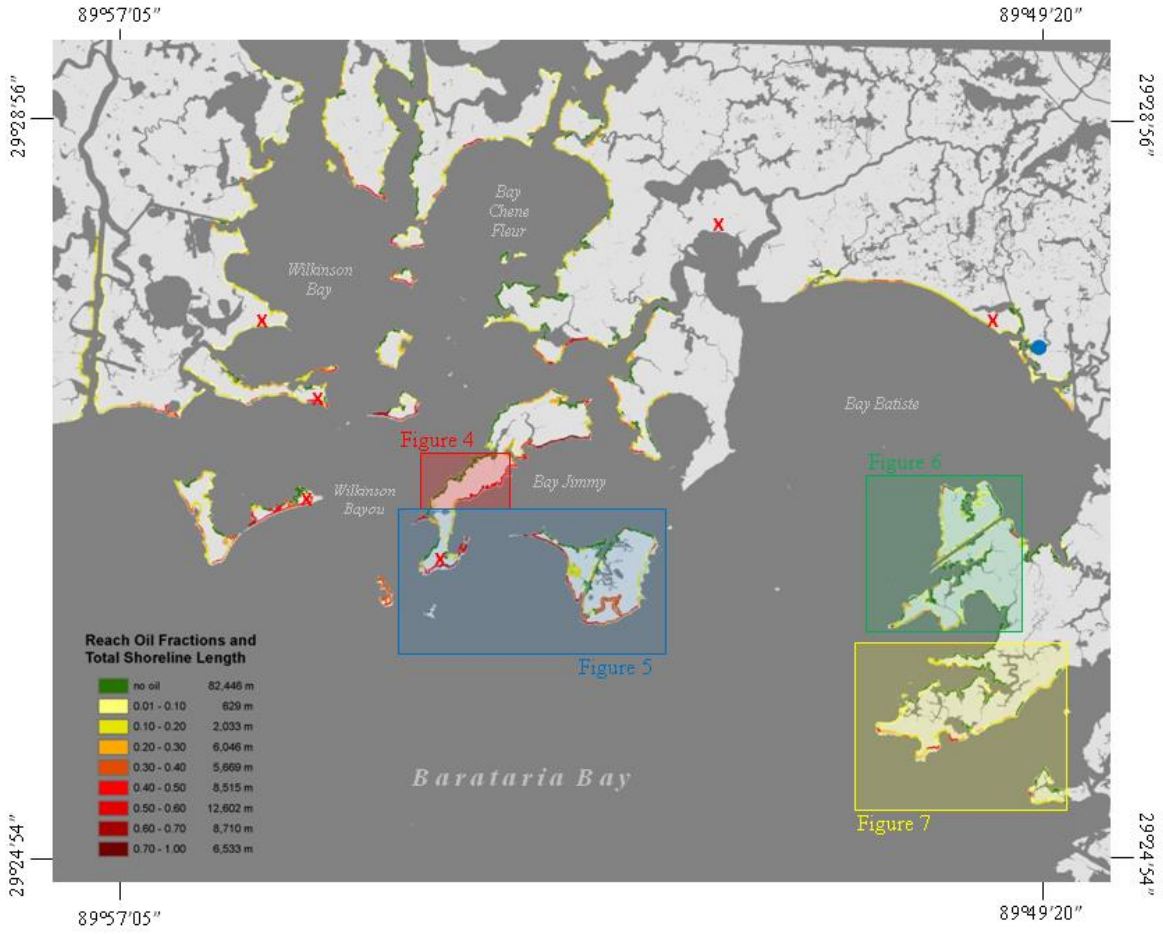

Figure 3.1: Upper Barataria Bay study area. Shows shoreline reach oil fractions, NDVI validation locations (red x's), water level measurement site (blue circle).

Soils in the lower Barataria Basin form on sediment and are tidally redistributed in the lower basin (Li et al., 2011). Soils (Timbalier, Lafitte, Bellpass, Clovelly, Scatlake series) are very poorly drained and consists of a moderate to thick layer (30-310 cm) of muck and fibrous peat (20% organic content) over clayey (coarse silt) alluvium with 0-0.2% slopes (Hatton et al., 1983). The lower Barataria Basin is a microtidal environment with a diurnal spring tidal range less than 0.6 m (Li et al., 2011). Diurnal tides and wind-driven winter storms account for frequent water exchanges between the lower Barataria Basin marshes and the Gulf of Mexico, while tropical storms account for infrequent, yet pronounced flooding of the marsh platform with saline water (Chuang and Wiseman, 1983).

Salt marshes of Barataria Bay are vegetated by dense monotypic stands of polyhaline and mesohaline macrophytes, with *Spartina alterniflora* and *Juncus roemerianus* commonly comprising more than 80% of the vegetation cover. *Distichlis spicata*, *Spartina patens*, *Phragmites australis*, *Schoenoplectus americanus* and *Schoenoplectus robustus* are also common (Visser et al., 1998; Lin and Mendelssohn, 2012; Beland et al., 2016). Non-inundated bare soil (e.g. mudflats, salt pannes, unvegetated marsh edges) cover accounts for < 2% of the total marsh area (Beland et al., 2016).

3.2.2 Oil fraction cover maps

The oil maps used here were generated using MESMA applied to Airborne Visible/Infrared Imaging Spectrometer (AVIRIS) imagery and published in Peterson et al. (2015). AVIRIS datasets were radiometrically calibrated, converted to apparent surface reflectance using Atmospheric Correction Now (ACORN 6.0, ImSpec LLC, Seattle), and ground-reflectance spectra from a calibration site (airport tarmac) were used to remove residual atmospheric features (Peterson et al., 2015). Peterson et al. (2015) used iterative

endmember selection (IES: Roth et al., 2012) to produce a spectral library of green vegetation, non-photosynthetic vegetation, soil and oiled marsh endmembers. Stable Zone Unmixing (SZU: Somers et al., 2010), InStability Index (ISI: Somers et al., 2009) and synthetic mixture modeling were used to identify an optimal subset of nine bands for discriminating endmembers, particularly bands that effectively separated spectrally similar oiled marsh and non-photosynthetic vegetation. Finally, two, three and four endmember models were run on each image, followed by an automated extraction process in which endmember combinations with the lowest RMSE and least complexity (fewest endmembers) were selected for each pixel and merged into a multiple endmember fractional cover dataset. The models were run on images from July 31, August 15, September 14, October 4, 2010 and May 4, 2011 to capture the movement of oil around Barataria Bay (Peterson et al., 2015). Accuracies for the image dates ranged from 87.5% to 93.3% with zero false positive detections (Peterson et al., 2015). Here, we created marsh oiling zones of 0-21m from the shoreline edge, and extracted the maximum oil fraction (per 3.5 m pixel) over a multi-temporal data set of oil maps (i.e. July 31, August 15, September 14, October 4, 2010 and May 4, 2011). Overall, the oil maps used here were consistent with the Shoreline Cleanup Assessment Technique (SCAT) maps used in previous studies (Michel et al., 2013; Rangoonwala et al., 2016), however, some discrepancies in oil coverage along shorelines were apparent. These variations were likely due to differing methodologies, reach extents and oil surface cover categories.

3.2.3 Mapping shoreline change: Remote sensing techniques

High resolution (0.30-0.64 m) orthorectified image datasets were acquired from DigitalGlobe (https://www.digitalglobe.com) and Aerometric Inc.

(http://gis.aerometric.net/dirlists.htm) for the four dates used in this study (S1 Table). The DigitalGlobe products were captured on the QuickBird-2 and WorldView-2 & 3 instruments (panchromatic and multispectral) at ground sample distances (GSD) ranging from 0.31 m to 0.64 m (Table 3.1). Aerometric Inc. four band (blue, green, red, near infrared) stereoscopic photographs have a GSD of 0.30m (RMSE < 1.2 m). A relative image-to-image accuracy of 0.77 m (RMSE) was achieved across all image dates.

We generated binary classification maps of marsh cover and open water for each image (S2 Figure). Marsh vegetation cover and open water are easily distinguishable in bands 4 (NIR) and 3 (red), so we utilized the Normalized Difference Vegetation Index (NDVI), and a binary threshold of -0.03 to create marsh land and open water cover classification maps. A -0.03 threshold was used to include mudflats in the marsh land class. Maps were assessed using field observations made contemporaneous with image acquisition dates (n = 289) from six field sites located along the marsh edge (Figure 3.1). Land and water were classified accurately for 97% of the observations. Mudflats and lakes located within the marsh interior that had no connectivity with large channels and bays were removed by converting the raster of water pixels into a polygon. This process was followed for all four image dates. Post-classification change detection analysis was performed to determine if marsh area was retained from the previous imaging date, or if a conversion from marsh to open water (i.e. land loss) had occurred.

Image acquisition time could affect the amount of water mapped due to tides, therefore, image data captured at or below mean low water (MLW) are ideal and acquisition at 1-2 feet (0.31 - 0.62 m) above MLW is acceptable for the northern Gulf of Mexico (Jensen et al., 1993; Dobson et al., 1995). Here, acquisition times for the data were at 17:10 (2006),

17:00 (2010), 21:25-21:31 (2013) and 16:44 UTC (2016), corresponding to tidal heights of 0.007, -0.031, 0.140 and 0.185 m from MLW (S1 Table). The tidal range (0.22 m) over all image acquisition periods is relatively small, and the maximum tidal height of 0.185 m above MLW (2016) is well within the preferred tidal range (< 0.31 m) stated previously (Jensen et al., 1993; Dobson et al., 1995). In addition, the ratio of erosion in oiled and non-oiled reaches should be insensitive to tidal effects because the background rate for non-oiled reaches is determined from the same image pair as the oiled reaches (see *Land loss analysis* section).

3.2.4 Land loss analysis

Image change analysis often uses pixel-wise comparisons over time. For analysis of marsh land loss along shorelines, both total area loss and the distance of shoreline retreat are important, so we aggregated the pixel data by shoreline reaches with a single orientation and oil fraction. A vector of the 2006 marsh shoreline was used as a baseline for generating transects every 100m using an onshore transect sampling algorithm. The sinuosity of the marsh shorelines and number of small marsh islands (< 1000 m^2) in the southern Barataria Basin resulted in frequently overlapping onshore transects and created shoreline reaches that were variable in length (S1 Figure). Where overlapping transects generated longshore reaches that were less than 15 m, the transects were manually removed, resulting in reaches that ranged in length from 15-172 m (S2 Table). We then examined land loss in relation to oil fractional cover along the segmented longshore reaches (N=1443, 133 km of marsh shoreline) (S2 Table). The ArcGIS zonal statistics tool was used to calculate the area of land loss per reach over each time period, and to calculate the mean oil fractional cover over the same shoreline reaches. Finally, the ArcGIS spatial join tool was used to link all the reach

attributes (shoreline reach length, land loss area for each time period and mean oil fraction) to a single shoreline vector file.

To account for the variable lengths of the created longshore reaches (15-172 m), we normalized the total land loss by the reach length to get a standardized loss rate (*slr*) in m yr^{-1}:

$$slr = \left(\frac{a}{l}\right)\Big/_{t} \qquad (1)$$

where *slr* is calculated as the land area loss (*a*) over the segmented longshore reach length (*l*) divided by the number of years between image acquisitions (*t*). The time intervals (*t*) between imaging dates were 3.4 (2006-2010), 3.6 (2010-2013) and 2.5 (2013-2016) years. We performed reach-level pair-wise T-tests, and then summarized the p-values for each oiling category to determine if post-oiling land loss rates were significantly different from the pre-oiling rates (Table 3.1).

Post-spill land loss rates were higher for all shoreline reaches, including non-oiled reaches, presumably due to normal erosion forces affecting all reaches, such as wave energy, currents, tides and sediment supply. Additionally, storm surge from Hurricane Isaac, which made landfall in the study area in August 2012, likely contributed to increased land losses during the first post-oiling period (2010-2013). Therefore, we estimated background loss rates (*blr*) for a given oiling category (*j*) for the post-oiling periods as:

$$blr_j = k(slr_j^{pre}) \qquad (2)$$

where k is the ratio of *slr* for post-oil (*slr post,no.oil*) and pre-oil (*slr, pre,no.oil*) periods for non-oiled reaches (oil cover = 0):

$$k = \frac{slr_{post,no.oil}}{slr_{pre,no.oil}} \quad (3)$$

For instance, the post-oiling (2010-2013) change coefficient (k_1 = 1.36) was calculated by dividing the post-oiling (2010-2013) period *slr* (0.36 m^2 m^{-1} yr^{-1}) by the pre-oiling *slr* (0.26 m^2 m^{-1} yr^{-1}) for non-oiled reaches. The oil-related loss rate (*olr*) is the difference between the observed *slr* and the *blr*. All three loss rates were converted into an area loss rate by multiplying the loss rate by the length of shoreline for each oiling category.

3.3. Results

3.3.1 General land loss patterns over the three periods

Sixty-two percent of the shoreline (N=993; 82,446 m) exhibited no detectable oiling (i.e. oil cover = 0) from July 2010 - April 2011 (Figure 3.1, Table 3.1, S2 Figure). Twenty-one percent of the shoreline had mean oil fractions greater than 50%, and the remaining 17% had mean oil fractions between 3 and 49% (Figure 3.1, Table 3.1). Shorter reaches (< 50m) could have a disproportionate effect on land loss rates along the shoreline, however, these reaches only accounted for 7% of the total shoreline length. Additionally, 91% of the shorter reaches (< 50 m) were along non-oiled shorelines.

Table 3.1. Annual land loss rates by reach oiling category and time period. Rows (oiling categories) and columns (time periods) also include background annual loss estimates and

resulting p-values for the reach-level pair-wise T-tests for Period 1 (2006-2010), Period 2 (2010-2013) and Period 3 (2013-2016) and for each oil category.

oil category	shoreline length (m)	2006-2010 (m^2/yr)	2010-2013 (m^2/yr)	2010-2013 *background*	2013-2016 (m^2/yr)	2013-2016 *background*	periods 1 & 2	periods 2 & 3	periods 1 & 3
no oiling	82,446	43,348	58,762	58,762	51,904	51,904	0.129	0.249	0.581
>0-10	629	29	402	39	132	34	0.146	0.302	0.095
20-Oct	2,033	385	1,070	522	1,074	461	0.253	0.91	0.143
20-30	6,046	2,254	7,351	3,056	2,378	2,699	***0.001***	***0.002***	0.849
30-40	5,669	1,923	9,481	2,607	2,313	2,302	***<0.001***	***0.002***	0.484
40-50	8,515	6,973	20,461	9,453	5,550	8,350	***0.006***	***<0.001***	0.368
50-60	12,602	9,771	29,840	13,245	9,701	11,699	***<0.001***	***<0.001***	0.357
60-70	8,710	6,022	16,748	8,163	7,626	7,211	***<0.001***	***<0.001***	0.616
70+	6,533	4,087	9,792	5,540	4,749	4,894	***0.023***	***0.046***	0.248
Total:	133,183	74,792	153,909	101,387	85,427	89,553	***<0.001***	***<0.001***	0.56

Total land loss during post-oiling period 1 (2010-2013) more than doubled the losses from the pre-oiling period (2006-2010) (Figure 3.2A), and then returned to near the pre-oiled rate in the post-oiling period 2 (2013-2016). Total land loss for all reaches increased from 74,702 m^2 yr^{-1} (0.49 m^2 m^{-1} yr^{-1}) to 153,676 m^2 yr^{-1} (1.44 m^2 m^{-1} yr^{-1}) from 2010-2013, and decreased to 85,388 m^2 yr^{-1} (0.58 m^2 m^{-1} yr^{-1}) from 2013-2016 (Figure 3.2A). For non-oiled reaches (82,446 m), the *slr* was highest during the first post-oil period (2010-2013, 0.71 m^2 m^{-1} yr^{-1}), however, there were no statistical differences in *slr* between 2010-2013 and the pre-oiling period (0.53 m^2 m^{-1} yr^{-1}, $p = 0.129$) or the 2013-2016 period (0.63 m^2 m^{-1} yr^{-1}, $p = 0.249$) (Table 3.1). Even though the land loss rates for non-oiled reaches were highest during the 2010-2013 period, their relative contribution to the total losses were low (Figure 3.2B). Land loss within non-oiled reaches contributed to 38% (58,762 m^2/yr) of the total land loss during 2010-2013, despite accounting for 62% of the shoreline length (Table 3.1). In comparison, land loss within non-oiled reaches accounted for 58% (43,348 m^2 yr^{-1}) and 61% (51,904 m^2 yr^{-1}) of the total land loss during the 2006-2010 and 2013-2016 periods,

respectively (Table 3.1), which is comparable to the percent shoreline length, suggesting non-oiled and oiled shorelines had similar relative contributions to land loss in pre- and the second post-oiled periods (Figure 3.2B). Furthermore, there was no statistical difference observed for any reach oiling categories from pre-oiling and post-oiling period 2 (2013-2016), suggesting land loss had returned to background rates by the second post-oiling period (2013-2016) (Table 3.1).

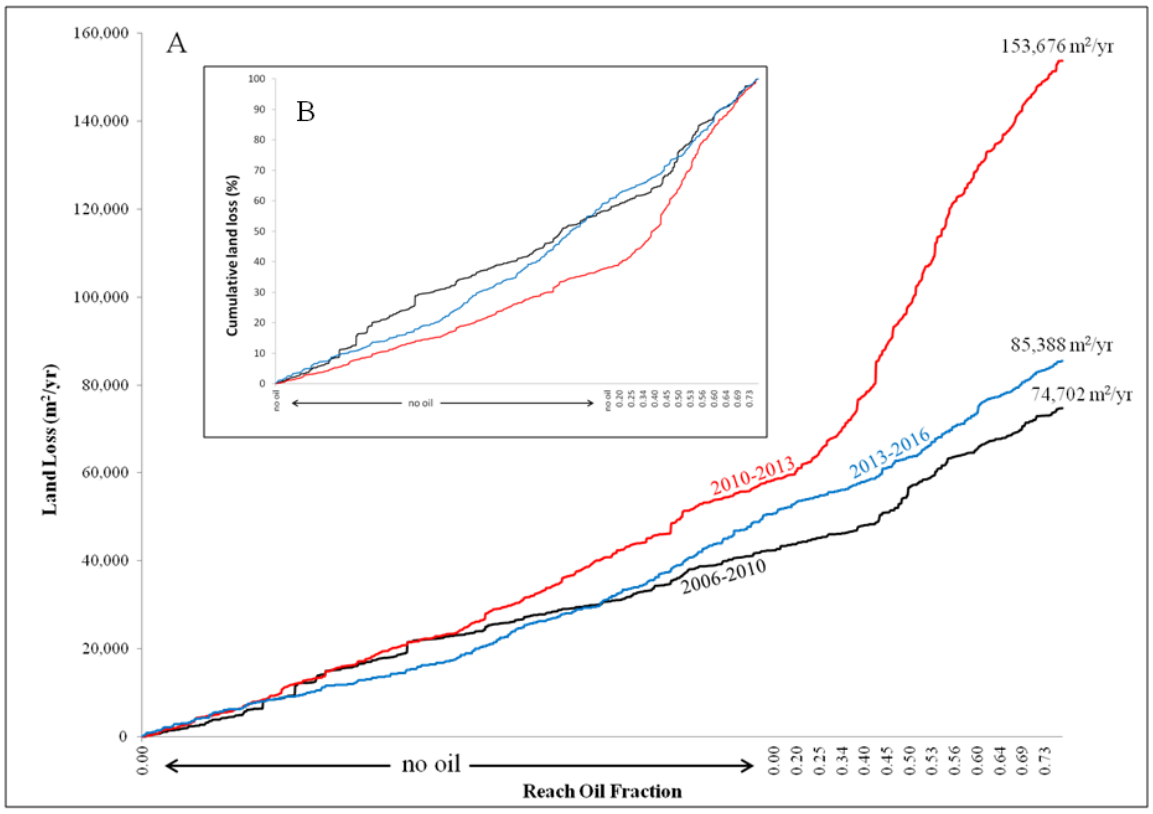

Figure 3.2: Cumulative land loss plots. Shows land losses in m^2yr^{-1} (A) and percent of cumulative losses (B) over reaches with increasing oil fractions for the three time periods.

3.3.2 Land loss trajectories along oiled reaches

Reaches with oiling, particularly mean oil fractions ≥20%, exhibited noticeably higher land loss rates during post-oiling period 1 (2010-2013) (Figure 3.3). Further, the trajectory of land loss rates during this period is significantly different than either the pre-oiling or post-oiling period 2 (2013-2016) (Figures 3.2 and 3.3, Table 3.1). The loss rates during the first post-oiling period are consistently and significantly higher ($p < 0.05$) than the pre-oiling period and post-oiling period 2 (2013-2016) for reaches with ≥20% oiling (Figure 3.3, Table 3.1), though land loss rates in post-oiling period 1 (2010-2013) do not increase monotonically with oiling and reached a maximum at 40-60% oiling. The decrease in loss rate for shorelines with >60% oiling may partly be a product of remediation efforts along the heaviest oiled shorelines as discussed in Zengel et al. (2015). For instance, the island in Bay Jimmy in Figure 3.4 (red box) received extensive treatment following oiling, including both mechanical and manual treatments, which may have contributed to suppressed shoreline erosion (Zengel et al., 2015). The average loss rates in post-oiling period 1 (2010-2013) for reaches with ≥20% oiling are more than three times the rates of both the pre-oiling and the post-oiling period 2 (Table 3.1). Reaches with ≥20% oiling (36% of shoreline length) accounted for 93,674 m^2 yr^{-1} of land loss, or 62% of the total land loss for the post-oiling period 1 (2010-2013). In comparison, the land losses from the pre-oiling period (31,030 m^2 yr^{-1}, 42% of total loss) and post-oiling period 2 (2013-2016: 32,317 m^2 yr^{-1}, 38% of total loss) are more similar to the relative length of the shorelines. Reaches with ≥50% oiling contributed 37% of the land loss during the post-oiling period 1 (2010-2013), while accounting for 21% of the shoreline length (Table 3.1).

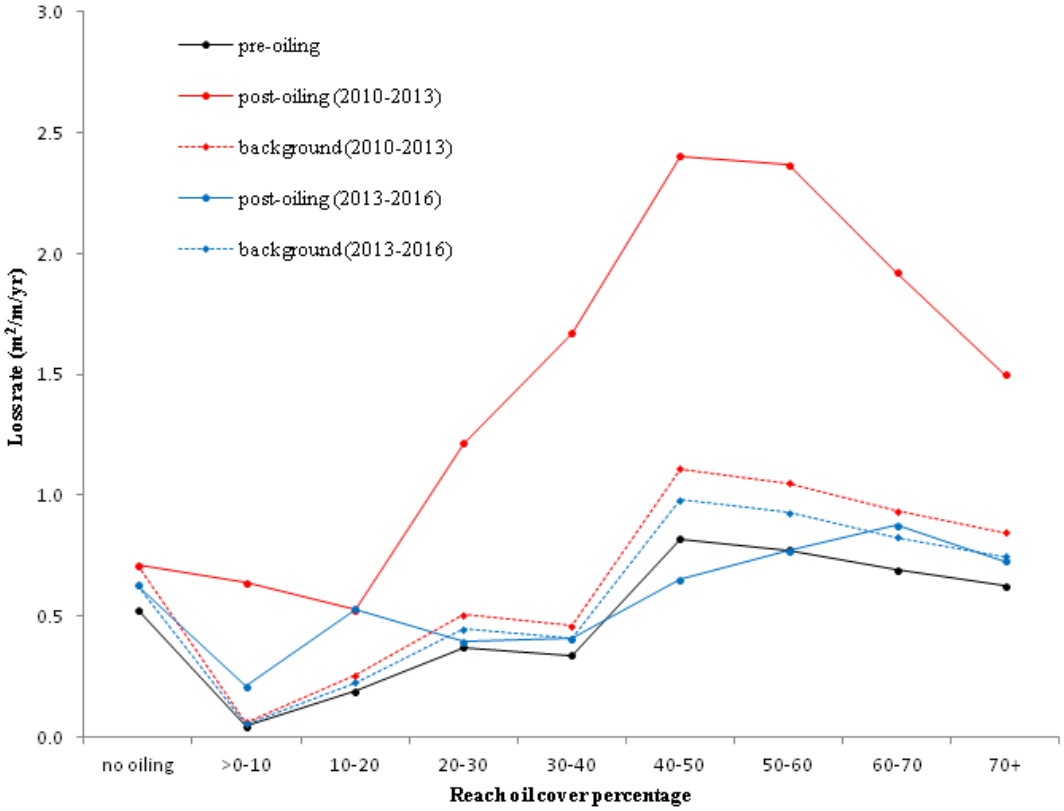

Figure 3.3: Land loss rates over reach oiling categories. Pre-oiling (2006-2010), post-oiling (2010-2013), post-oiling (2013-2016), and background land loss rates over reach oiling categories.

3.3.3 Background rates and oil-related land losses

Mean background loss rates along the shoreline are 0.65 and 0.58 m^2 m^{-1} yr^{-1} for oiled reaches, and range from 0.06-1.11 and 0.05-0.98 m^2/m/yr over the two consecutive post-oiling periods (Figure 3.3). Background land loss area for oiled reaches are 42,635 and 37,650 m^2/yr for the two post-oiled periods, accounting for 28% and 44% of the total losses (Table 3.1).

Total land losses along oiled reaches increased by 55%, or 52,521 m^2 yr^{-1}, in the first post-oil period (2010-2013), more than 80% of which are attributable to the 30-70% oiled reaches (Table 3.1). The background loss rate for post-oiling period 2 (2013-2016) accounts for all of the erosion observed. The estimated background loss rates were slightly higher than the observed loss rates for some reaches in the second post-oil period, which resulted in area loss estimates that were above the observed losses for the 40-60% oiled reaches (Figure 3.3, Table 3.1).

3.3.4 Spatial patterns of land loss

Two distinct spatial patterns are observed in the maps of progressive land loss over the three time periods (Figures 3.4-3.7). First, we observed substantial land loss along non-oiled, north facing shorelines. In Figure 3.5, non-oiled reaches (A) along the northern shoreline exhibit shoreline retreat and land loss over all three periods. A similar pattern of land loss is shown in Figure 3.6B, along the northeast facing non-oiled reach. Second, moderate to heavily oiled shorelines show the greatest losses, particularly in the post-oiling period 1 (2010-2013), and highest rates of land loss are predominantly along south and southeast facing shorelines as seen in Figures 3.4-3.7. In Figures 3.4,3.5 and 3.7, the south to southeast facing shorelines exhibit heavy oiling (A), and extensive land loss from 2010-2013 (B). These reaches exhibited far less shoreline retreat and land loss during the pre-oiling and 2013-2016 time periods (Figures 3.4B, 3.5B and 3.7B).

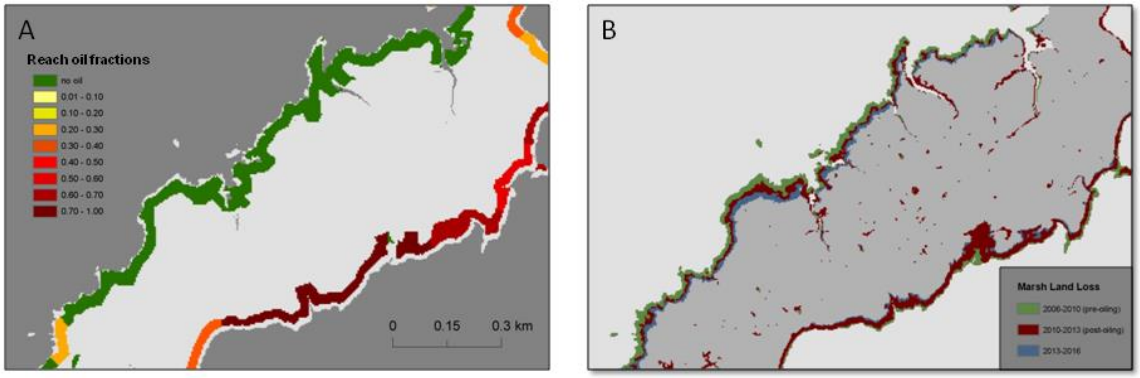

Figure 3.4: Maps of shoreline oiling category and corresponding land loss in Bay Jimmy (map location is shown in Fig.1). Map A shows shoreline zones and reach mean oil fractions, and map B shows marsh land loss along the same reaches over the three time periods. Narrow strip of the Bay Jimmy island (red box) is an area that experienced extensive oiling treatments for remediation.

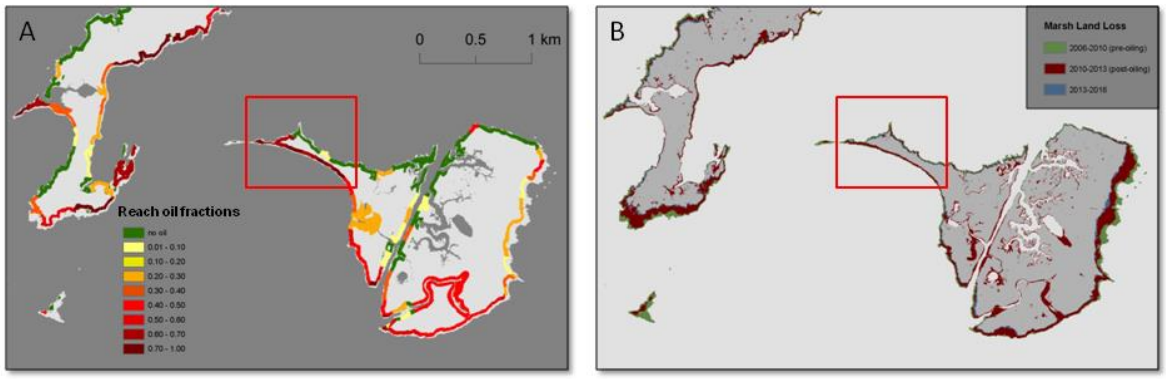

Figure 3.5. Maps of shoreline oiling category and corresponding land loss (map location is shown in Figure1). Map A shows shoreline zones and reach mean oil fractions, and map B shows marsh land loss along the same reaches of northern Bay Jimmy over the three time periods.

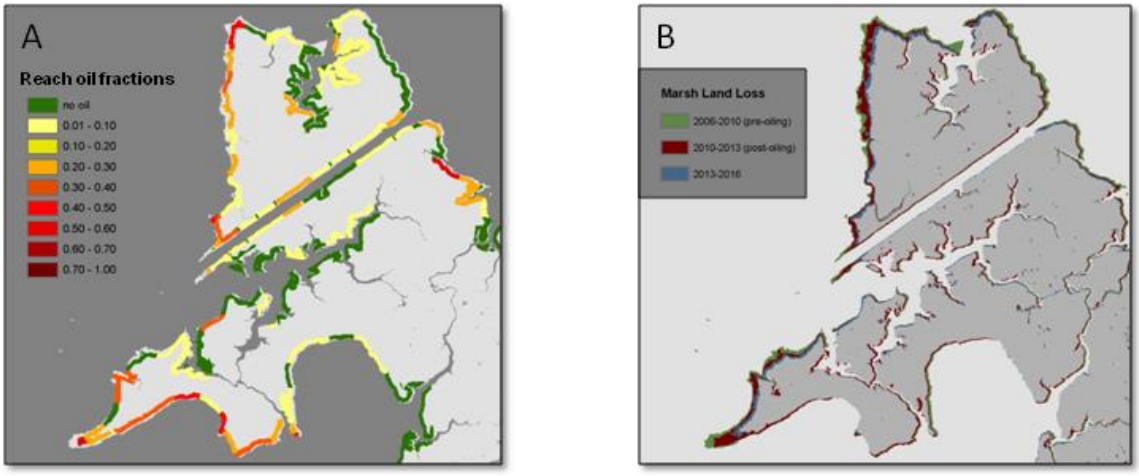

Figure 3.6: Maps of shoreline oiling category and corresponding land loss in Bay Batiste (map location is shown in Figure1). Map A shows shoreline zones and reach mean oil fractions, and map B shows marsh land loss along the same reaches of eastern Bay Batiste over the three time periods.

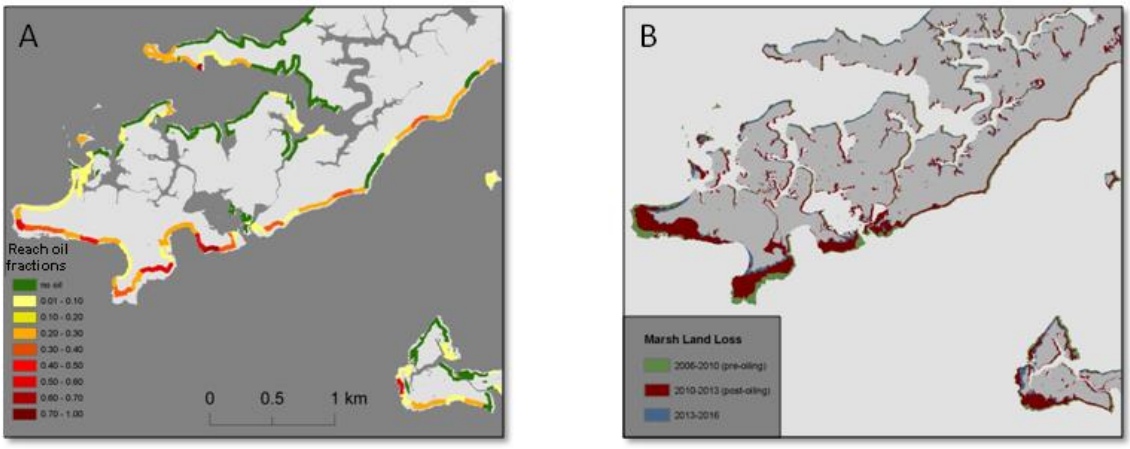

Figure 3.7: Maps of shoreline oiling category and corresponding land loss in Bay Batiste (map location is shown in Figure1). Map A shows shoreline zones and reach mean oil fractions, and map B shows marsh land loss along the same reaches of southeastern Bay Batiste over the three time periods.

3.4. Discussion

3.4.1 Land losses in historical context

The Mississippi River Delta, particularly the Terrebonne and Barataria basins, has among the highest land loss rates of any deltaic system in the United States (Couvillion et al., 2011), which is driven by both natural and anthropogenic forcings (DeLaune et al., 1994; Nyman et al., 1994; Ko and Day, 2004; Day et al., 2007; Morton and Bernier, 2010; Turner, 2011). Vertical erosion processes have been attributed to canal dredging, river channelization, land subsidence and sea-level-rise (Ko and Day, 2004; Day et al., 2007; Morton and Bernier, 2010; Turner, 2011), while wave energy has been the primary contributor to lateral erosion (i.e. marsh edge undercutting) forcings (DeLaune et al., 1994; Nyman et al., 1994; Sasser et al., 1986). Herein, we report overall land loss rates of 1.03% (2006-2010), 1.40% (2010-2013) and 1.23% (2013-2016) wetland area per year for non-oiled shoreline zones (i.e. $\leq$ 21m from marsh edge), which are consistent with earlier periods of land loss in Barataria Bay. Similar rates were reported for the 1956-1970 (0.70 - 1.2%) (Adams et al., 1976; Gagliano et al., 1981; Sasser et al., 1986; Turner, 1990; Evers et al., 1992) and the 1990-2000 time periods (0.90%; Barras et al., 2003). Our findings are higher than the rates reported from 1933-1956 (0.20 - 0.37%; Sasser et al., 1986; Evers et al., 1992; Couvillion et al., 2011) and 2000-2010 (0.49%); ; Couvillion et al., 2011), but less than the 1970-1990 peak loss period (1.90 - 2.04%; Sasser et al., 1986; Evers et al., 1992; Barras et al., 2007), which suggests that 2006-2016 was a period of intermediate rates of erosion from non-oiling related forces. The lower rates of land loss, during the 1933-1956 and 1990-2010 periods, are consistent with rates averaged over geological time scales that are attributable to sediment compaction and deep crustal loading (Morton and Bernier, 2010). The peak land

loss rates during the 1970-1990 period are likely the direct result of accelerated subsidence from fluid extraction for oil and gas production, which increased in the Mississippi Delta during the 1960's and 1970's (Morton and Bernier, 2010).

Our reported rates (i.e. 1.03%, 1.40% and 1.23% for the three periods) are somewhat higher than what Barras et al. (2007) (0.90%) and Couvillion et al. (2011) (0.49%) reported for the most recent pre-oil period (1990-2010). The observations of land loss conducted during these earlier studies used coarser spatial resolution imagery (Landsat: 30 m), which may account for some of the discrepancy in land loss rates. The difference in rates is more likely a result of our focus on near-shore marshes (i.e. $\leq$ 21m from marsh edge). Historically, interior marshes of Barataria Bay have comparatively low land loss rates (Couvillion et al., 2011), therefore, we expect that the percentage of total wetland loss would decrease to around the previously reported rates attributable to natural processes (i.e. 0.40-0.90 % yr^{-1}), if interior marshes were included in the analysis. A more appropriate comparison of non-oiled near-shore marsh loss rates is with the bay islands of Barataria Bay, due to their similar biogeomorphic profiles, which are comprised of low, relatively flat monotypic (i.e. *Spartina alterniflora* dominant) marsh platforms behind 30-50 cm natural levees at the marsh edge (Rangoonwala et al., 2016; Turner et al., 2016). Our annual wetland loss rates post-oiling (2010-2013: 1.40 % yr^{-1} and 2013-2016: 1.23% yr^{-1}) are comparable to the marsh island area loss rates of 1.5-1.6% reported in Turner et al. (2016) for non-oiled islands. Rates of shoreline retreat along non-oiled shorelines that are reported in our analysis (0.99 - 1.21 m yr^{-1}) are also similar to the rates reported previously in specific study sites of Barataria Bay (0.80-1.38 m yr^{-1}) (Wilson and Allison, 2008; Silliman et al., 2012; McClenachan et al., 2013).

3.4.2 Impact of oiling on land loss trajectory

Several recent studies have used remote sensing techniques to assess the impacts of oiling on salt marsh vegetation (Van Eerdt, 1985; Michel and Kirchner, 2002; Hester et al., 2001; Khanna et al., 2013; Beland et al., 2016) and marsh land loss (Beland et al., 2016; Rangoonwala et al., 2016; Turner et al., 2016). Herein, we take a unique approach to quantifying the impact of oiling on reach-scale and bay-wide loss rates, while controlling for temporal variability in natural background erosion rates. The most notable results from our analysis are: 1) the differences in land loss trajectories reported for the first 3-years post-oiling (2010-2013) and the other two periods, and 2) the magnitude of land loss beyond background rates. The curves of cumulative land loss by oiled fraction are relatively similar for the pre-oiling period and 3-6 years after oiling (2013-2016), and exhibit no significant differences across all reaches (Figure 3.2, Table 3.1). There is a striking increase in land loss rates during the 2010-2013 period for all reaches with oiling ≥20% (Figure 3.3). As expected, the substantial increase in loss rates contributed to total land losses that are more than double the period before (2006-2010) or after (2013-2016) (Table 3.1).

Heavy oiling has complex and interactive effects on the structural and physiological traits of marsh macrophytes that likely influence recovery success (Pezeshki and DeLaune, 1993; Delaune et al., 2003; Lin et al., 2016). Plant community composition (i.e. stem density, above- and belowground productivity) may influence residual oil concentrations and ecosystem response (Lin and Mendelssohn, 1996; DeLaune et al., 2003; Pezeshki et al., 2000; Lin and Mendelssohn, 2012). Most petroleum crude oils (e.g. south Louisiana crude) are nonionic, and therefore, associate more readily with organic particles (Pezeshki et al., 2000). Consequently, soil organic matter (SOM) in a marsh substrate impacts oil

concentrations, and SOM content varies depending on plant species composition (Lin and Mendelssohn, 1996). Lin and Mendelssohn (1996) reported both higher SOM content and higher oil residual concentrations in plots dominated by *Spartina patens* than those dominated by *S. alterniflora*. In both field and mesocosm experiments, *S. alterniflora* has exhibited a greater recovery rate than *Juncus roemerianus,* indicating a higher tolerance limit for oil contamination (Lin and Mendelssohn, 2012; Lin et al., 2016). Live aboveground biomass and stem density were about 10 times greater for *S. alterniflora* than *J. roemerianus* after 18 months under heavy oiling conditions (Lin and Mendelssohn, 2012). Recently, Beland et al. (2016) reported that only *S. alterniflora* dominated marshes were extensively degraded following the DWH spill, losing 15% (354,604 m^2) cover along oiled shorelines, suggesting that marsh degradation might have been worse if the oil-impacted marshes were dominated by other species i.e. (*J. roemerianus* or *S. patens*).

For heavily oiled shorelines (>50% oil fraction), we report loss rates 2.7 times greater (2.1 times for all oiled reaches) than that of non-oiled shorelines for the first 3-years after oiling. This magnitude of impact from oiling is consistent with observations of land loss on Barataria Bay marsh islands from Turner et al. (2016) and from site-specific studies (Silliman et al., 2012; Zengel et al., 2015), which have reported erosion rates at heavily oiled plots that were 2-3 times that of reference, non-oiled plots within 2 years of initial oiling. Our bay-wide results show that oiled shorelines experienced 2.1 times the loss rate of non-oiled shorelines over 3 years, which is in agreement with Turner et al. (2016) observations of oiled island shorelines that were 2.0 times greater than non-oiled islands over 2.5 years. Accounting for bay-wide background land losses from natural processes (42,625 $m^2\ yr^{-1}$), we determined

52,521 $m^2\ yr^{-1}$ of land was lost due to oiling, increasing the land losses by 52% over the background rate.

Two marsh erosion processes, driven by heavy oiling, were presumably contributing to the accelerated rates of land loss that we observed. Exposure to heavy oiling obstructs critical, adaptive mechanisms for reducing oxygen stress in anoxic soils (Pezeshki et al., 2000), and for controlling tissue salt (Na+ or Cl−) concentrations through osmotic adjustment (Pezeshki et al., 2000). Further, long-term (months to years) exposure to heavy residual oiling has resulted in reduced aboveground primary productivity and root matrix mortality, which are critical components of soil strength (Lin et al., 2002; Mishra et al., 2012; Lin et al., 2016; Ramsey et al., 2016; Shapiro et al., 2016). Consequently, above- and belowground plant loss and reductions in primary productivity have resulted in substrate instability and increased potential for shoreline erosion (Silliman et al., 2012; McClenachan et al., 2013; Zengel et al., 2015; Lin et al., 2016). Early assessments following the DWH spill reported widespread vegetation mortality and deterioration of the aboveground vegetation structure and function at heavily oiled sites (Lin and Mendelssohn, 2012; Silliman et al., 2012; Zengel et al., 2015), resulting in slow rates of recovery with aboveground biomass reaching only 50% of that in reference sites after 3.5 years (Zengel et al., 2015; Lin et al., 2016), and accelerated surface subsidence (vertical erosion) (Silliman et al., 2012; Lin et al., 2016). Further, heavily oiling in marsh soils have also resulted in losses of belowground biomass, weakening soil shear strength and accelerating the undercutting along marsh edges (McClenachan et al., 2013; Zengel et al., 2015).

The influence of other factors, including: oiling characteristics (Alexander and Webb, 1987; Mendelssohn et al., 1990; Hoff et al., 1993; Mendelssohn et al., 2012; Lin and

Mendelssohn, 1996; Hester and Mendelssohn, 2000; Pezeshki et al., 2000; DeLaune et al., 2003) and treatment methods (Baker et al., 1993; Sell et al., 1995; Hoff, 1995; Zengel and Michel, 2013; Zengel et al., 2015), environmental stressors (e.g. salinity, flooding, nutrients, predation) (Bertness and Shumway, 1993; Pennings and Bertness, 2001; Silliman and Bertness, 2002; Pennings et al., 2005), as well as complex and interactive marsh biogeochemical processes (Atlas et al., 2015; Marton et al., 2015; Bernhard et al., 2016; Turner and Bodker, 2016) make attributing the landscape-scale progression of marsh deterioration and land loss to oiling difficult (Hester et al., 2016; Rabalais and Turner, 2016; Turner et al., 2016). We attempt to control for the influence of these factors on land loss by calculating reach-scale background rates over the three periods between image acquisition dates.

This study is the first to show that land loss rates returned to pre-oiling levels within 3-6 years after oiling, and that no significant differences in land loss rates are exhibited for any oiling category between the pre-oiling and latter post-oiling periods ($p \geq 0.095$) (Table 3.1). Land loss was higher in the second post-oiling period (2013-2016) compared with pre-oiling, but non-oiled reaches accounted for 81% of this increase, which suggests that any increases in land loss related to oiling is negligible from three to six years after initial contamination.

We provided a landscape-scale, bay-wide quantification of land loss, while documenting the return to background erosion rates 3-6 years after oiling. Yet, several obvious questions remain unaddressed, such as: What is the relative importance of lateral erosional forces from wave action in comparison to vertical forces (i.e. reduced sediment accretion and subsidence) in Barataria Bay? Wilson and Allison (2008) estimated that 25%

of wetland losses in southeastern Louisiana are due to lateral erosion from wave action, particularly along shorelines exposed to long fetches and predominant direction of wave approach. Over the last century, shoreline erosion has likely accelerated in Barataria Bay as the conversion from marsh platform to open water has increased the fetch and wave energy on exposed marsh edges (Wilson and Allison, 2008). Oiling in Barataria Bay occurred most frequently on the south side of landmasses and marsh islands (Kokaly et al., 2012; Khanna et al., 2013), and we anticipated oil distribution might be correlated with pre-oiling shoreline erosion rates, due to the strong influence of currents, wave energy and tides on both processes (Turner et al., 2016). Yet, the land loss along non-oiled shorelines was substantial and relatively similar during all three time periods, and these loss rates were at least equal to the rates of oiled reaches during the pre-oiling period. Future research will need to explicitly investigate the compounding role wave action has on lateral erosion and overall land loss rates.

The impact of marsh treatments on bay-wide land losses is still largely unknown. Clean-up and treatment efforts affect the recovery process, both positively and negatively (Sell et al., 1995; Hoff, 1995). Aggressive treatment strategies, including the use of large cleanup crews or heavy machinery, have delayed marsh recovery or increased degradation by trampling live vegetation and churning oil into underlying sediments (Baker et l., 1993; Hoff, 1995; Zengel and Michel, 2013). Conversely, less intrusive treatments, which include the use of sorbents, bioremediation, and restricted cutting, have been shown to accelerate the rates of recovery (Sell et al., 1993; Lin and Mendelssohn, 2009). Two years after the DWH spill, Zengel et al. (2015) reported both mechanical and manual treatments exhibited greater improvements in oiling conditions and vegetation characteristics than the natural recovery

(reference sites). However, mechanical treatments increased oil mixing in soils and accelerated shoreline erosion (Zengel et al., 2015). Other analysis has indicated that shoreline erosion was similar on both treated and non-treated shorelines (Rangoonwala et al., 2016). Due to the potential impact of treatments, the location and treatment type should be regarded as a factor in a future analysis of marsh responses to oiling.

Finally, we showed that land losses increased significantly for the first three years after oiling, followed by a return to background erosion levels after three years. To date, this process of returning to background rates of erosion remains unexplained, and should be addressed in future research. Hester et al. (2016) reported evidence of vegetation stress (chlorosis), lower stem densities and productivity for the first 2.5 years, but few significant impacts to plant aboveground productivity (for plots that did not erode away) for heavily oiled plots 3.5 years after the DWH spill, which may suggest that vegetation recovery and presumably substrate stability had returned to heavily oiled marshes that were not eroded in the first three years. Conversely, Lin et al. (2016) reported that belowground biomass (0-12 cm) at heavily oiled plots was 76% less than reference sites after 3.5 years, which may suggest substrate instability is an ongoing problem. Further research is required on the interactions among belowground biomass recovery, resistance to wave-driven erosion, the sequence and magnitude of wave events, and subsequent shoreline erosion.

3.5. Conclusion

We examined the relative land loss rates of oiled shoreline reaches compared to non-oiled reaches of Barataria Bay over three consecutive time periods. Oiling increased total

land losses by 52,521 m^2 yr^{-1}, in the first post-oil period (2010-2013), more than 80% of which are attributable to the 30-70% oiled reaches. No statistical difference was observed for any reach oiling categories from pre-oiling and post-oiling period 2 (2013-2016). Oiling increased land loss by more than 50%, but land loss rates returned to background levels within 3-6 years after oiling, suggesting that oiling results in a large but temporary increase in shoreline loss.

We attempted to control for effect of other erosional forces (i.e. wave energy, variability in landscape position and geomorphic profile) on land loss by calculating the background rates (*blr*) derived from pre-oiling land loss patterns and post-oiling land loss in non-oiled reaches. Our calculation of *blr* assumes that the ratio between the loss rate in the pre-oil and post-oil period is the same under non-oiled conditions for all shoreline orientations and locations in the bay. Wave modeling could be included in future analysis to control for changes in shoreline orientations, wind direction and fetch between periods.

This study does not examine the relative contributions of oiling as it relates to other drivers of land loss, or efforts to suppress shoreline erosion following oil contamination. For instance, Rangoonwala et al. (2016) showed that storm surge from Hurricane Isaac (August 2012) contributed to a 2.5x increase in the shoreline length that experienced lateral recession of >12 m over a 4-month period. Further, Zengel et al. (2015) documented significant differences in the ecological responses of oiled marshes that received manual and mechanical treatments, and those not receiving remediation. Going forward, a spatially explicit model could determine the relative importance of multiple factors, including oiling (oil fractional cover), wave energy (significant wave height, period and length), vegetation composition (green and non-photosynthetic vegetation, aboveground biomass) and treatment type

(manual, mechanical and no remediation) on predicting land loss. The results from this analysis, along with a spatially-explicit predictive model, would help inform future management decisions regarding coastal wetland ecosystems.

3.6. References

Adams, R. D., Barrett, B. B., Blackmon, J. H., Gane, B. W., & McIntire, W. G. (1976). Barataria Basin: Geologic processes and framework. *Sea Grant Publication Louisiana State University Center Wetland Resources*, (8), 111.

Alexander, S.K., & Webb, J.W. (1987). Relationship of Spartina alterniflora growth to sediment oil content following an oil spill. Proceeding of the 1987 Oil Spill Conference. American Petroleum Institute, Washington, DC, pp. 445–449.

Atlas, R.M., Stoeckel, D.M. Faith, S.A. & Minard-Smith, A. (2015). Oil biodegradation and oil-degrading microbial populations in marsh sediments impacted by oil from the Deepwater Horizon well blowout. *Environmental Science & Technology* 49:8,356–8,366.

Baker, J.M., Guzman, L.M., Bartlett, P.D., Little, D.I., Wilson, C.M. (1993). Long-term fate and effects of untreated thick oil deposits on salt marshes. Proceedings, 1993 International Oil Spill Conference, American Petroleum Institute, Washington, D.C., pp. 395-399.

Barras, J., Beville, S., Britsch, D., Hartley, S., Hawes, S., Johnston, J., et al. (2003). *Historical and projected coastal Louisiana land changes: 1978-2050* (p. 39p). United States Geological Survey.

Barrett, B. (1970). Water measurements of coastal Louisiana: Louisiana Wildlife and Fisheries Commission, Division of Oysters, Water Bottoms and Seafood, p. 196.

Beland, M., Roberts, D. A., Peterson, S. H., Biggs, T. W., Kokaly, R. F., Piazza, S., et al. (2016). Mapping changing distributions of dominant species in oil-contaminated salt marshes of Louisiana using imaging spectroscopy. *Remote Sensing of Environment*, 182, 192-207.

Bernhard, A. E., Sheffer, R., Giblin, A. E., Marton, J. M., & Roberts, B. J. (2016). Population Dynamics and Community Composition of Ammonia Oxidizers in Salt Marshes after the Deepwater Horizon Oil Spill. *Frontiers in Microbiology*, 7, 854.

Bertness, M. D., & Shumway, S. W. (1993). Competition and facilitation in marsh plants. *The American Naturalist*, 142(4), 718-724.

Britsch, L. D., & Dunbar, J. B. (1993). Land loss rates: Louisiana coastal plain. *Journal of coastal research*, 324-338.

Chabreck, R H., "Vegetation, water and soil characteristics of the Louisiana coastal region" (1972).*LSU Agricultural Experiment Station Reports*. 147.

Chuang, W. S., & Wiseman, W. J. (1983). Coastal sea level response to frontal passages on the Louisiana-Texas shelf. *Journal of Geophysical Research: Oceans*, 88(C4), 2615-2620.

Couvillion, B.R., Barras, J.A., Steyer, G.D., Sleavin, W., Fischer, M., Beck, H., et al. (2011). Land area change in coastal Louisiana from 1932 to 2010: U.S. Geological Survey Scientific Investigations Map 3164, scale 1:265,000, 12 p. pamphlet.

Craig, N. J., Turner, R. E., & Day Jr, J. W. (1979). Land loss in coastal Louisiana (USA). *Environmental Management*, *3*(2), 133-144.

Culbertson, J. B., Valiela, I., Pickart, M., Peacock, E. E., & Reddy, C. M. (2008). Long-term consequences of residual petroleum on salt marsh grass. *Journal of Applied Ecology*, 45(4), 1284–1292.

Day, J. W., Boesch, D. F., Clairain, E. J., Kemp, G. P., Laska, S. B., Mitsch, W. J., et al. (2007). Restoration of the Mississippi Delta: lessons from hurricanes Katrina and Rita. *Science*, 315(5819), 1679-1684.

Day, J. W., Britsch, L. D., Hawes, S. R., Shaffer, G. P., Reed, D. J., & Cahoon, D. (2000). Pattern and process of land loss in the Mississippi Delta: a spatial and temporal analysis of wetland habitat change. *Estuaries*, 23(4), 425-438.

Deegan L., Kennedy H., and Neill C. (1984). Natural factors and human modifications contributing to marsh loss in Louisiana's Mississippi River deltaic plain. *Environmental Management*, 8 519–27.

DeLaune, R. D., Nyman, J. A., & Patrick Jr, W. H. (1994). Peat collapse, ponding and wetland loss in a rapidly submerging coastal marsh. *Journal of Coastal Research*, 1021-1030.

DeLaune, R. D., Pezeshki, S. R., Jugsujinda, A., & Lindau, C. W. (2003). Sensitivity of US Gulf of Mexico coastal marsh vegetation to crude oil: Comparison of greenhouse and field responses. *Aquatic Ecology*, 37(4), 351-360.

Dobson, J. E., Bright, E. A., Ferguson, R. L., Field, D. W., Wood, L. L., Haddad, K. D., et al. (1995). *NOAA Coastal Change Analysis Program (C-CAP): guidance for regional implementation* (p. 92). US Department of Commerce, National Oceanic and Atmospheric Administration, National Marine Fisheries Service.

Evers, D. E., Gosselink, J. G., Sasser, C. E., & Hill, J. M. (1992). Wetland loss dynamics in southwestern Barataria basin, Louisiana (USA), 1945–1985. *Wetlands Ecology and Management*, *2*(3), 103-118.

Feagin, R. A., Lozada-Bernard, S. M., Ravens, T. M., Möller, I., Yeager, K. M., & Baird, A. H. (2009). Does vegetation prevent wave erosion of salt marsh edges?. *Proceedings of the National Academy of Sciences*, 106(25), 10109-10113.

FitzGerald, D., Kulp, M., Hughes, Z., Georgiou, I., Miner, M., Penland, S., & Howes, N. (2007). Impacts of rising sea level to backbarrier wetlands, tidal inlets, and barrier islands: Barataria Coast, Louisiana. In *Proceedings of Coastal Sediments* (Vol. 7, pp. 179-1192).

Francalanci, S., Bendoni, M., Rinaldi, M., & Solari, L. (2013). Ecomorphodynamic evolution of salt marshes: Experimental observations of bank retreat processes. *Geomorphology*, 195, 53-65.

Gabet, E. J. (1998). Lateral migration and bank erosion in a saltmarsh tidal channel in San Francisco Bay, California. *Estuaries*, 21(4), 745-753.

Gagliano, S. M., Ashby, F. A., & Guidry, J. (1981). *Special report on marsh deterioration and land loss in the deltaic plain of coastal Louisiana*. Coastal Environments, Incorporated.

Gagliano, S. M., Kwon, H. J., & Van Beek, J. L. (1970). Deterioration and restoration of coastal wetlands. *Coastal Engineering Proceedings*, 1(12).

Gedan, K. B., Silliman, B. R., and Bertness, M. D. (2009). Centuries of human-driven change in salt marsh ecosystems. *Annual Review of Marine Science*, *1*, 117–141.

Hatton, R. S., DeLaune, R. D., & Patrick Jr, W. E. I. (1983). Sedimentation, accretion, and subsidence in marshes of Bar&aria Basin, Louisiana1. *Limnol. Oceanogr*, 28(3), 494-502.

Hershner, C., & Lake, J. (1980). Effects of chronic oil pollution on a salt-marsh grass community. *Marine Biology*, 56(2), 163-173.

Hester, M. W., & Mendelssohn, I. A. (2000). Long-term recovery of a Louisiana brackish marsh plant community from oil-spill impact: Vegetation response and mitigating effects of marsh surface elevation. *Marine Environmental Research*, 49(3), 233–254.

Hester, M. W., Mendelssohn, I. A., & McKee, K. L. (2001). Species and population variation to salinity stress in Panicum hemitomon, Spartina patens, and Spartina alterniflora: morphological and physiological constraints. *Environmental and Experimental Botany*, 46(3), 277-297.

Hester, M. W., Willis, J. M., Rouhani, S., Steinhoff, M. A., & Baker, M. C. (2016). Impacts of the Deepwater Horizon oil spill on the salt marsh vegetation of Louisiana. *Environmental Pollution*, 216, 361-370.

Hoff, R.Z., Shigenaka, G., & Henry, C.B. (1993). Saltmarsh recovery from a crude oil spill: vegetation, oil weathering, and response. Proceeding of the 1993 International Oil Spill Conference, pp. 307–311.

Hoff, R. (1995). Responding to oil spills in coastal marshes: The fine line between help and hindrance. HAZMAT Report 96-1. Hazardous Materials Response and Assessment Division, NOAA, Seattle, WA, 17 pp.

Jensen, J. R., Cowen, D. J., Althausen, J. D., Narumalani, S., & Weatherbee, O. (1993). The detection and prediction of sea level changes on coastal wetlands using satellite imagery and a geographic information system. *Geocarto International*, 8(4), 87-98.

Khanna, S., Santos, M. J., Koltunov, A., Shapiro, K. D., Lay, M., & Ustin, S. L. (2017). Marsh Loss Due to Cumulative Impacts of Hurricane Isaac and the Deepwater Horizon Oil Spill in Louisiana. *Remote Sensing*, 9(2), 169.

Khanna, S., Santos, M. J., Ustin, S. L., Koltunov, A., Kokaly, R. F., & Roberts, D. A. (2013). Detection of salt marsh vegetation stress and recovery after the deepwater horizon oil spill in barataria bay, Gulf of Mexico using AVIRIS data. *PloS one*, 8(11), e78989.

Ko, J.-Y., & Day, J. W. (2004). A review of ecological impacts of oil and gas development on coastal ecosystems in the Mississippi Delta. *Ocean & Coastal Management*, 47(11-12), 597–623.

Kokaly, R. F., Couvillion, B. R., Holloway, J. M., Roberts, D. A., Ustin, S. L., Peterson, S. H., et al. (2013). Spectroscopic remote sensing of the distribution and persistence of oil from the Deepwater Horizon spill in Barataria Bay marshes. *Remote Sensing of Environment*, 129, 210-230.

Lehr, B., Nristol, S., & Possolo, A. (2010). Oil Budget Calculator—Deepwater Horizon, technical documentation: a report to the National Incident Command. *Coastal Response Research Cent*er.

Li, C., White, J. R., Chen, C., Lin, H., Weeks, E., Galvan, K., & Bargu, S. (2011). Summertime tidal flushing of Barataria Bay: Transports of water and suspended sediments. *Journal of Geophysical Research: Oceans*, 116(C4).

Lin, Q., & Mendelssohn, I. A. (1996). A comparative investigation of the effects of south Louisiana crude oil on the vegetation of fresh, brackish and salt marshes. *Marine Pollution Bulletin*, 32(2), 202-209.

Lin, Q., & Mendelssohn, I.A. (2009). Potential of restoration and phytoremediation with Juncus roemerianus for diesel-contaminated coastal wetlands. *Ecological Engineering,* 35, 85–91.

Lin, Q., & Mendelssohn, I. A. (2012). Impacts and recovery of the Deepwater Horizon oil spill on vegetation structure and function of coastal salt marshes in the northern Gulf of Mexico. *Environmental science & technology*, 46(7), 3737-3743.

Lin, Q., Mendelssohn, I. A., Graham, S. A., Hou, A., Fleeger, J. W., & Deis, D. R. (2016). Response of salt marshes to oiling from the Deepwater Horizon spill: Implications for plant growth, soil surface-erosion, and shoreline stability. *Science of the Total Environment*, 557, 369-377.

Lin, Q., Mendelssohn, I. A., Suidan, M. T., Lee, K., & Venosa, A. D. (2002). The dose-response relationship between No. 2 fuel oil and the growth of the salt marsh grass, Spartina alterniflora. *Marine Pollution Bulletin*, 44(9), 897-902.

McClenachan, G., Eugene Turner, R., & Tweel, A. W. (2013). Effects of oil on the rate and trajectory of Louisiana marsh shoreline erosion. *Environmental Research Letters*, 8(4), 044030.

Mendelssohn, I.A., Anderson, G.L., Baltz, D., Caffey, R., Carman, K.R., Fleeger, J.W., et al. (2012). Oil impacts to coastal wetland: implications for the Mississippi River delta ecosystem after the Deepwater Horizon oil spill. *Biosciences*, 62, 562–574.

Mendelssohn, I.A., Hester, M.W., Sasser, C., & Fischel, M. (1990). The effect of Louisiana crude oil discharge from a pipeline break on the vegetation of a southeast Louisiana brackish marsh. *Oil and Chemical Pollution,* 7, 1–15.

Michel, E. R., & Kirchner, J. W. (2002). Effects of wet meadow riparian vegetation on streambank erosion. 2. Measurements of vegetated bank strength and consequences for failure mechanics. *Earth Surface Processes and Landforms*, 27(7), 687-697.

Michel, J., Owens, E. H., Zengel, S., Graham, A., Nixon, Z., Allard, T., et al. (2013). Extent and degree of shoreline oiling: Deepwater Horizon oil spill, Gulf of Mexico, USA. *PloS one*, 8(6), e65087.

Mishra, D. R., Cho, H. J., Ghosh, S., Fox, A., Downs, C., Merani, P. B., et al. (2012). Post-spill state of the marsh: Remote estimation of the ecological impact of the Gulf of Mexico oil spill on Louisiana Salt Marshes. *Remote Sensing of Environment*, 118, 176-185.

Marton, J. M., Roberts, B. J., Bernhard, A. E., & Giblin, A. E. (2015). Spatial and temporal variability of nitrification potential and ammonia-oxidizer abundances in louisiana salt marshes. *Estuaries and coasts*, 38(6), 1824-1837.

Morton, R. A., & Bernier, J. C. (2010). Recent subsidence-rate reductions in the Mississippi Delta and their geological implications. *Journal of Coastal Research*, 555-561.

Niering W.A., Warren R.S., Weymouth C.G. (1977). Our dynamic tidal marshes: vegetation changes as revealed by peat analysis. *Connecticut Arboretum Bulletin*, 22:2–12.

Nyman, J. A., Carloss, M., DeLaune, R. D., & Patrick Jr, W. H. (1994). Erosion rather than plant dieback as the mechanism of marsh loss in an estuarine marsh. *Earth Surface Processes and Landforms*, 19(1), 69-84.

Penland, S., & Ramsey, K. E. (1990). Relative sea-level rise in Louisiana and the Gulf of Mexico: 1908-1988. *Journal of Coastal Research*, 323-342.

Pennings S.C., Bertness M.D. (2001). Salt marsh communities. In: M.D. Bertness SDG, Hay ME, editors. Marine Community Ecology: Sinauer Associates.

Pennings, S. C., Grant, M. B., & Bertness, M. D. (2005). Plant zonation in low-latitude salt marshes: disentangling the roles of flooding, salinity and competition. *Journal of Ecology*, *93*(1), 159-167.

Peterson, S. H., Roberts, D. A., Beland, M., Kokaly, R. F., & Ustin, S. L. (2015). Oil detection in the coastal marshes of Louisiana using MESMA applied to band subsets of AVIRIS data. *Remote Sensing of Environment*, 159, 222-231.

Pezeshki, S. R., Hester, M. W., Lin, Q., & Nyman, J. A. (2000). The effects of oil spill and clean-up on dominant US Gulf coast marsh macrophytes: a review. *Environmental pollution*, 108(2), 129-139.

Pezeshki, S. R., & Laune, R. D. (1993). Effect of crude oil on gas exchange functions of Juncus roemerianus and Spartina alterniflora. *Water, Air, & Soil Pollution*, 68(3), 461-468.

Rabalais, N. N., & Turner, R. E. (2016). Effects of the Deepwater Horizon Oil Spill on Coastal Marshes and Associated Organisms. *Oceanography*, 29(3), 150-159.

Ramsey, E., Rangoonwala, A., & Jones, C. E. (2016). Marsh canopy structure changes and the Deepwater Horizon oil spill. *Remote Sensing of Environment*, 186, 350-357.

Rangoonwala, A., Jones, C. E., & Ramsey, E. (2016). Wetland shoreline recession in the Mississippi River Delta from petroleum oiling and cyclonic storms. *Geophysical Research Letters*, 43(22).

Roth, K. L., Dennison, P. E., & Roberts, D. A. (2012). Comparing endmember selection techniques for accurate mapping of plant species and land cover using imaging spectrometer data. *Remote Sensing of Environment*, *127*, 139-152.

Sasser, C. E., Dozier, M. D., Gosselink, J. G., & Hill, J. M. (1986). Spatial and temporal changes in Louisiana's Barataria Basin marshes, 1945–1980. *Environmental Management*, 10(5), 671-680.

Sasser, C. E., Gosselink, J. G., Swenson, E. M., & Evers, D. E. (1995). Hydrologic, vegetation, and substrate characteristics of floating marshes in sediment-rich wetlands of the Mississippi river delta plain, Louisiana, USA. *Wetlands Ecology and Management*, 3(3), 171-187.

Sell, D., Conway, L., Clark, T., Picken, G. B., Baker, J. M., Dunnet, G. M., et al. (1995). Scientific criteria to optimize oil spill cleanup. In *International Oil Spill Conference* (Vol. 1995, No. 1, pp. 595-610). American Petroleum Institute.

Shapiro, K., Khanna, S., & Ustin, S. L. (2016). Vegetation Impact and Recovery from Oil-Induced Stress on Three Ecologically Distinct Wetland Sites in the Gulf of Mexico. *Journal of Marine Science and Engineering*, 4(2), 33.

Silliman, B.R., & Bertness, M.D. (2002). A trophic cascade regulates salt marsh primary production. *Proceedings of the National Academy of Sciences*, 99, 10500–10505.

Silliman, B. R., van de Koppel, J., McCoy, M. W., Diller, J., Kasozi, G. N., Earl, K., et al. (2012). Degradation and resilience in Louisiana salt marshes after the BP–Deepwater Horizon oil spill. *Proceedings of the National Academy of Sciences*, 109(28), 11234–11239.

Smart, R. M., & Barko, J. W. (1978). Influence of sediment salinity and nutrients on the physiological ecology of selected salt marsh plants. *Estuarine and Coastal Marine Science*, 7(5), 487–495.

Somers, B., Delalieux, S., Verstraeten, W. W., Van Aardt, J. A. N., Albrigo, G. L., & Coppin, P. (2010). An automated waveband selection technique for optimized hyperspectral mixture analysis. *International Journal of Remote Sensing*, 31(20), 5549-5568.

Somers, B., Delalieux, S., Stuckens, J., Verstraeten, W. W., & Coppin, P. (2009). A weighted linear spectral mixture analysis approach to address endmember variability in agricultural production systems. *International Journal of Remote Sensing*, 30(1), 139-147.

Stedman, S. M., & Dahl, T. E. (2008). *Status and trends of wetlands in the coastal watersheds of the eastern United States, 1998 to 2004*. National Oceanic and Atmospheric Administration, National Marine Fisheries Service.

Turner, R.E. (1976). Geographic variations in salt marsh macrophyte production: a review. *Contributions in Marine Science*, 20:47–68.

Turner, R. E. (1990). Landscape development and coastal wetland losses in the northern Gulf of Mexico. *American Zoologist*, 30(1), 89-105.

Turner, R. E. (2011). Beneath the salt marsh canopy: loss of soil strength with increasing nutrient loads. *Estuaries and Coasts*, 34(5), 1084-1093.

Turner, R. E., & Bodker, J. E. (2016). The effects of N, P and crude oil on the decomposition of Spartina alterniflora. *Wetlands Ecology and Management*, 24(3), 373-380.

Turner, R. E., McClenachan, G., & Tweel, A. W. (2016). Islands in the oil: Quantifying salt marsh shoreline erosion after the Deepwater Horizon oiling. *Marine Pollution Bulletin*, 110(1), 316-323.

van de Koppel, J., van der Wal, D., Bakker, J. P., & Herman, P. M. (2005). Self-organization and vegetation collapse in salt marsh ecosystems. *The American Naturalist*, 165(1), E1-E12.

Van Eerdt, M. M. (1985). Salt marsh cliff stability in the Oosterschelde. *Earth Surface Processes and Landforms*, 10(2), 95-106.

Visser, J. M., Sasser, C. E., Chabreck, R. H., & Linscombe, R. G. (1998). Marsh vegetation types of the Mississippi River deltaic plain. *Estuaries*, 21(4), 818-828.

Weis J.S., & Weis P. (2004) Metal uptake, transport and release by wetland plants: implications for phytoremediation and restoration. *Environmental International*, 30:685–700b.

Wilson, C. A., & Allison, M. A. (2008). An equilibrium profile model for retreating marsh shorelines in southeast Louisiana. *Estuarine, Coastal and Shelf Science*, 80(4), 483-494.

Wu, T. H. (2013). Root reinforcement of soil: review of analytical models, test results, and applications to design. *Canadian Geotechnical Journal*, 50(3), 259-274.

Zengel, S., Bernik, B. M., Rutherford, N., Nixon, Z., & Michel, J. (2015). Heavily oiled salt marsh following the Deepwater Horizon oil spill, ecological comparisons of shoreline cleanup treatments and recovery. *PloS one*, 10(7), e0132324.

Zengel, S. & Michel, J. (2013). *Deepwater Horizon* Oil Spill: Salt Marsh Oiling Conditions, Treatment Testing, and Treatment History in Northern Barataria Bay, Louisiana (Interim Report October 2011). *U.S. Dept. of Commerce, NOAA Technical Memorandum NOS OR&R 42*. Seattle, WA: Emergency Response Division, NOAA. 74 pp.

Chapter 4: Interactive Contributions of Oiling and Wave Energy on Land Loss along Salt Marsh Boundaries

Abstract

The 2010 Deepwater Horizon (DWH) oil spill damaged salt marshes in the Mississippi River Delta, which have for decades experienced some of the highest land loss rates in the United States. Along marsh boundaries, where oiling was concentrated, wave action is the dominant physical driver of erosion and land loss. Disentangling the contribution of oiling and physical processes of erosion, in particular the effects of wave energy, on marsh boundary land loss is challenging. Here, we integrate a simple, fetch-limited wave climate model with high spatial resolution imagery that documents shoreline oiling and land loss to examine the interacting effects of wave characteristics and oiling on bay-wide land loss rates. Oiling was most severe along reaches with the highest wave energy, suggesting that it can be predicted with a simple wave model, and land loss rates correlated with wave energy in both oiled and non-oiled reaches. Land loss rates were higher on oiled reaches in the first post-oiling period (2010-2013) after controlling for wave height, but only for reaches with wave heights greater than 0.5 m (18 % of all reaches). Loss rates on oiled reaches decreased to less than that of non-oiled reaches in the second post-oiling period (2013-2016). Our results support previous findings that indicate oiling accelerates land loss rates, highlighting that high wave energy was necessary for oil-induced land loss.

4.1. Introduction

Salt marsh ecosystems of the Mississippi River Delta (MRD) provide a multitude of important ecosystem services, including storm surge protection, water quality enhancements, carbon sequestration, wildlife habitat, fisheries, and recreational opportunities (Mitsch and Gosselink, 2000; Reddy and DeLaune, 2008). However, human activities have altered the natural hydrologic regime and sediment loads for over a century (Deegan et al., 1984), resulting in coastal wetlands that are among the most vulnerable in the world to current and future land loss (Tessler et al., 2015). Mechanisms of both vertical and lateral erosion are contributing to high loss rates, which have been described colloquially as "a football field per hour" (Couvillion et al., 2011). The importance of specific physical factors and mechanisms that drive land loss are largely dependent on landscape position. For example, vertical erosion in the interiors of marshes, which accounts for ~75% of all wetland loss, is primarily the result of marsh platform subsidence and a lack of sediment accumulation, due to either reduced river discharge and reduced sediment deposition, or degraded substrate stability (Penland and Ramsey, 1990). Lateral erosion from direct exposure to wind-generated waves is the dominant erosional process along marsh boundaries (Delaune et al., 1994; Nyman et al., 1994; Sasser et al., 1995). Lateral erosion accounts for approximately 25% of all wetland losses in Louisiana, which is particularly prevalent along shorelines exposed to long fetches and predominant direction of wave approach (Penland and Ramsey, 1990; Wilson and Allison, 2008).

Oil spills have been shown to accelerate land loss rates (Lin and Mendelssohn, 2012; Silliman et al., 2012; Turner et al., 2016; Beland et al., 2017). Oil exposure from the DWH spill led to plant stress, reduced function, and mortality of marsh organisms (Lin and

Mendelssohn 2012; Silliman et al., 2012; Khanna et al., 2013; Zengel et al., 2015). Heavy oiling can cause an obstruction of critical, adaptive mechanisms for reducing oxygen stress and controlling tissue salt concentrations (Na^+ or Cl^-), resulting in long-term reductions in aboveground primary productivity, root matrix mortality, substrate instability, and increased potential for accelerated rates of shoreline erosion (Silliman et al., 2012; McClenachan et al., 2013; Zengel et al., 2015; Lin and Mendelssohn, 2016).

Tropical storms and hurricanes can act as both destructive and marsh building agents, and the spatial distribution of coastal wetland impacts from a single storm can vary greatly, depending on a marsh's position in relation to the storm track, antecedent conditions, and geomorphology (Guntenspergen et al., 1995; Stone et al., 1997). Tropical disturbances can cause severe vegetation damage, scouring of the marsh platform, and subsequent accumulation of wrack that hinders recovery (Cahoon et al., 1995; Guntenspergen et al., 1995; Khanna et al., 2017). Conversely, tropical storms and hurricanes are important mechanisms of sediment replenishment, particularly for vertically deteriorating marshes that have been cut off from fluvial sources of sedimentation (Cahoon et al., 1995; Guntenspergen et al., 1995).

Multiple disturbances in succession (e.g. oil spill followed by a high energy tropical storm) have the potential to hinder ecosystem recovery (Rangoonwala et al., 2016; Khanna et al., 2017). Given sufficient time to recover, salt marsh ecosystems are resilient to physical disturbances, due to their high productivity and intrinsic physiological traits for coping with stressful environmental conditions (Turner, 1976; Niering et al., 1977; Smart and Barko, 1978; Pezeshki and DeLaune, 1993). However, sequential disturbances, occurring repetitively in short time intervals, can result in greatly amplified land loss rates

(Rangoonwala et al., 2016; Khanna et al., 2017). Oiling weakens substrate stability along marsh boundaries by damaging vegetation and reducing above- and belowground biomass (Lin et al., 2002; Lin and Mendelssohn, 2012), and high winds and high energy waves associated with tropical storms and hurricanes can scour weak-rooted marsh platforms and remove unconsolidated topsoil along open water boundaries (Wilson and Allison, 2008; Rangoonwala et al., 2016).

Barataria Bay, a rapidly eroding abandoned delta, perhaps best exemplifies the state of intertidal marshes in the MRD (Craig et al., 1979; Fitzgerald et al., 2007). A combination of natural and anthropogenic factors, including reduced sediment deposition from the Mississippi River, compaction and subsidence of underlying deltaic deposits, flood control practices, and canal dredging have caused the rapid deterioration of marsh platforms in the lower Barataria Basin (Craig et al., 1979; Evers et al., 1992; Britsch and Dunbar, 1993; Ko and Day, 2004; Fitzgerald et al., 2007; Wilson and Allison, 2008). Since 1932, the lower Barataria Basin has been losing 15.1 km^2 of wetland area per year out of a total of 3833 km^2 (Britsch and Dunbar, 1993; Couvillion et al., 2011). Fetch and wind-generated waves have increased as more wetland area has been converted to open water, creating an erosion feedback mechanism (Wilson and Allison 2008).

In the spring of 2010, the largest oil spill in U.S. history occurred off the coast of Louisiana, when an explosion at the Deepwater Horizon (DWH) offshore drilling resulted in the release of 780,000 m^3 of crude oil before it was capped on July 15 (Lehr et al., 2010). Due in part to the prevailing currents and tides, the marshes of Barataria Bay were among the most severely impacted in the MRD (Michel et al., 2013). Oiling was concentrated along marsh boundaries (<21 m from the marsh edge).

Several recent studies conducted in Barataria Bay have linked the acceleration of land loss rates to the distribution of heavy oiling (Silliman et al., 2012, McClenahan et al., 2013, Rangoonwala et al., 2016; Khanna et al., 2017, Beland et al., 2017). Rangoonwala et al. (2016) investigated shoreline erosion following the DWH oil spill and Hurricane Isaac and reported a distinctive pattern of erosion caused by marsh boundary oiling. In the first year, shorelines that were heavily oiled and exposed to higher wave energy eroded; this was followed by erosion extending into areas subjected to less severe oiling and lower wave energy in the second year (Rangoonwala et al., 2016). Other work has pointed out that heavy-oiling occurred most frequently along seaward facing boundaries exposed to long fetches and thus potentially more vulnerable to lateral erosion from wave action (Turner et al., 2016). Yet, disentangling marsh responses to oiling from other physical factors remains a challenge.

To control for variations in physical erosion between controlled and oiled sites, two site-specific studies integrated wave models (Silliman et al., 2012; McClenachan et al., 2013). However, to date, we know of no research that has quantified the relationship between wave climate and heavily oiling along marsh boundaries, or determined the role played by wave energy in both the distribution of oil and land loss rates.

Here, we investigate the effects of wave energy on bay-wide trends in land loss rates along marsh boundaries, while controlling for variations in oiling along boundary segments. Our goal is to better explain the distribution of land losses after oiling by integrating a spatially explicit, yet simple, wave climate model to determine the spatial distribution of background rates of erosion before and after oil contamination. The following questions provide a framework for the analysis: 1) How strong is the relationship between marsh boundary oiling distribution and exposure to wave energy? 2) How do land loss rates differ

along heavily-oiled and non-oiled marsh boundaries across a range of wave energy exposures? and 3) Which factor (oiling or wave energy) has the strongest influence on erosion rates at three and six years after oiling? To address these questions, we generate a wind-wave model for Barataria Bay to compare marsh boundary wave energy characteristics and land loss rates for non-oiled and heavily-oiled (>20% areal surface cover) segments over a time period prior to oil exposure (2006-2010) and two periods following shoreline oiling (2010-2013, 2013-2016).

4.2. Methods

We used a combination of remote sensing, GIS, and wave modeling techniques to examine marsh boundary responses to oiling and wave action. The primary response variables are a time series of land loss rates (L_R) derived from a time series of high resolution (0.30-0.64 m) orthorectified image datasets (September 29, 2006; February 17, 2010; October 9, 2013; April 3, 2016). The rationale for examining land loss at near-three year time intervals derived from the shorter-term (~ 1 – 2.5 years) response patterns that have been well-documented by past investigations of land loss following the DWH oil spill (Silliman et al., 2012; Lin and Mendelssohn, 2012; McClenachan et al., 2013; Khanna et al., 2017; Rangoonwala et al., 2017; Turner et al., 2017); Further, the time intervals between image acquisition dates (1237, 1330, and 907 days) used in the analysis were constrained by the availability of high resolution images.

The variables used to predict L_R are surface oiling (%) and the 95th percentile significant wave height (H_s95). We calculated the background L_R for both oiled and non-oiled boundaries based on pre-spill observations (2006-2010) to determine the relationship

between L_R and H_s95 and to examine the oil-related amplification of L_R along heavily oiled boundaries.

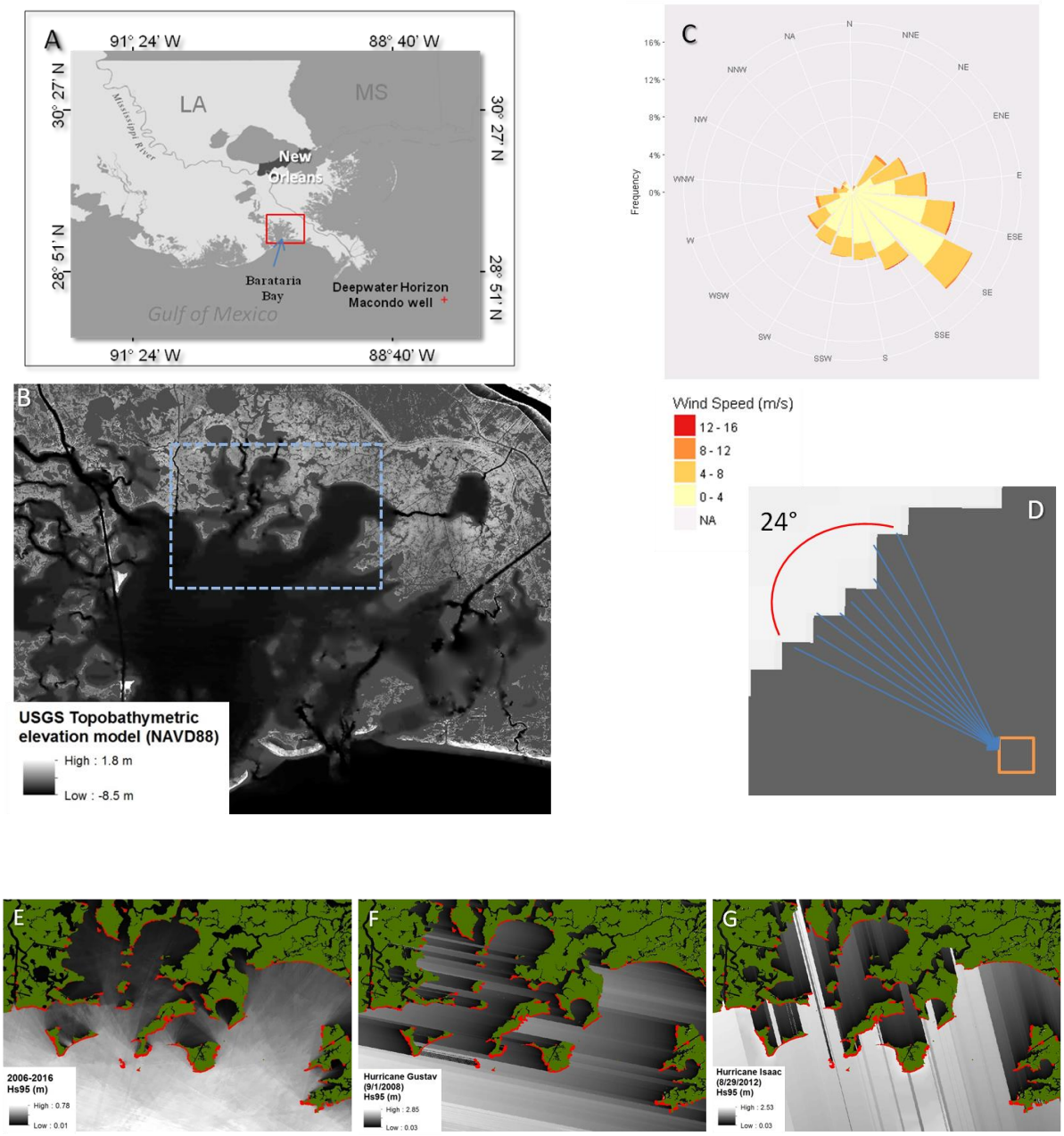

Figure 4.1: Study area map location (A) in Louisiana and within Barataria Bay (B). Topobathymetric range is shown in map B. Wind rose shows the prevailing wind direction over the study period (C). An example of the nine radials (3° interval) used in the fetch-limited method (D). Maps E-G show H_S95 results for the full study period (E), Hurricane Gustav (F) and Hurricane Isaac (G).

4.2.1 Study Area Description

The study area covers approximately 197 km^2 in northern Barataria Bay, Louisiana (29.43°N, 89.88°W) and consists of 41 km^2 of marsh and 133 km of marsh-ocean boundary (excluding interior channels and canal banks; Figure 4.1A-B). The Bay and surrounding wetlands are cut off from freshwater and sediment inputs from the Mississippi River and LaFourche Bayou. Surface elevations of salt marshes of Barataria Bay are fractions of a meter above sea level, are being impacted by sea level rise (Penland and Ramsey, 1990), and are highly vulnerable to natural and anthropogenic disturbances (Craig et al., 1979; Ko and Day, 2004; Day et al., 2000). Barrier islands, which form the southern boundary of Barataria Bay, are predominantly exposed to low-energy wind-generated waves (< 0.4 m) from the Gulf of Mexico, except during the passage of winter storms and infrequent hurricanes, when waves can exceed 3.0 m and cause widespread erosion, overwash, and breaches (Stone et al., 2005). Diurnal tides with a spring tide range of 0.46 m and wind-driven winter storms account for frequent water exchanges between the lower Barataria Basin marshes and the Gulf of Mexico, while tropical storms account for infrequent (1 every 7 years; Muller and Stone, 2001) yet pronounced flooding of the marsh platform with saline water (Chuang and Wiseman, 1983). Salt marshes of Barataria Bay are vegetated by dense monotypic stands of polyhaline and mesohaline macrophytes, with *Spartina alterniflora* and *Juncus roemerianus* commonly comprising more than 80% of the vegetation cover. Soils are very poorly drained and consist of vegetative mats that are 10 – 20 cm thick and moderate to thick layers (30 - 310 cm) of fibrous peat (20% organic content) over clayey (coarse silt) alluvium with negligible slopes (Hatton et al., 1983).

4.2.2 Marsh Boundary Land Loss Analysis

High spatial resolution (0.30-0.64 m) orthorectified image datasets were acquired from DigitalGlobe's QuickBird-2 and WorldView-2 & 3 instruments (https://www.digitalglobe.com) and stereoscopic aerial photographs from Aerometric Inc. (http://gis.aerometric.net/dirlists.htm), which collectively covered the four dates used in this study (Beland et al., 2017). Acquisition times for the DigitalGlobe datasets were at 17:10 (September 29, 2006), 17:00 (February 17, 2010), and 16:44 UTC (April 3, 2016), corresponding to tidal heights of 0.007, -0.031, and 0.185 m from mean low water (MLW). Image acquisition times for the Aerometric dataset were between 21:25 - 21:31 UTC on October 9, 2013, corresponding to a tidal height of 0.140 m MLW. The maximum tidal height of 0.185 m MLW (2016) is well within the tidal range (< 0.31 m) stated in previous works for minimizing change detection errors in intertidal environments (Jensen et al., 1993; Dobson et al., 1995). Images were resampled to 0.64 m, and a relative image-to-image registration root-mean-square error (RMSE) of 0.77 m was achieved across all image dates.

A Normalized Difference Vegetation Index (NDVI) and a binary classification system (i.e. marsh, including vegetation, bare soil, and open water) were applied to QuickBird (2006), WorldView (2010 and 2016) and Aerometric (2013) images to generate a time series of maps documenting marsh boundary land loss. Further details of the image processing techniques used to generate these maps were published in Beland et al. (2017). Following land and water classification, image masks were used to create shoreline vectors for each image acquisition date and to generate polygons of the land loss that occurred between each date.

4.2.3 Shoreline Segmentation and Land Loss Analysis

For land loss analysis, both total area loss and the distance of shoreline retreat are valuable measures of change, so we aggregated pixel-scale data into shoreline segments, or reaches (Beland et al., 2017). Determining the appropriate lengths of reaches along marsh boundaries is an important component of land loss analysis as the relative influence of different erosional processes changes with scale (Priestas et al., 2015). Through visual examination of previously published oil maps (Kokaly et al., 2013; Michel et al., 2013; Peterson et al., 2015), we concluded that reaches of approximately 30 m would sufficiently capture the patchiness of oil exposure, while reducing the effects of localized influences (<10 m), like macrofauna burrowing and herbivory, on reach-scale observations (Holdredge et al., 2009; Davidson and De Rivera, 2010).

Longshore segments of 30 m were created for each of the four imaging dates using an onshore transect sampling algorithm (N = 2440, 138 km of marsh shoreline). Boundary sinuosity, small marsh peninsulas, and islands (< 1000 m^2) created overlap of onshore transects that resulted in longshore reaches of variable length, and in some cases, boundary absence in the latter time periods. Some overlapping onshore transects along peninsular and island boundaries were manually removed to eliminate short longshore reaches (< 15 m) and to avoid boundary absence problems, which resulted in wide ranging segment lengths (15-619 m). However, more than 90% of the reaches were between 20 - 99 m.

Our preliminary analysis included reach-scale marsh boundary sinuosity calculations. However, the degree of shoreline sinuosity appeared to have no statistical effect on land loss rates ($R^2 < 0.01$; $p > 0.01$). Therefore we omitted shoreline sinuosity from this analysis, but acknowledge that marsh boundary geometry and morphology are likely factors in lateral

erosion rates at finer temporal (i.e. months to a year) and spatial scales (i.e. < 30 m) as reported in previous studies (Priestas et al., 2015).

4.2.4 Shoreline Oiling

Mean surface oiling percentages were calculated for each reach from the maps generated in Peterson et al. (2015) and used in previous analyses of oil impacts (Beland et al., 2016; 2017). Peterson et al. (2015) used multiple endmember spectral mixture analysis (MESMA), applied to Airborne Visible/Infrared Imaging Spectrometer (AVIRIS) imagery (*see* Peterson et al., 2015, *for details on MESMA*). AVIRIS datasets were radiometrically calibrated and converted to apparent surface reflectance using Atmospheric Correction Now (ACORN 6.0, ImSpec LLC, Seattle). Ground-reflectance spectra from a calibration site (airport tarmac) were used to remove residual atmospheric features (Peterson et al., 2015). Using a spectral library of green vegetation, non-photosynthetic (senesced) vegetation, soil, and oiled marsh endmembers, MESMA was run on radiometrically corrected images from July 31, August 15, September 14, October 4, 2010, and May 4, 2011 to capture the movement and deposition of oil around Barataria Bay. Accuracies for the image dates ranged from 87.5% to 93.3% with zero false positive detections (Peterson et al., 2015). Overall, the MESMA-generated oil maps were consistent with the Shoreline Cleanup Assessment Technique (SCAT) maps used in previous studies (Michel et al., 2013; Rangoonwala et al., 2016). The discrepancies that were observed between these oil maps were likely the result of differing methodologies, reach extents, and oil surface cover categories. For instance, we used MESMA-generated fractional (per pixel) oil maps derived from images, rather than descriptive categories (i.e. low, moderate, and high) based on field observations.

We created oiling zones of 0-21 m from the marsh boundary edge and extracted the maximum oil percentage (per 3.5 m pixel) over for the four dates of AVIRIS imagery (July 31, August 15, September 14, October 4, 2010, and May 4, 2011; Figure 4.1E-G). Our designation of "heavily oiled" for those shoreline reaches exhibiting surface oiling of ≥ 20% was in agreement with the SCAT surveys (Michel et al., 2013). In total, 92% of the reaches with ≥ 20% oiling on our MESMA-generated oil maps were classified as either "heavily" or "moderately" oiled during the SCAT field surveys (Michel et al., 2013).

4.2.5 Wind-wave Model

Wave characteristics were computed for each reach using the United States Geological Survey (USGS) Waves model (Rohweder et al., 2008), which uses wind fetch, wind direction, wind speed (two-minute means), and bathymetric data as inputs to hindcast significant wave height, wavelength and peak spectral period according to equations documented in the United States Army Corps of Engineers Shore Protection Manual (USACE, 1984) and the Coastal Engineering Manual (USACE, 2002). Effective fetch was calculated using the method recommended by the USACE Shore Protection Manual for fetch-limited water bodies as wave generation is often significantly lower for inland waters when compared to open waters under the same generating conditions (USACE, 1977). The fetch-limited method spreads nine radials about the wind direction at 3-degree increments and calculates the mean fetch length from the nine radials (Figure 4.1D: USACE, 1984; Rohweder et al., 2008). For water depth, we used an integrated topobathymetric elevation model (spatial resolution = 3 m) created by the USGS National Geospatial Technical Operations Center (USGS dataset accessed December 17, 2014 at http://earthexplorer.usgs.gov). The Barataria Bay portion of the project (Barataria LiDAR

Data Collection Project) was conducted from March 5-8, 2013. Fetch lengths were calculated along the bearing of potential wind directions (i.e. 0° - 360°) for all cells in the topobathymetric elevation model using the aforementioned fetch-limited method. Topobathymetric elevations ranged from -8.5 – 1.8 m relative to the North American Vertical Datum of 1988 (NAVD88, Figure 4.1B). Wind data for the three periods between image dates were obtained from the National Oceanic and Atmospheric Administration (NOAA) meteorological station in Grand Isle, LA (Station ID: 8761724, https://tidesandcurrents.noaa.gov). The Grand Isle station is located approximately 21 km southwest of our study area.

Using the Rohweder et al. (2008) 2-dimensional wave model and inputs for fetch length, wind speed and direction (6-minute means), water density (1025 kg/m^3), and topobathymetric data, we derived cell-by-cell (3 m resolution) daily significant wave height, spectral wave peak period, and wave length. We examined the relationships among several wave action variables and background land loss rates, including the 50th percentile significant wave height (H_s50) and spectral peak wave period (T_p50) to estimate the frequent, low-energy events, and the 95th percentile significant wave height (H_s95) to estimate the infrequent, high-energy events. We averaged these parameters over each time period between image acquisition dates (hereafter referred to as the "three time periods") and for each marsh boundary reach.

Wave energy flux, or wave power, is proportional to T_p times the square of H_s (Young and Verhagen 1996; McLouglin et al., 2015; Leonardi et al., 2016); therefore, we used H_s50 and T_p50 for the three time periods leading up to imaging dates to estimate the wave energy flux (P) for each marsh boundary segment using:

$$P_i = \frac{\rho g^2 T_p H_s^2}{32\pi} \quad (4)$$

where P_i is the wave power (expressed in W/m of crest length) for the ith boundary segment, $\rho$is the water density (1025 kg/m^3), g^2 is the gravitational acceleration constant (9.8 m/**s**^{2}) squared, H_s^2 is the significant wave height squared, and T_p is the peak wave period.

4.2.6 Analysis

The relationships between land loss rates *(L_R)* and the main driving factors (wave energy, wave power and marsh boundary oiling percentage) were explored and tested using simple linear regression and analysis of variance (ANOVA). Through regression analysis, we explored relationships between: a) H_s, b) P_i , c) L_R for the pre-oiling (2006-2010) and post-oiling (2010-2013, 2013-2016) time periods, and d) wave energy and oiling. ANOVA was utilized to determine if the mean values for oiling and wave energy groups were significantly different for oiled and non-oiled shorelines and over the three time periods.

4.3. Results

4.3.1 Wind-wave climate

The prevailing winds over the ten-year timeframe (2006-2016) were out of the south, southeast (SE), and east directions, accounting for 35% of the mean daily wind direction (Figure 4.1C). Wind direction was similar over the three time periods; however, SE winds were more prevalent during the pre-oil (2006-2010) period (Table 4.1). The mean wind speeds over the three time periods were 3.6, 3.8 and 4.0 m/s, respectively, and mean hourly wind speeds ranged from 0.0 - 25.5, 0.0 - 27.2, and 0.0 -17.6 m/s over the three time periods.

Generally, the marsh boundaries with the longest fetches faced S and SE, and these fetches ranged from approximately 4 to 21 km (Figure 4.1B).

Two extreme events, Hurricanes Isaac (August 2012) and Gustav (September 2008), accounted for the top 19 mean hourly wind speeds over the study period (2006-2016) ranging from 17.8 to 27.2 m/s (Figure 4.1F-G). Hurricane Isaac sustained mean hourly wind speeds of >17.5 m/s for a ten hour period between August 28-29, 2012, and Hurricane Gustav sustained mean hourly wind speeds ≥15.9 m/s for a ten hour period on September 1, 2008. The average for the top 5% mean hourly wind speeds was 13.5 m/s with observed wind speeds that were slightly greater over the first two time periods (2006-2010 = 13.7 m/s, 2010-2013 = 13.8 m/s) than the last time period (2013-2016 = 12.8 m/s) (Table 4.1). The prevailing wind directions of the top 5% mean hourly wind speeds were SSE and ESE.

Table 4.1: Wind speeds, wave period (T_p50), significant wave height (H_s50 and H_s95), wave power (P_i), and land loss rates (L_R).

Time Period	daily mean wd spd (ms^{-1})	95% wd spd (ms^{-1})	T_p50 (s)	H_s50 (m)	P_i(Wm^{-1})	H_s95 (m)		L_R ($m^2m^{-1}yr^{-1}$)	
						NO OIL	*OIL*	*NO OIL*	*OIL*
2006-2010	3.6	13.7	0.69	0.04	32.30	0.20	0.38	0.72	1.29
2010-2013	3.8	13.8	0.79	0.06	98.94	0.23	0.44	1.04	2.71
2013-2016	4.0	12.8	0.78	0.06	91.60	0.24	0.42	0.84	0.86

4.3.2 Wave height, period and energy flux

The mean spectral peak wave periods (T_p50) varied between 0.24 and 2.66 s with an overall mean of 0.76 sec, and only a 0.1 sec difference for the three periods between imaging dates (Table 4.1). Mean H_s50 and mean H_s95 were 5 and 29 cm with ranges from 1 to 31 cm and 5 to 71 cm, respectively (Table 4.1). Mean H_s50 and mean H_s95 are consistent for the

three time periods with only 2 cm and 4 cm differences between them, respectively (Table 4.1). Further, the T_p50 showed only a 0.1 sec difference for the three periods between imaging dates (Table 4.1). The mean wave power was 74.28 Wm^{-1} (Table 4.1); however, the estimates varied greatly, increasing by four orders of magnitude from the lowest (0.02 Wm^{-1}) to the highest (253.37 Wm^{-1}) power.

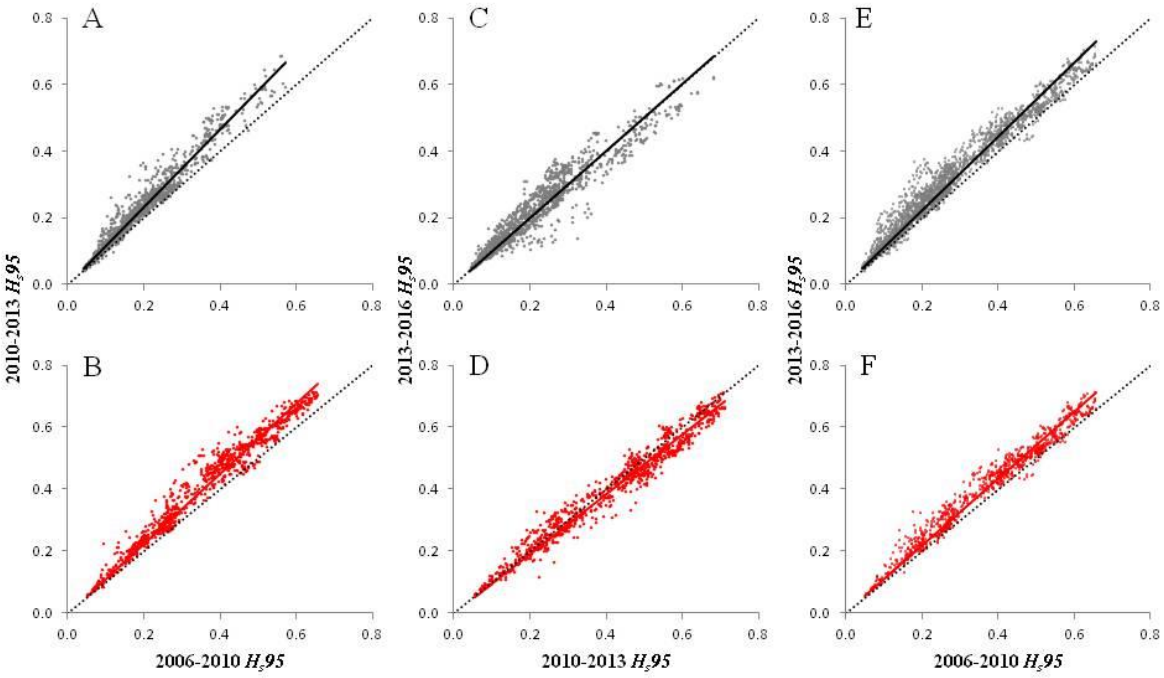

Figure 4.2: Time period comparisons of reach-scale H_s95 (m) for non-oiled (A,C,E) and oiled shorelines (B,D,F). Plots A & B show the relationships in H_s95 between the 2006-2010 and the 2010-2013 periods for non-oiled reaches (R^2 = 0.96) and oiled reaches (R^2 = 0.96). Plots C & D show the relationships in H_s95 between the 2010-2013 and the 2013-2016 periods for non-oiled reaches (R^2 = 0.91) and oiled reaches (R^2 = 0.96). Plots E & F show the relationships in H_s95 between the 2006-2010 and the 2013-2016 periods for non-oiled reaches (R^2 = 0.96) and oiled reaches (R^2 = 0.96).

The relationship between reach-level H_S95 and land loss rates is significant but weak ($R^2 = 0.28$, p value <0.0001) but it is stronger than for the H_S50 ($R^2 = 0.19$), T_p50 ($R^2 = 0.17$) and P_i ($R^2 = 0.15$). Therefore, we selected H_S95 as the wave energy variable for predicting land loss rates under non-oiled conditions. Time period comparisons of reach-level H_S95 showed that all three periods are highly correlated (R2 > 0.90, p< 0.0001) and exhibit little variability (SE < 0.026) for both oiled and non-oiled boundaries (Figure 4.2). The slopes of the regression lines are between 0.83 and 1.17 (Figure 4.2). Overall, the H_S95 for 2010-2013 and 2013-2016 are slightly higher than for 2006-2010 (Figure 4.2).

Generally, the south- and southeast-facing marsh boundaries exhibit the highest surface oiling percentages, due in part to their direct exposure to currents and tides (Turner et al., 2016). Interestingly, many of the same boundaries were exposed to the longest fetches in the study area, resulting in the highest significant wave heights (Figure 4.1E-G). Therefore, we expected the boundary reaches with the highest H_s95 would be good predictors of heavy oiling. H_S95 was a moderately good predictor of the degree of marsh boundary surface oiling ($R^2 = 0.34$; $p < 0.0001$, Figure 4.3). In general, the marsh boundaries that experienced heavy oiling in 2010 had the highest H_s95 in all three time periods (Table 4.1). Further, oiling percentage increases monotonically when the H_S95 is grouped by 10 cm intervals (Figure 4.3).

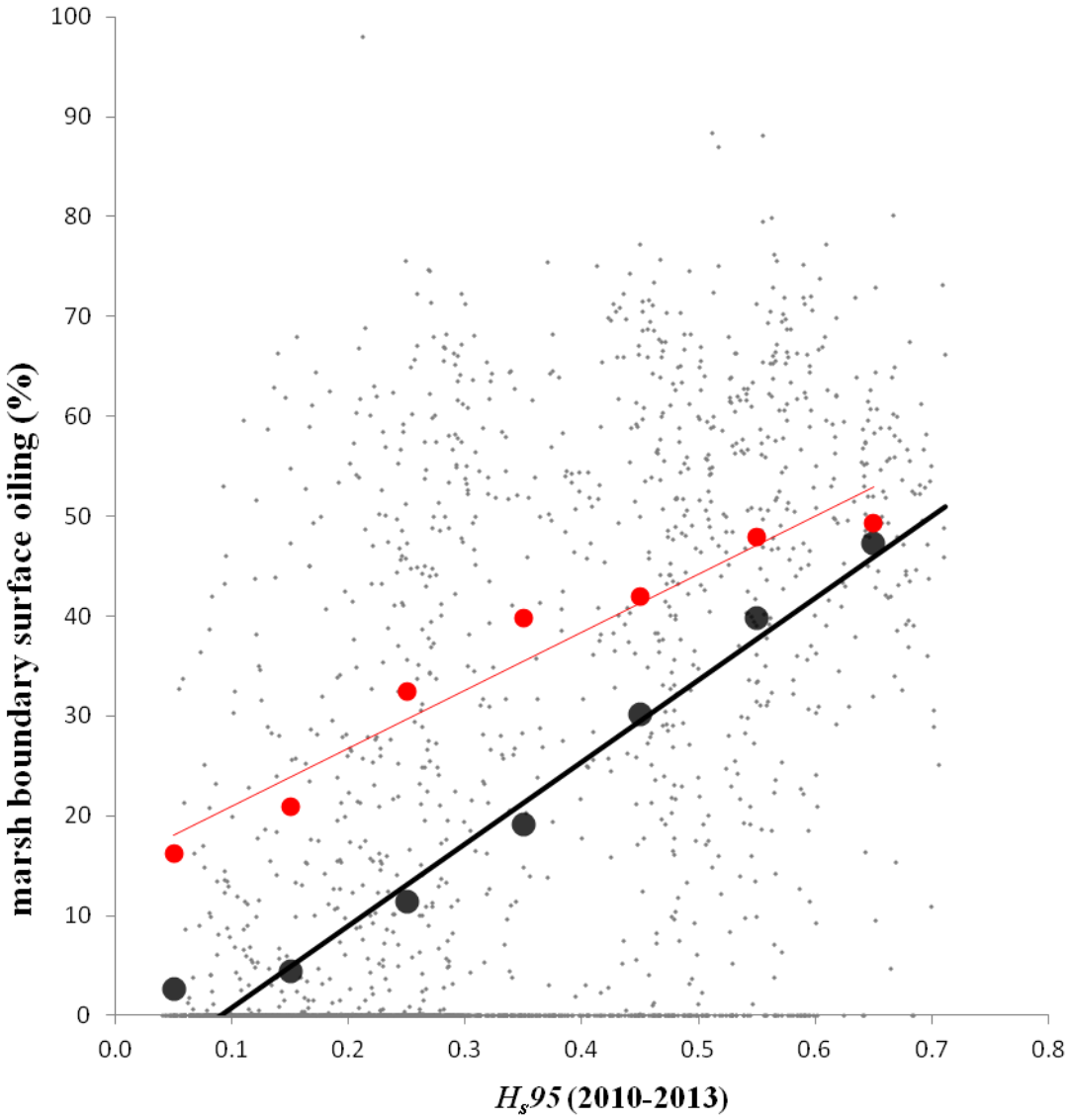

Figure 4.3: Relationship between the 95th percentile significant wave heights and percentage of shoreline oiled surface for all marsh boundary reaches (R^2 = 0.34; p < 0.0001; N = 2420). Large black circles show the averaged percent oil coverage over 0.10 m wave height intervals to highlight the overall trend. Large red circles show the averaged percent oil coverage with non-oiled (0%) reaches excluded from calculation.

4.3.3 Land loss, significant wave height, and oiling

For heavily-oiled marsh boundaries, mean L_R increased by an average of 0.99 $m^2m^{-1}yr^{-1}$ for every 10 cm increase in the H_S95 from a low of 0.84 $m^2m^{-1}yr^{-1}$ (10-20 cm) to 5.79

$m^2m^{-1}yr^{-1}$ (>60 cm) during the period from 2010-2013 (Figure 4.4A-C). The increase in mean L_R was non-linear for H_S95 above 40 cm, highlighted by a tripling of the mean L_R from the H_S95 interval of 40-50 cm to >60 cm (Figure 4.4A-C). Heavily oiled boundaries exhibited a different mean L_R during the following period (2013-2016) than observed in the 2010-2013 period. During the second post-oiling period (2013-2016), mean L_R ranged from a low of 0.27 $m^2m^{-1}yr^{-1}$ (10-20 cm) to a high of 1.61 $m^2m^{-1}yr^{-1}$ (50-60 cm) and increased by an average of 0.34 $m^2m^{-1}yr^{-1}$ for every 10 cm increase in the H_S95, before dropping to 1.27 $m^2m^{-1}yr^{-1}$ for the highest H_S95 (Figure 4.4C). The mean L_R for heavily-oiled boundary reaches from 2013-2016 were less than half the background L_R of the pre-oiling (2006-2010) period along the same reaches, despite exhibiting H_s95 in the 2013-2016 period that were slightly greater (Figure 4.2F). Mean L_R for non-oiled boundaries ranged from 0.27 $m^2m^{-1}yr^{-1}$ (0-10 cm) to 2.96 $m^2m^{-1}yr^{-1}$ (>60 cm) and increased, on average, 0.42 $m^2m^{-1}yr^{-1}$ for every 10 cm increase in the H_s95 (Figure 4.4A-C). There are few shoreline reaches that were both non-oiled and exposed to high H_S95, which could introduce bias into the analysis of L_R-H_S95. Accordingly, we examined the sensitivity of non-oiled and oiled shoreline L_R-H_S95 relationships to outliers by removing all reaches with H_S95 >0.40 m. Removal of the reaches with H_S95 > 0.40 m reduced the slope of the H_S95-L_R relationship to a similar degree for both oiled and non-oiled shorelines, indicating the relationship is consistent for a range of H_S95, and is not sensitive to outliers at high H_S95 (Figure 4.4D-F).

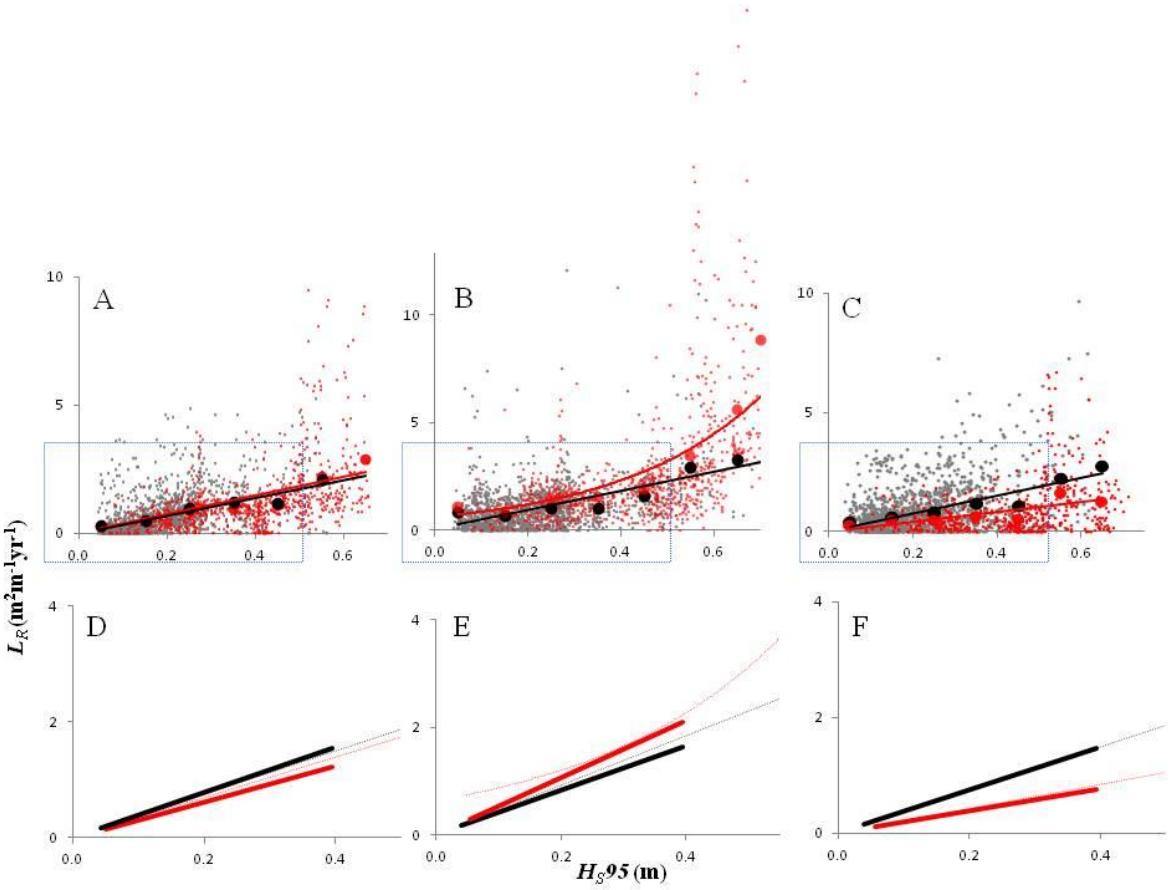

Figure 4.4: Land loss rates (L_R) with increasing significant wave height (H_s95). Small gray (non-oiled) and red (heavily-oiled) points show overall distribution of marsh boundary L_R for each period: 2006-2010 (A), 2010-2013 (B) and 2013-2016 (C). Large black (non-oiled) and red (oiled) points represent grouped H_s95 (0.10 m intervals). The zoom inserts for the 2006-2010 (D), 2010-2013 (E) and 2013-2016 (F) show L_R trends (bold lines) for reaches without H_S95 > 0.40 m and with H_S95 > 0.40 m.

Heavily-oiled boundaries exhibited similar overall covariability for L_R - H_S95 (R^2 = 0.21, R^2 = 0.24, and R^2 = 0.11; $p < 0.0001$).The mean L_R for each H_S95 category was not significantly different for the non-oiled and heavily-oiled marsh boundaries during the pre-oil period (2006-2010, $p = 0.29$). L_R along non-oiled marsh boundaries were weakly but significantly correlated with H_s95 in all three periods (R^2 = 0.20, R^2 = 0.14, and R^2 = 0.12; $p < 0.0001$; Figure 4.4A-C). L_R for oiled reaches behaved differently than L_R for non-oiled reaches in 2010-2013 ($p < 0.1$) and 2013-2016 ($p < 0.05$; Figure 4.4B-C). A difference in L_R

between oiled and non-oiled reaches occurred in the first post-oil period (2010-2013) for H_S95 > ~0.4 m, suggesting that oiling had the largest impact on reaches with the highest waves. The L_R-H_S95 relationship for heavily-oiled boundaries (≥20% oiled) in 2010-2013 was exponential, which differs from the linear L_R-H_S95 relationship for the other time periods (i.e. 2006-2010, and 2013-2016; Figure 4.4A-C) and non-oiled boundaries (Figure 4.4B). The L_R-H_S95 relationship for the same heavily-oiled boundaries was linear during the second post-oil period (2013-2016; Figure 4.4C), similar to the non-oiled boundary background rates (Figure 4.5), but the slope of the line was less steep than the non-oiled (<25% oiled) boundaries, which suggests L_R for heavily-oiled marsh boundaries dropped below the background rates (Figure 4.6E-F).

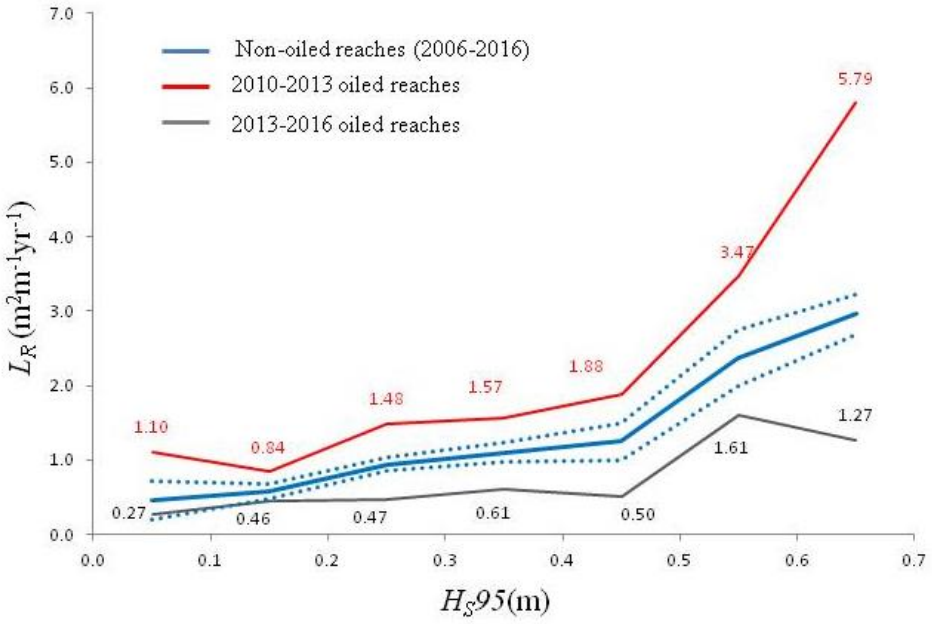

Figure 4.5: Comparison of land loss rates (L_R), grouped and averaged by H_S95, for oiled reaches and reaches (red and gray lines) without oiling (blue line) and ± sd (dashed lines).

Overall, L_R were generally higher during 2006-2010 and 2010-2013 than during the 2013-2016 period (Figure 4.6A-F). The greatest differences in L_R were determined for heavily oiled boundary reaches between 2010-2013 and 2013-2016 (Figure 4.6D), followed by the non-oiled reaches of the same time periods (Figure 4.6C). These results suggest a considerable decline in L_R over the latter period, even though H_s95 was comparable between the pre-oil and second post-oil periods (Figure 4.2C-D). Interestingly, L_R along non-oiled boundaries were slightly higher during the 2006-2010 period than the 2010-2013 period (Figure 4.6A), despite overall H_s95 being slightly higher in the latter period (Figure 4.2). Conversely, L_R were substantially higher during the 2010-2013 period than the 2006-2010 period along oiled shorelines (Figure 4.6B), despite the H_s95 slope differences being virtually the same for oiled and non-oiled shorelines (Figure 4.2). This further suggests that oiling accelerated L_R from 2010-2013. All three time period comparisons of L_R showed highly significant relationships ($p < 0.001$) for both oiled and non-oiled boundaries, except for non-oiled reaches between time periods 2010-2013 and 2013-2016 ($R^2 = 0.001$, $p = 0.34$).

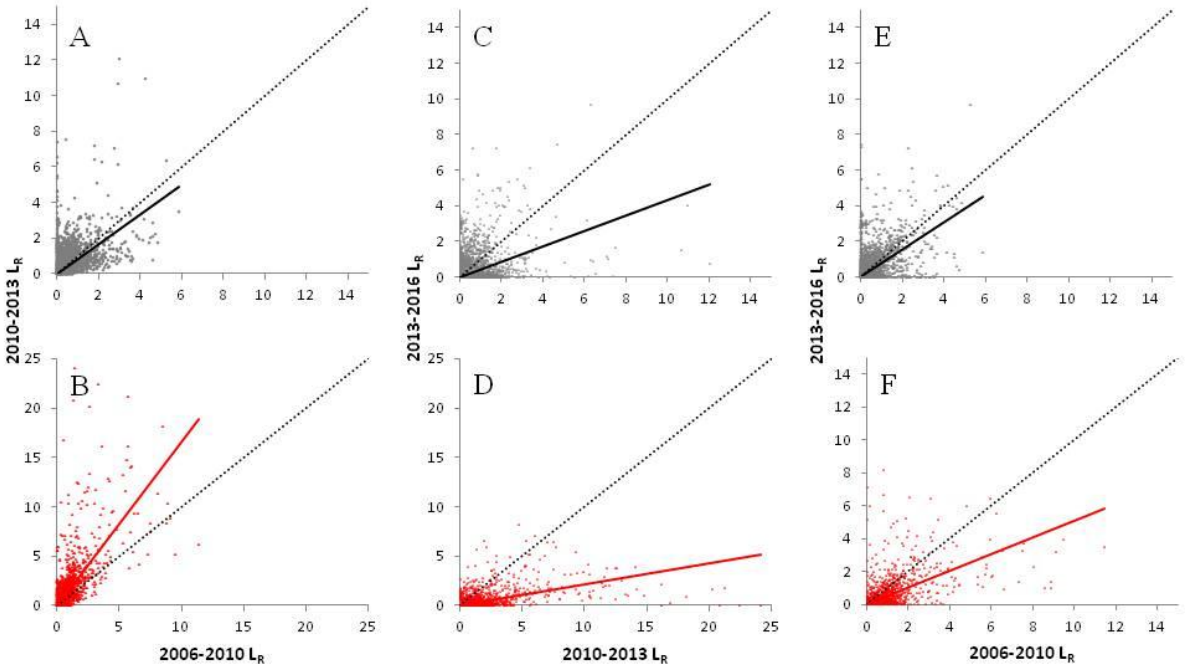

Figure 4.6: Time period comparisons of reach-scale L_R($m^2m^{-1}yr^{-1}$) for non-oiled (A,C,E) and oiled shorelines (B,D,F). Plots A & B show the relationships in L_R between the 2006-2010 and the 2010-2013 periods for non-oiled reaches (R^2 = 0.13, SE = 1.01) and oiled reaches (R^2 = 0.34, SE = 2.32). Plots C & D show the relationships in L_R between the 2010-2013 and the 2013-2016 periods for non-oiled reaches (R^2 = 0.001, SE = 1.02) and oiled reaches (R^2 = 0.11, SE = 1.02). Plots E & F show the relationships in L_R between the 2006-2010 and the 2013-2016 periods for non-oiled reaches (R^2 = 0.13, SE = 0.97) and oiled reaches (R^2 = 0.19, SE = 0.97).

4.4. Discussion

The marsh platform of Barataria Bay has been eroding since 1932, losing ~31% of its marsh area between 1932 and 2010 (Couvillion et al., 2011), through human activity and natural forcings (DeLaune et al., 1994; Nyman et al., 1994; Day et al., 2007; Morton and Bernier, 2010; Turner, 2011). From 1932-1990, twenty-five percent of land loss in salt marshes occurred along shorelines, driven predominantly by waves and tidal currents (Penland et al., 2000; Wilson and Allison, 2008). Over decades, the loss of marsh platform to

open water further lengthens fetches and increases the wind-generated wave power (Wilson and Allison, 2008). The compounding effect of greater wave energy, in addition to subsidence and reduced sediment supply, resulted in peak loss rates of 1.90 - 2.04% per year of total marsh area from 1970-1990 (Sasser et al., 1986; Evers et al., 1992; Barras et al., 2003). Loss rates declined from 1990-2010 (0.49 - 0.90 % per year), which was likely a result of reduced fluid extraction for oil and gas production after the 1970's (Morton and Bernier, 2010).

Turner et al. (2016) suggested that the distribution of oil along marsh boundaries immediately following the DWH spill event may be directly related to the variance in shoreline erosion rates prior to the DWH spill because both are strongly influenced by local currents and tides. Wave energy has been widely reported to drive lateral erosion processes, and the strong relationship between the spatial distribution of oiling and variance in shoreline erosion rates implies that oiling along marsh shorelines may be correlated with exposure to wave energy. Our analysis showed that the marsh boundaries that experienced the highest wave energy were also the most severely oiled following the DWH oil spill (Figure 4.3). Only 2% of the marsh boundary reaches (totaling 2627 m) with H_S95 greater than 50 cm experienced no oiling (according to the MESMA maps), while 91% of these reaches exhibited surface oiling greater than 20%. Conversely, 26% of reaches with H_S95 less than 30 cm exhibited oiling greater than 20%, suggesting that heavy oiling was concentrated along shorelines with high wave energy.

Our observations of accelerated land losses along oiled marsh shorelines are in general agreement with several recent studies conducted in Barataria Bay that have documented marsh responses following the 2010 DWH oil spill (Silliman et al., 2012;

McClenahan et al., 2013; Zengel et al., 2015; Rangoonwala et al., 2016; Turner et al., 2016; Beland et al., 2017; Khanna et al., 2017). Our analysis shows that land loss rates are correlated with wave energy for both oiled and non-oiled boundaries, and that loss rates were amplified along oiled reaches with wave heights (H_S95) greater than 50 cm (18% of all reaches) in the first post-oiling period (2010-2013). Land loss rates for heavily-oiled shorelines (> 20% oiling) were 75% higher than background rates for reaches with wave heights (H_S95) greater than 50 cm (Figure 4.5). These findings are in agreement with two recent studies that documented the distinct land loss patterns observed over the same period following the DWH oil spill and Hurricane Isaac, which made landfall in the Barataria Bay area (Rangoonwala et al., 2016; Khanna et al., 2017). Hurricane Isaac, a category 1 storm, made landfall twice in the vicinity of Barataria Bay on August 29, 2012, roughly two years after oil washed ashore from the DWH spill. While the maximum sustained wind speeds only reached tropical storm levels (~27 m/s), the storm's long dwell time in the area worsened the damage (Rangoonwala et al., 2016). Khanna et al. (2017) reported land loss rates for oiled boundaries that were 31% higher along the marsh zone closest to the shoreline (0-7 m), and 84% higher 7-14 m from the shoreline. By contrast, Rangoonwala et al. (2016) found that land loss along marsh shorelines was far more spatially extensive than that caused by wave-induced erosion, concluding that, perhaps the greatest impact of oil exposure was the acceleration of loss rates along boundaries protected from high wave energy. Our analysis of land loss rates found that oiling increased marsh loss even along shorelines exposed to low wave energy. However, loss rate increases were not as significant as exhibited by the boundaries subjected to high wave energy (Figures 4.4B & 5), suggesting that oiling and wave energy interact to produce rapid land loss.

The elevated land loss over background rates (i.e. + 75% background loss rates from 2006-2016) would likely have been even greater if not for the impacts of Hurricane Gustav, which made landfall in September of 2008. Hurricane Gustav likely damaged marsh boundaries, particularly along the high wave energy shorelines, thus resulting in elevated background rates used in the analysis. We suspect periods with light tropical cyclonic storm activity would exhibit background loss rates that are more in line with 2013-2016 observations. However, the accelerated losses along reaches with the highest wave energy reported here highlight the importance of landscape position, physical forces, and biogeomorphological feedbacks in predicting marsh responses to disturbances (Silliman et al., 2012; McClenahan et al., 2015).

Finally, land loss rates along oiled reaches decreased to less than the loss rates of non-oiled reaches in the second post-oil period (2013-2016). While this result was unanticipated, recent research has documented a similar trend in decreases in land loss rates in the MRD (Couvillion et al., 2017). Couvillion et al. (2017) offered several potential reasons for the reduced rate of loss, some of which may apply to the oil impacted, high wave energy exposure marshes of Barataria Bay. One possibility is the lack of major hurricane effects that have occurred over the last 5+ years (2013-2017; Couvillion et al., 2017). As observed in our analysis among others (e.g. Rangoonwala et al., 2016; Khanna et al., 2017), hurricanes can severely degrade vegetated shorelines and convert marsh platform area to open water, particularly along marsh boundaries that are vulnerable to direct, high energy waves. An equally compelling explanation for the decreased loss rates in our study area is that the most exposed and vulnerable marshes had already been lost by the second post-oil period (2013-2016), and therefore, the loss rates declined (Couvilion et al., 2017). For instance, heavily

oiled portions of marsh boundaries eroded more rapidly than non-oiled or low oiled portions creating headlands along the boundaries (McClenachan et al., 2013). As a result, these headlands were exposed to wave energy from more directions, which led to the rapid erosion of these micro-peninsulas (McClenachan et al., 2013). This process of oiling, heightened exposure to wave energy, and increased erosion rates may explain the acceleration of losses. Further, the subsequent decrease in rates below that of background land loss rates may be due to the removal of "points" or "heads" as discussed in previous studies of shoreline morphodynamics (Priestas et al., 2015). More research will be required to address the questions regarding the effects of shoreline morphology on recent trends in loss rates.

4.5. Conclusion

We examined the interactive contributions of wave action (H_S95) and oiling to marsh boundary land loss rates (L_R) in Barataria Bay over three consecutive time periods. Significant wave height was a moderately good predictor of heavily oiled marsh boundary locations, and surface oiling (%) increased monotonically with 10 cm increments of H_S95. Land loss rates were higher on oiled reaches in the first post-oiling period (2010-2013) after controlling for wave height, but only for reaches with wave heights greater than 0.5 m (18 % of all reaches) did the L_R - H_S95 relationship change from linear to exponential. Marsh responses to oil contamination were highly variable, and that wave action and degree of marsh boundary oiling were both significant factors in driving land loss for years after initial oiling. Three to six years after oiling, reaches returned to background rates across all wave

energy categories. These results highlight the importance of exposure to high wave energy in accelerating L_R following oiling.

4.6. References

Barras, J., Beville, S., Britsch, D., Hartley, S., Hawes, S., Johnston, J., et al. (2003). *Historical and projected coastal Louisiana land changes: 1978-2050* (p. 39p). United States Geological Survey.

Beland, M., Biggs, T. W., Roberts, D. A., Peterson, S. H., Kokaly, R. F., & Piazza, S. (2017). Oiling accelerates loss of salt marshes, southeastern Louisiana. *PloS one*, *12*(8), e0181197.

Beland, M., Roberts, D. A., Peterson, S. H., Biggs, T. W., Kokaly, R. F., Piazza, S., ... & Ustin, S. L. (2016). Mapping changing distributions of dominant species in oil-contaminated salt marshes of Louisiana using imaging spectroscopy. *Remote Sensing of Environment*, *182*, 192-207.

Britsch, L. D., & Dunbar, J. B. (1993). Land loss rates: Louisiana coastal plain. *Journal of Coastal Research*, 324-338.

Cahoon, D. R., Reed, D. J., Day Jr, J. W., Steyer, G. D., Boumans, R. M., Lynch, J. C., ... & Latif, N. (1995). The influence of Hurricane Andrew on sediment distribution in Louisiana coastal marshes. *Journal of Coastal Research*, 280-294.

Chuang, W. S., & Wiseman, W. J. (1983). Coastal sea level response to frontal passages on the Louisiana-Texas shelf. *Journal of Geophysical Research: Oceans*, *88*(C4), 2615-2620.

Couvillion, B.R., Barras, J.A., Steyer, G.D., Sleavin, W., Fischer, M., Beck, H., Trahan, N., Griffin, B., Heckman, D. (2011). Land area change in coastal Louisiana from 1932 to 2010: U.S. Geological Survey Scientific Investigations Map 3164, scale 1:265,000, 12 p. pamphlet.

Couvillion, B. R., Beck, H., Schoolmaster, D., & Fischer, M. (2017). Land area change in coastal Louisiana 1932 to 2016: US Geological Survey Scientific Investigations Map 3381: p 16. *Pamphlet, doi*, *10*.

Craig, N. J., Turner, R. E., & Day Jr, J. W. (1979). Land loss in coastal Louisiana (USA). *Environmental Management*, *3*(2), 133-144.

Davidson, T.M.; De Rivera, C.E. Accelerated erosion of saltmarshes infested by the non-native burrowing crustacean Sphaeroma quoianum. *Marine Ecology Progress Series*. 2010, 419, 129–136.

Day, J. W., Britsch, L. D., Hawes, S. R., Shaffer, G. P., Reed, D. J., & Cahoon, D. (2000). Pattern and process of land loss in the Mississippi Delta: a spatial and temporal analysis of wetland habitat change. *Estuaries*, *23*(4), 425-438.

Deegan L., Kennedy H., and Neill C. (1984). Natural factors and human modifications contributing to marsh loss in Louisiana's Mississippi River deltaic plain. *Environment Management*. 8 519–27.

DeLaune, R. D., Nyman, J. A., & Patrick Jr, W. H. (1994). Peat collapse, ponding and wetland loss in a rapidly submerging coastal marsh. *Journal of Coastal Research*, 1021-1030.

Dobson, J. E., Bright, E. A., Ferguson, R. L., Field, D. W., Wood, L. L., Haddad, K. D., et al. (1995). *NOAA Coastal Change Analysis Program (C-CAP): guidance for regional implementation* (p. 92). US Department of Commerce, National Oceanic and Atmospheric Administration, National Marine Fisheries Service.

Evers, D. E., Gosselink, J. G., Sasser, C. E., & Hill, J. M. (1992). Wetland loss dynamics in southwestern Barataria basin, Louisiana (USA), 1945–1985. *Wetlands Ecology and Management*, *2*(3), 103-118.

FitzGerald, D., Kulp, M., Hughes, Z., Georgiou, I., Miner, M., Penland, S., & Howes, N. (2007, May). Impacts of rising sea level to backbarrier wetlands, tidal inlets, and barrier islands: Barataria Coast, Louisiana. In *Proceedings of Coastal Sediments* (Vol. 7, pp. 179-1192).

Guntenspergen, G. R., Cahoon, D. R., Grace, J., Steyer, G. D., Fournet, S., Townson, M. A., & Foote, A. L. (1995). Disturbance and recovery of the Louisiana coastal marsh landscape from the impacts of Hurricane Andrew. *Journal of Coastal Research*, 324-339.

Hatton, R. S., DeLaune, R. D., & Patrick Jr, W. E. I. (1983). Sedimentation, accretion, and subsidence in marshes of Barataria Basin, Louisiana1. *Limnology Oceanographer*, *28*(3), 494-502.

Holdredge, C.; Bertness, M.D.; Altieri, A.H. (2009) Role of Crab Herbivory in Die-Off of New England Salt Marshes. *Conservation Biology*, 23, 672–679.

Jensen, J. R., Cowen, D. J., Althausen, J. D., Narumalani, S., & Weatherbee, O. (1993). The detection and prediction of sea level changes on coastal wetlands using satellite imagery and a geographic information system. *Geocarto International*, *8*(4), 87-98.

Khanna, S., Santos, M. J., Koltunov, A., Shapiro, K. D., Lay, M., & Ustin, S. L. (2017). Marsh Loss Due to Cumulative Impacts of Hurricane Isaac and the Deepwater Horizon Oil Spill in Louisiana. *Remote Sensing*, *9*(2), 169.

Khanna, S., Santos, M. J., Ustin, S. L., Koltunov, A., Kokaly, R. F., & Roberts, D. A. (2013). Detection of salt marsh vegetation stress and recovery after the deepwater horizon oil spill in barataria bay, Gulf of Mexico using AVIRIS data. *PloS one*, *8*(11), e78989.

Ko, J.-Y., & Day, J. W. (2004). A review of ecological impacts of oil and gas development on coastal ecosystems in the Mississippi Delta. *Ocean & Coastal Management*, *47*(11-12), 597–623.

Kokaly, R. F., Couvillion, B. R., Holloway, J. M., Roberts, D. A., Ustin, S. L., Peterson, S. H., ... & Piazza, S. C. (2013). Spectroscopic remote sensing of the distribution and persistence of oil from the Deepwater Horizon spill in Barataria Bay marshes. *Remote Sensing of Environment*, *129*, 210-230.

Lehr, B., Nristol, S., & Possolo, A. (2010). Oil Budget Calculator—Deepwater Horizon, technical documentation: a report to the National Incident Command. *Coastal Response Res. Cent*.

Leonardi, N., Ganju, N. K., & Fagherazzi, S. (2016). A linear relationship between wave power and erosion determines salt-marsh resilience to violent storms and hurricanes. *Proceedings of the National Academy of Sciences*, 113(1), 64-68.

Lin, Q., Mendelssohn, I. A., Graham, S. A., Hou, A., Fleeger, J. W., & Deis, D. R. (2016). Response of salt marshes to oiling from the Deepwater Horizon spill: Implications for plant growth, soil surface-erosion, and shoreline stability. *Science of the Total Environment*, *557*, 369-377.

Lin, Q., & Mendelssohn, I. A. (2012). Impacts and recovery of the Deepwater Horizon oil spill on vegetation structure and function of coastal salt marshes in the northern Gulf of Mexico. *Environmental science & technology*, *46*(7), 3737-3743.

Lin, Q., Mendelssohn, I. A., Suidan, M. T., Lee, K., & Venosa, A. D. (2002). The dose-response relationship between No. 2 fuel oil and the growth of the salt marsh grass, Spartina alterniflora. *Marine Pollution Bulletin*, *44*(9), 897-902.

McClenachan, G., Eugene Turner, R., & Tweel, A. W. (2013). Effects of oil on the rate and trajectory of Louisiana marsh shoreline erosion. *Environmental Research Letters*, *8*(4), 044030.

McLoughlin, S. M., Wiberg, P. L., Safak, I., & McGlathery, K. J. (2015). Rates and forcing of marsh edge erosion in a shallow coastal bay. *Estuaries and Coasts*, 38(2), 620-638.

Mendelssohn, I. A., McKee, K. L., & Patrick, W. H. (1981). Oxygen deficiency in *Spartina alterniflora* roots: metabolic adaptation to anoxia. *Science*, *214*(4519), 439-441.

Michel, J., Owens, E. H., Zengel, S., Graham, A., Nixon, Z., Allard, T., ... & Taylor, E. (2013). Extent and degree of shoreline oiling: Deepwater Horizon oil spill, Gulf of Mexico, USA. *PloS one*, *8*(6), e65087.

Mitsch, W.J., Gosselink, J.G., 2000. Wetlands, 3rd ed. John Wiley, New York.

Morton, R. A., & Bernier, J. C. (2010). Recent subsidence-rate reductions in the Mississippi Delta and their geological implications. *Journal of Coastal Research*, 555-561.

Muller, R. A., & Stone, G. W. (2001). A climatology of tropical storm and hurricane strikes to enhance vulnerability prediction for the southeast US coast. *Journal of Coastal Research*, 949-956.

Niering W.A., Warren R.S., Weymouth CG (1977). Our dynamic tidal marshes: vegetation changes as revealed by peat analysis. Connecticut Arboretum Bulletin, 22:2–12.

Nyman, J. A., Carloss, M., DeLaune, R. D., & Patrick Jr, W. H. (1994). Erosion rather than plant dieback as the mechanism of marsh loss in an estuarine marsh. *Earth Surface Processes and Landforms*, *19*(1), 69-84.

Penland, S., & Ramsey, K. E. (1990). Relative sea-level rise in Louisiana and the Gulf of Mexico: 1908-1988. *Journal of Coastal Research*, 323-342.

Peterson, S. H., Roberts, D. A., Beland, M., Kokaly, R. F., & Ustin, S. L. (2015). Oil detection in the coastal marshes of Louisiana using MESMA applied to band subsets of AVIRIS data. *Remote Sensing of Environment*, *159*, 222-231.

Pezeshki R. D., S. R. D. (1993). Effect of crude oil on gas exchange functions of *Juncus roemerianus* and *Spartina alterniflora*. *Water, Air, Soil Pollution*, *68*(3), 461–468.

Priestas, A. M., Mariotti, G., Leonardi, N., & Fagherazzi, S. (2015). Coupled wave energy and erosion dynamics along a salt marsh boundary, Hog Island Bay, Virginia, USA. *Journal of Marine Science and Engineering*, *3*(3), 1041-1065.

Rangoonwala, A., Jones, C. E., & Ramsey, E. (2016). Wetland shoreline recession in the Mississippi River Delta from petroleum oiling and cyclonic storms. *Geophysical Research Letters*.

Reddy, K. Ramesh, Delaune, Ronald, D. (2008). *Biogeochemistry of Wetlands: Science and Applications*. Boca Raton, FL: CRC Press, Taylor and Francis Group (757 pp).

Rohweder, J. J., Rogala, J. T., Johnson, B. L., Anderson, D., Clark, S., Chamberlin, F., & Runyon, K. (2008). *Application of wind fetch and wave models for habitat rehabilitation and enhancement projects* (No. 2008-1200, pp. 0-0). Geological Survey (US).

Sasser, C. E., Gosselink, J. G., Swenson, E. M., & Evers, D. E. (1995). Hydrologic, vegetation, and substrate characteristics of floating marshes in sediment-rich wetlands of the Mississippi river delta plain, Louisiana, USA. *Wetlands Ecology and Management, 3*(3), 171-187.

Silliman, B. R., van de Koppel, J., McCoy, M. W., Diller, J., Kasozi, G. N., Earl, K., … Zimmerman, A. R. (2012). Degradation and resilience in Louisiana salt marshes after the BP–Deepwater Horizon oil spill. *Proceedings of the National Academy of Sciences , 109* (28), 11234–11239.

Smart, R. M., & Barko, J. W. (1978). Influence of sediment salinity and nutrients on the physiological ecology of selected salt marsh plants. *Estuarine and Coastal Marine Science, 7*(5), 487–495.

Stone, G. W., Grymes III, J. M., Dingler, J. R., & Pepper, D. A. (1997). Overview and significance of hurricanes on the Louisiana coast, USA. *Journal of Coastal Research*, 656-669.

Stone, G. W., Zhang, X., & Sheremet, A. (2005). The role of barrier islands, muddy shelf and reefs in mitigating the wave field along coastal Louisiana. *Journal of Coastal Research*, 40-55.

Tessler, Z. D., Vörösmarty, C. J., Grossberg, M., Gladkova, I., Aizenman, H., Syvitski, J. P. M., & Foufoula-Georgiou, E. (2015). Profiling risk and sustainability in coastal deltas of the world. *Science, 349*(6248), 638-643.

Turner R.E. (1976). Geographic variations in salt marsh macrophyte production: a review. Contributions in Marine Science. 20:47–68.

Turner, R. E. (2011). Beneath the salt marsh canopy: loss of soil strength with increasing nutrient loads. *Estuaries and Coasts, 34*(5), 1084-1093.

Turner, R. E., McClenachan, G., & Tweel, A. W. (2016). Islands in the oil: Quantifying salt marsh shoreline erosion after the Deepwater Horizon oiling. *Marine Pollution Bulletin, 110*(1), 316-323.

U.S. Army Corps of Engineers (1977) Shore Protection Manual (3d ed.): Fort Belvoir, Va., Coastal Engineering Research Center.

U.S. Army Corps of Engineers (1984) Shore Protection Manual: Fort Belvoir, Va., Coastal Engineering Research Center.

U.S. Army Corps of Engineers (2002) Coastal Engineering Manual: Washington, D.C., U.S. Army Corps of Engineers, Engineer Manual 1110-2-1100, 6 vol.

Wilson, C. A., & Allison, M. A. (2008). An equilibrium profile model for retreating marsh shorelines in southeast Louisiana. *Estuarine, Coastal and Shelf Science*, *80*(4), 483-494.

Young, I. R., & Verhagen, L. A. (1996). The growth of fetch limited waves in water of finite depth. Part 1. Total energy and peak frequency. *Coastal Engineering*, 29(1-2), 47-78.

Zengel, S., Bernik, B. M., Rutherford, N., Nixon, Z., & Michel, J. (2015). Heavily oiled salt marsh following the Deepwater Horizon oil spill, ecological comparisons of shoreline cleanup treatments and recovery. *PloS one*, *10*(7), e0132324.

Chapter 5: Conclusions

Globally, coastal wetlands are under threat from rising sea level and reduced sediment supplies (Kirwan et al., 2010). Nowhere is this more evident than in coastal Louisiana, which has been losing ~62 km^2yr^{-1} since the early 1930's (Couvillion et al., 2017). The DWH oil spill and subsequent oiling along marsh shorelines added a compounding effect onto existing high rates of land loss exhibited by these ecosystems. This dissertation shows that the marsh responses to oil contamination are highly variable, and that wave action and degree of marsh boundary oiling are both significant factors in determining marsh recovery trajectories. For instance, the results suggest that marshes that are heavily-oiled, but protected from wave action, show signs of vegetation regrowth and recovery within 3 years of oil contamination. This is demonstrated in Chapter 2, where some of the heavily oiled shorelines showed signs of recovery in 2011 and 2012 as sub-climax, pioneer species revegetated disturbed marsh. Conversely, heavily oiled marsh boundaries that were exposed to high wave energy exhibited land loss rates that were amplified from 2010-2013. For example, in Chapter 3, the results show that oiling increased total land losses by 50% (52,521 m^2yr^{-1}) from 2010-2013 (more than 80% of which are attributable to reaches with > 30% oil cover), and the relationship between land loss and wave height for heavily-oiled (>20%) reaches was exponential during the 2010-2013 post-oil period.

The findings highlight the importance of wave action in determining ecosystem responses following oiling, and demonstrate how an integrated oil-wave action exposure

model could be used more broadly to prioritize the most vulnerable marsh boundaries for immediate restoration and substrate stabilization efforts. The dissertation also accounted for background rates of land loss attributable to natural erosional forcings. While the rates are likely substantially higher for Barataria Bay than would be reported for estuarine marshes in other regions, these results are a valuable reference for comparison with other estuaries in the Mississippi River Delta and elsewhere. Additionally, the dissertation provides a simple method for calculating background rates of land loss that can be used in future assessments of impacts following disturbances.

The findings related to oil effects on marsh communities and land loss will likely have limited applicability beyond the Gulf Coast region, due to the unique set of physical and biological factors that govern the ecosystem responses in these estuaries. Past studies have demonstrated that coastal wetlands exposed to oil in warmer (equatorial or sub-tropical) regions, like the Gulf of Mexico, have the capacity to recover more rapidly than in temperate or polar regions because of the enhanced activity by hydrocarbon-utilizing microorganisms in warmer water and marsh sediments (Pezeshki et al., 2000; Atlas et al., 2015). Weather events, like hurricanes, also influence the distinctive ecosystem response of this region. Elevated wave energy flux during tropical storm events can result in severe lateral erosion along marsh boundaries and scouring of the marsh platform (Cahoon et al., 1995; Guntenspergen et al., 1995). Conversely, warm regions or locations where tropical storms and high wave energy events are infrequent will likely exhibit greater ecosystem resilience in response to an oiling disturbance. Further, climatic factors (i.e. temperature and precipitation) largely determine the plant community composition for a particular region, which would also influence ecosystem response to oiling. For example, the forested

wetlands of the Niger Delta or mangrove swamps of Southeast Asia are likely to response differently to oil exposure than marshes along the Gulf Coast region of the United Sates.

Finally, the general applicability of this research lies predominantly in the advanced remote sensing and GIS techniques developed here to assess the ecosystem responses to a large-scale disturbance. In Chapter 2, the dissertation demonstrates the capacity of the IES/CDA classification system to accurately and consistently map spectrally similar salt marsh species across multiple datasets and image acquisition dates (overall accuracy = 82%, kappa = 0.78). This approach has also performed well in forested ecosystems (Roth et al., 2015), making it a good candidate for further application following future ecosystem disturbances. In Chapter 3, a methodology is developed to assess reach-scale wetland loss attributable to oiling and to account for variability in background erosion rates over multiple time periods. This approach could be broadly applied to future investigations of ecosystem degradation along vegetated shorelines following a disturbance. A limitation of Chapter 3 is that non-oiled shorelines in all locations within Barataria Bay are assumed to have the same background land loss rate for a given time period. This limitation is addressed in Chapter 4 by integrating a simple, fetch-limited wave model to determine the interactive contributions of wave energy and oiling on marsh boundary land loss rates. This model could help explain land loss rates across many regions where estuarine shorelines are exposed to variable wave energy which influence recovery trajectories following disturbances.

5.1. Limitations

A limitation of this dissertation is the potential influence of spatiotemporal autocorrelation in the statistical analysis of the relationships among the land loss rates, wave

energy, and oiling variables. Based on visual interpretation and preliminary spatial autocorrelation results ($I \approx 0.70$, z-score > 10, $p < 0.005$), there is a high probability (>95%) of clustering of L_R. Going forward, a major challenge will be determining which factors are the primary drivers of the spatial dependence for L_R. For instance, an important question will be to address whether or not the spatial autocorrelation of L_R is caused by the spatial dependence of exogenous variables (i.e. wave action, oiling, vegetation, macrofauna), or is due to endogenous factors (i.e. boundary elevation and plant biomass) and, therefore, unexplained (statistically) by these other factors.

Another limitation of this dissertation is that there are other factors, in addition to wave energy and oil exposure, contributing to the dynamics of L_R. Priestas et al. (2015) notes that variability in L_R is strongly influenced by local geomorphic and biological factors. For instance, sediment composition along with above- and belowground biomass composition have a substantial effect on marsh boundary resistance to erosional forces. In addition, slight differences in marsh boundary elevations can have a measurable effect on erosion rates at a local scale.

5.2. Future Research

An analysis of the spatial dependence of explanatory (oiling and wave energy) and response (land loss) variables could increase our understanding of oil exposure and land loss characteristics, and assist in forecasting later disturbance events. Other future studies that integrate local variables into the landscape-scale model introduced here would likely enhance our capacity to analyze the dynamic response of salt marshes to disturbance events such as oil spills and hurricanes.

5.3. References

Atlas, R.M., Stoeckel, D.M. Faith, S.A. & Minard-Smith, A. (2015). Oil biodegradation and oil-degrading microbial populations in marsh sediments impacted by oil from the Deepwater Horizon well blowout. *Environmental Science & Technology* 49:8,356–8,366.

Cahoon, D. R., Reed, D. J., Day Jr, J. W., Steyer, G. D., Boumans, R. M., Lynch, J. C., ... & Latif, N. (1995). The influence of Hurricane Andrew on sediment distribution in Louisiana coastal marshes. *Journal of Coastal Research*, 280-294.

Couvillion, B. R., Beck, H., Schoolmaster, D., & Fischer, M. (2017). Land area change in coastal Louisiana 1932 to 2016: US Geological Survey Scientific Investigations Map 3381: p 16. *Pamphlet, doi, 10*.

Guntenspergen, G. R., Cahoon, D. R., Grace, J., Steyer, G. D., Fournet, S., Townson, M. A., & Foote, A. L. (1995). Disturbance and recovery of the Louisiana coastal marsh landscape from the impacts of Hurricane Andrew. *Journal of Coastal Research*, 324-339.

Kirwan, M. L., Guntenspergen, G. R., D'Alpaos, A., Morris, J. T., Mudd, S. M., & Temmerman, S. (2010). Limits on the adaptability of coastal marshes to rising sea level. *Geophysical Research Letters*, 37(23).

Pezeshki, S. R., Hester, M. W., Lin, Q., & Nyman, J. A. (2000). The effects of oil spill and clean-up on dominant US Gulf coast marsh macrophytes: a review. *Environmental pollution*, 108(2), 129-139.

Priestas, A. M., Mariotti, G., Leonardi, N., & Fagherazzi, S. (2015). Coupled wave energy and erosion dynamics along a salt marsh boundary, Hog Island Bay, Virginia, USA. *Journal of Marine Science and Engineering*, 3(3), 1041-1065.

Roth, K. L., Roberts, D. A., Dennison, P. E., Alonzo, M., Peterson, S. H., & Beland, M. (2015). Differentiating plant species within and across diverse ecosystems with imaging spectroscopy. *Remote Sensing of Environment*, 167, 135-151.